ORSAY
n° d'ordre : 2667

UNIVERSITE DE PARIS-SUD

CENTRE D'ORSAY

THESE

présentée

Pour obtenir

Le GRADE de DOCTEUR d'ETAT

Spécialité: Sciences Physiques

PAR

Mme Monique LASSAUT

SUJET : Etude microscopique du potentiel optique alpha-noyau à basse et moyenne énergies. Application à l'analyse simultanée de la diffusion élastique (α,α) et de la réaction de transfert $(^3He,\alpha)$.

soutenue le 15 Février 1983 devant la Commission d'examen

MM. M. JEAN Président

R. SCHAEFFER

Mme M. ERICSON

M. C. MAHAUX

Mmes N. MARTY

N. VINH MAU

UNIV.
LEIDEN
1936

ORSAY
n° d'ordre : 2667

UNIVERSITE DE PARIS-SUD

CENTRE D'ORSAY

THESE

présentée

Pour obtenir

Le GRADE de DOCTEUR d'ETAT

Spécialité: Sciences Physiques

PAR

Mme Monique LASSAUT

SUJET : Etude microscopique du potentiel optique alpha-noyau à basse et moyenne énergies. Application à l'analyse simultanée de la diffusion élastique (α,α) et de la réaction de transfert $(^3He,\alpha)$.

soutenue le 15 Février 1983 devant la Commission d'examen

MM. M. JEAN Président

R. SCHAEFFER

Mme M. ERICSON

M. C. MAHAUX

Mmes N. MARTY

N. VINH MAU

Je tiens à remercier Mme N. Vinh Mau de m'avoir acceuillie à la Division de Physique Théorique de l'Institut de Physique Nucléaire d'Orsay.

Je remercie Mr Jean, Mme Ericson, Mr Mahaux ainsi que Mme Marty de l'intérêt qu'ils ont manifesté pour ce travail en acceptant d'être président et membres du jury de cette thèse.

Il m'est particulièrement agréable de pouvoir exprimer ici toute ma gratitude à N. Vinh Mau, qui a suggéré ce travail, pour les nombreux conseils et encouragements qu'elle n'a cessé de me prodiguer avec beaucoup de bienveillance et de patience.

Je suis très reconnaissante à R. Schaeffer d'avoir suivi dès son début le développement de cette étude, en me faisant bénéficier de sa confiance et de ses encouragements, et d'avoir accepté d'en être le rapporteur.

Je remercie vivement toutes les personnes qui ont contribué à la réalisation de ce travail, en particulier F. Michel pour son amicale et précieuse collaboration et J. Van de Wiele dont la collaboration m'a permis de mener à bien la dernière partie de cette étude. J'exprime également toute ma gratitude à H. Langevin qui s'est toujours vivement intéressée à ce travail. Ses remarques et ses suggestions m'ont été très précieuses.

Je suis très reconnaissante à tous les membres de l'Institut de Physique Nucléaire et aux visiteurs qui m'ont aidée de leurs conseils et de leurs encouragements, en particulier F. Duggan, E. Gerlic, M. L'Huillier, S. Marcos, C. Marty, M.C. Nemes, H. Ngô et D. Vautherin.

Je remercie vivement tous les personnels techniques et administratifs de la Division de Physique Théorique dont j'ai beaucoup apprécié la disponibilité et la gentillesse. J'exprime en particulier toute ma gratitude à A. Fercoq qui a dactylographié le manuscrit avec autant de soin que de rapidité, ainsi qu'à M. Dormeau, C. Marchal et J. Rouvet pour la réalisation des nombreuses figures. M. Malézieux, O. Le Royer et C. Séguy ont aussi contribué à la réalisation matérielle de cette thèse. Qu'elles trouvent ici l'expression de ma reconnaissance.

SOMMAIRE

	INTRODUCTION	1
I	INTERACTION α-NUCLEON A BASSE ENERGIE	11
II	POTENTIEL OPTIQUE α-NOYAU	18
	A- Approximation locale du potentiel optique non local	21
	B- Etude de la partie réelle du potentiel α-noyau à l'approximation de convolution	28
	C- Etude de la correction au modèle de convolution et de la partie imaginaire du potentiel α-noyau	61
	1. Calcul du potentiel absorptif α-^{40}Ca à basse énergie.	62
	2. Calcul du potentiel absorptif α-noyau et de correction au modèle de convolution aux énergies intermédiaires.	70
III	ETUDE AVEC NOS POTENTIELS MICROSCOPIQUES DE LA DIFFUSION ELASTIQUE (α,α) ET DE LA REACTION DE TRANSFERT (^{3}He,α)	97
	CONCLUSION	11

Résumé

Une étude microscopique du potentiel α-noyau est effectuée dans le cadre de la théorie de Feshbach pour des énergies comprises entre 20 et 200 MeV. Le potentiel réel du modèle de convolution est calculé directement à partir de l'interaction α-nucléon non locale déduite à l'approximation Hartree-Fock de diverses interactions nucléon-nucléon. Pour les interactions dépendant de la densité, nous avons proposé un choix différent de densité locale et inclus les termes de réarrangement, qui se sont révélés importants à courtes distances. Notre étude montre l'importance des effets de non-localité de l'interaction α-nucléon et de dépendance en densité du noyau de l'interaction nucléon-nucléon effective pour la détermination du potentiel réel. A basse énergie, nous avons calculé le potentiel absorptif α-^{40}Ca en tenant compte de tous les états qui peuvent être excités et en utilisant les fonctions d'onde RPA du ^{40}Ca. Aux énergies intermédiaires, nous avons dérivé une expression simple du potentiel imaginaire et de la correction au modèle de convolution pour tous les noyaux, en utilisant la relation de fermeture sur la base complète des états du noyau. Nous montrons que la correction au modèle de convolution est très faible. La détermination du potentiel imaginaire local équivalent au potentiel de Feshbach est fortement influencée par la non-localité du potentiel réel. Nos potentiels α-noyau reproduisent correctement les propriétés globales des potentiels déduits des analyses de diffusion et nous ont permis une description cohérente de la diffusion élastique (α,α) et de la réaction de transfert (^{3}He, α) au-delà de 100 MeV.

Mots-clés

Interaction α-noyau - Potentiel optique -
Diffusion élastique - Réaction de transfert.

ABSTRACT

The α-nucleus potential is investigated within the framework of Feshbach theory for energies ranging from 20 MeV up to 200 MeV. The folding model real potential is directly derived from the non local α-nucleon interaction calculated in the Hartree-Fock approximation from different nucleon-nucleon interactions. For density-dependent forces, we have proposed a different choice of the local density and included the rearrangement terms, which were found to be significant at small distances. Both effects of the non-locality of the α-nucleon interaction and the target density dependence of the effective nucleon-nucleon interaction are shown to be important to determine the real potential. At low energy, the α-^{40}Ca absorptive potential is calculated including the contribution of all opened inelastic channels and using the RPA wave function of ^{40}Ca. At intermediate energy, a simple expression of the imaginary potential and the correction to the folding model potential is derived for all nuclei, by using the closure relation over the complete basis of nucleus states. The correction to the folding model potential is shown to be very weak. The determination of the local imaginary potential equivalent to the Feshbach potential is strongly influenced by the non-locality of the real potential. Our microscopic α-nucleus potentials reproduce the global properties of empirical potentials correctly and allow a coherent description of both (α,α) elastic scattering and (^{3}He,α) transfer reaction for incident energies above 100 MeV.

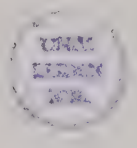

INTRODUCTION

Un grand nombre d'informations sur le potentiel optique alpha-noyau ont été accumulées au cours de ces dernières années grâce à de nombreuses expériences de diffusion élastique de particules alpha. Les analyses phénoménologiques globales des données expérimentales de diffusion élastique sur un grand domaine d'énergies et d'angles de diffusion ont réduit les ambiguïtés pour la détermination de la partie réelle du potentiel,et bien que conduisant à une connaissance moins précise de sa partie imaginaire ont néanmoins permis d'en établir certaines propriétés globales [GR78] . Outre les expériences de diffusion, les expériences de transfert (^{3}He,α) constituent également une source d'informations sur le potentiel optique α-noyau. Or les analyses phénoménologiques semblent indiquer que les potentiels ajustés sur la diffusion élastique ne peuvent reproduire les sections efficaces de la réaction de transfert dès que l'énergie est supérieure à 100 MeV [CH77, DJ80, VDW78] . Un potentiel α-noyau microscopique qui puisse,dans une certaine mesure, expliquer les propriétés et le comportement des potentiels phénoménologiques nous a semblé souhaitable et le but de notre travail a donc été d'essayer de construire un tel potentiel et de le confronter simultanément aux données expérimentales de la diffusion élastique (α,α) et de la réaction de transfert (^{3}He,α).

Le grand nombre de données expérimentales disponibles a suscité de nombreuses études théoriques du potentiel α-noyau réel. La plupart de ces études sont effectuées dans le cadre du modèle de convolution [SI75a, BA77, SA79] où le potentiel α-noyau réel est simplement décrit par le produit de convolution de l'interaction α-nucléon par la densité du noyau cible. Dans les premiers travaux de Budzanowski et al. [BU70] où l'interaction α-nucléon est elle-même calculée comme produit de convolution de l'interaction nucléon-nucléon

par la densité de la particule alpha, tous les effets dus à l'antisymétrisation sont négligés. Des études plus récentes tiennent compte partiellement des effets dus à l'échange d'un nucléon entre le projectile et le noyau cible, en partant de l'interaction α-nucléon calculée dans le modèle de convolution antisymétrisé ou à l'approximation Hartree-Fock [EI76, MA78, SI75a, VM77]. Cette interaction α-nucléon non locale est alors approchée par un potentiel local, dont le produit de convolution par la densité du noyau cible engendre un potentiel α-noyau local. Une autre approche possible du potentiel α-noyau réel dans le cadre de ce modèle, mais qui à l'encontre de la précédente n'a suscité que peu d'études théoriques [SI75b, MA78, MA80], consiste à convoluer l'interaction nucléon-noyau par la densité de la particule alpha. Dans les travaux de Majka et al [MA78, MA80], cette interaction nucléon-noyau est elle-même calculée dans le modèle de convolution antisymétrisé. De telles approches, où l'interaction nucléon-noyau ou nucléon-α est calculée au premier ordre de la théorie de Feshbach, supposent que les corrections à ce potentiel dues au processus en deux étapes sont faibles. Alors que cette propriété est vérifiée pour le potentiel nucléon-α, du fait que la particule alpha n'a pas d'états excités collectifs de basse énergie, elle n'est plus vraie pour le potentiel nucléon-noyau et de ce point de vue la première approche du potentiel α-noyau réel est plus réaliste. Parallèlement à ces travaux, plusieurs études consacrées au potentiel α-noyau réel sont effectuées dans le cadre du modèle du groupe résonant [TA78, WI77] (ou des modèles qui lui sont apparentés telle la méthode de la coordonée génératrice) qui, à l'encontre du précédent, traite exactement les effets dus au principe de Pauli et permet une description unifiée des états de diffusion et des états liés du système α + noyau. Néanmoins ces

potentiels sont non locaux, dépendent de l'énergie et du moment angulaire, et le potentiel local équivalent présente pour les états de faible moment angulaire un coeur répulsif qui est une conséquence directe du principe de Pauli. Bien que de tels potentiels soient différents des potentiels déduits du modèle de convolution qui, en particulier, n'ont pas de coeur répulsif, les résultats obtenus dans ces deux modèles ne sont pas incompatibles. En effet, s'inspirant du premier modèle de Saito [SA69], Buck et al ont montré que, moyennant certaines approximations, les équations du groupe résonant peuvent être ramenées à une équation de Schrödinger pour un potentiel effectif local, que Saito suggérait être le terme de double convolution, à condition d'imposer à la fonction d'onde d'être orthogonale aux états interdits par le principe de Pauli [BU77]. Dans le cas particulier où ces états interdits, qui sont de carré intégrable, sont voisins des états liés du potentiel local et sous réserve que l'interaction locale varie lentement en fonction de l'énergie pour que soit préservée l'orthonormalité des états propres, la condition d'orthogonalité est automatiquement satisfaite en résolvant l'équation de Schrödinger pour le potentiel local et en écartant les solutions correspondant aux premiers états liés interdits. Dans le même esprit, le potentiel nucléon-noyau, calculé à l'approximation Hartree-Fock, est utilisé soit pour décrire les états de diffusion [DO71], soit pour décrire les états liés permis pour le système nucléon + noyau. D'autre part, il semble que les potentiels phénoménologiques déduits des données expérimentales de diffusion,qui sont des potentiels profonds, soient capables de décrire le spectre des états liés permis du système α + noyau [BA78,a].

A l'encontre du potentiel réel, auquel sont consacrés de nombreux travaux théoriques, peu d'études microscopiques du potentiel α-noyau imaginaire ont été menées à bien. En particulier, les modèles théoriques exposés précédemment ne permettent pas de décrire le potentiel imaginaire (du moins lorsque les calculs effectués dans le formalisme du groupe résonant se limitent au seul canal élastique). Un modèle, reposant sur la théorie de Feshbach appliquée au système α-noyau et s'appuyant sur un certain nombre d'hypothèses simplificatrices qui ont permis notamment d'utiliser la relation de fermeture sur les états excités du noyau, a été proposé par N. Vinh Mau [VM77]. Dans la lignée de ce travail, Dermawan et al ont calculé récemment le potentiel imaginaire α-^{40}Ca en tenant compte explicitement de tous les états RPA du ^{40}Ca qui peuvent être excités au cours de la réaction [DE82]. Un autre modèle, proposé par Brink pour le potentiel entre deux ions lourds [BR78], a été appliqué récemment à l'étude du potentiel α-^{40}Ca [BO82]. Ce dernier article montre que le modèle de Brink, basé sur la méthode des chemins de Feynman, est équivalent à une approximation semi-classique de la formule de Feshbach, donc proche conceptuellement du modèle de N. Vinh Mau. Enfin, une approche du potentiel entre deux ions lourds, s'appuyant sur la théorie de Brueckner, a été proposée récemment par Faessler et al [FA81]. Ces auteurs ont en effet paramétrisé la matrice G, calculée pour deux nucléons en interaction situés dans deux fragments distincts de matière nucléaire, par une interaction effective locale et complexe. Le potentiel entre deux noyaux finis est ensuite calculé dans le modèle de double convolution. Toutefois, un tel modèle ne tient pas compte de la contribution due aux excitations collectives du système noyau-noyau, contribution qui est ensuite ajoutée séparément pour compenser le manque d'absorption du potentiel à la surface [KH81].

L'étude présentée ici repose sur la théorie de Feshbach appliquée à la diffusion de la particule alpha interagissant avec chaque nucléon du noyau cible. La particule alpha étant ainsi discernable des nucléons du noyau, nous appliquons la théorie de Feshbach sans antisymétrisation. Ce modèle suppose connue l'interaction α-nucléon et nous avons utilisé l'interaction calculée dans notre thèse de troisième cycle à l'approximation Hartree-Fock à partir de plusieurs interactions nucléon-nucléon effectives [LA78]. Le potentiel alpha-noyau s'écrit alors comme la somme de deux termes : le premier est le potentiel réel du modèle de convolution et le second contient à la fois la correction à ce modèle et le potentiel imaginaire.

Dans une première partie de notre travail, nous étudions le potentiel α-noyau réel approché par le produit de convolution de l'interaction α-nucléon non locale par la densité du noyau cible. Dans les travaux antérieurs où cette non localité n'était que globalement prise en compte par l'utilisation d'un potentiel local équivalent, le potentiel α-noyau était trop profond et son intégrale de volume variait linéairement en fonction de A, nombre de masse du noyau cible, contrairement à ce que semblent montrer les analyses de la diffusion élastique vers 100 MeV. D'après les travaux de Jackson et Johnson [JA74], qui ont dérivé l'expression formelle du potentiel noyau-noyau calculé dans le modèle de convolution pour une interaction nucléon-noyau non locale, le paramètre de non localité du potentiel α-noyau varie en fonction du nombre de nucléons du noyau cible et est beaucoup plus faible que le paramètre de non localité du potentiel α-nucléon. De ce fait, les approximations pour obtenir un potentiel local équivalent, qui reposent sur l'hypothèse que la non localité du potentiel est faible comparée à sa portée [FR57, FI66, PE80],sont mieux justifiées pour le potentiel α-noyau que pour le potentiel α-nucléon. Bien que l'on s'attende à ce que les poten-

tiels α-noyau calculés pour une interaction α-nucléon locale ou non locale aient sensiblement la même dépendance en énergie [JA74, VM 78], tout en étant différents à courtes distances [VM78], le fait d'utiliser l'interaction α- nucléon sous sa forme non locale, qui modifie la dépendance en A du potentiel α-noyau par le biais de sa non localité, pourrait expliquer le comportement en A du potentiel α-noyau prédit par les analyses phénoménologiques de Goldberg [GO73,GO75 Notre étude a été effectuée pour des interactions nucléon-nucléon dépendant et indépendantes de la densité. L'une des principales difficultés rencontrées pour étendre le formalisme du modèle de convolution aux interactions dépendant de la densité, qui seules à l'approximation Hartree-Fock sont capables de décrire correctement les états liés, est de définir la densité locale aux points 1 et 2,où sont situés les deux nucléons en interaction,en fonction des densités du projectile et de la cible. Généralement, cette densité est approchée par la somme des densités du projectile et de la cible [CO76, GU78, LO77, PE77, SA79, SI75a], approximation qui est certainement justifiée lorsque la distance entre les centres des deux noyaux est suffisamment grande pour que leur recouvrement soit faible, mais qui cependant conduit à petites distances à des densités très élevées pour lesquelles les interactions nucléon-nucléon effectives n'ont pas été déterminées. Ce problème a déjà été soulevé par Majka et al qui ont remplacé la somme simple par une somme pondérée des deux densités [MA78]. Nous avons alors proposé une expression différente de la densité locale en fonction des densités de la particule alpha et du noyau cible, expression qui conduit à des densités normales à courtes distances mais qui toutefois présente l'inconvénient de sous-estimer la densité totale, lorsque le recouvrement des deux noyaux est faible. Nous avons ensuite comparé les résultats obtenus avec ces deux prescriptions.

Une deuxième partie de notre travail est consacrée à l'étude de la correction au potentiel réel du modèle de convolution et au calcul du potentiel imaginaire, donnés par le deuxième terme de la formule de Feshbach qui tient compte de processus en deux étapes, correspondant à une excitation du noyau cible dans l'étape intermédiaire. Dans un tel processus, seuls les états excités du noyau d'énergie inférieure à l'énergie de la particule alpha incidente peuvent contribuer au potentiel imaginaire. A basse énergie où peu de voies inélastiques sont ouvertes, nous en avons tenu compte explicitement et calculé le potentiel α-^{40}Ca en décrivant les états excités du noyau par les fonctions d'onde RPA. Nous comparerons notre potentiel imaginaire à celui obtenu récemment par Dermawan et al dans une étude très similaire à la nôtre [DE82]. A plus haute énergie, le nombre de voies ouvertes est très important et nous avons fait des hypothèses simplificatrices qui nous ont permis d'utiliser la relation de fermeture sur la base complète des états du noyau. Nous avons ainsi obtenu des expressions simples pour la correction au modèle de convolution et pour le potentiel absorptif, qui peuvent être calculés aisément pour différents noyaux et différentes énergies. Remarquons que sommant sur tous les états du système à A particules, nous avons implicitement tenu compte des voies $(\alpha,\alpha a)$ avec émission d'une particule a par le noyau cible.

La dernière partie de notre travail est consacrée à l'étude simultanée de la diffusion élastique (α,α) et de la réaction de transfert $(^3He,\alpha)$ à partir de nos potentiels α-noyau calculés et pour des énergies supérieures à 100 MeV, là où la phénoménologie rencontre une difficulté. Dans une première analyse, nous avons conservé la forme de notre potentiel microscopique et introduit deux constantes multiplicatives de renormalisation pour

la partie réelle et la partie imaginaire du potentiel. Les potentiels ainsi renormalisés sur les sections efficaces élastiques ont été alors utilisés pour calculer les sections efficaces de la réaction (^{3}He,α). Toutefois, une telle méthode de renormalisation, destinée à simuler les processus qui ne sont pas inclus dans le calcul microscopique tel le break-up de la partie alpha, n'est certainement pas appropriée pour le potentiel imaginaire puisque l'on s'attend à ce que les voies de break-up contribuent à l'absorption principalement à la surface du noyau [BA78b, SH79, WA78, WU78]. Nous avons alors, dans une seconde analyse, ajouté à notre absorption calculée un terme de surface ajustable et comparé une telle approche à la précédente en ce qui concerne la diffusion élastique (α,α) et la réaction de transfert (^{3}He,α).

Ce travail a fait l'objet de quatre articles publiés à Nuclear Physics et Physics Letters qui seront présentés au cours de notre exposé. Dans le premier chapitre, nous résumons la dérivation des interactions α-nucléon utilisées dans ce travail. Le second chapitre est consacré au calcul du potentiel α-noyau partie réelle et partie imaginaire pour des énergies comprises entre 20 et 200 MeV. Dans le troisième chapitre, les résultats obtenus sont confrontés aux données expérimentales de la diffusion élastique (α,α) et de la réaction de transfert (^{3}He,α). A la suite de ce chapitre, nous présentons nos conclusions.

REFERENCES

[BA77] R.C. Barrett and D.F. Jackson, Nuclear size and structure (Clarendon, Oxford, 1977).

[BA78,a] D. Baye, Proc. Second Louvain Cracow Seminar on the Alpha Nucleus Interaction, Louvain-la-Neuve, 1978, ed. G. Grégoire and K. Grotowski, p.330.

[BA78,b] G. Baur, F. Rösel, R. Shyam and D. Trautmann, KFA Jülich, Annual Report (1978) p.131,132 et références internes.

[BO82] A. Bonaccorso and D.M. Brink, Nucl. Phys. A384 (1982) 161.

[BR78] D.M. Brink, Lectures Notes in Physics, vol.89 (Springer-Verlag, 1978).

[BU70] A. Budzanowski, A. Dudek, K. Grotowski and A. Strzalkowski, Phys. Lett. 32B (1970) 431.

[BU77] B. Buck, H. Friedrich and C.Wheatley, Nucl. Phys. A275 (1977) 246.

[CH77] N.S. Chant, H. Chen, D.A. Goldberg, A. Nadasen and P.G. Roos, University of Maryland, Progress Reports (1977), p.72.

[CO76] M.D. Cohler, B. Sinha, R.J. Griffiths and N.M. Clarke, Phys. Lett. 63B (1976) 377.

[DE82] H. Dermawan, F. Osterfeld and V.A. Madsen, Phys. Rev. C25 (1982) 180.

[DJ80] A. Djaloeis, C. Alderliesten, J. Bojowald, C. Mayer-Böricke, W. Oelert and P. Turek, Nucl. Phys. A342 (1980) 252.

[DO71] C.B. Dover and Nguyen Van Giai, Nucl. Phys. A177 (1971) 559.

[EI76] Y. Eisen and B. Day, Phys. Lett. 63B (1976) 253.

[FA81] A. Faessler, T. Izumoto, S. Krewald and R. Sartor, Nucl. Phys. A359 (1981) 509.

[FI66] H. Fiedeldey, Nucl. Phys. 77 (1966) 149.

[FR57] W.E. Frahn and R.H. Lemmer, Nuovo Cim. 5 (1957) 1564.

[GO73] D.A. Goldberg, S.M. Smith, H.G. Pugh, P.G. Roos and N.S. Wall, Phys. Rev. C7(1973) 1938.

[GO75] D.A. Goldberg, Phys. Lett. 55B(1975) 59.

[GR78] Proc. Second Louvain Cracow Seminar on the Alpha Nucleus Interaction, Louvain-la-Neuve, 1978, ed. G. Grégoire and K. Grotowski.

[GU78] S.K. Gupta and S. Kailas, Phys. Lett. 73B (1978) 398.

[JA74] D.F. Jackson and R.C. Johnson, Phys. Lett. 49B (1974) 249.

[KH81] S.B. Khadkikar, L. Rikus and A. Faessler, Nucl. Phys. A369 (1981) 495.

[LA78] M. Lassaut, Thèse de Troisième Cycle, Université Paris VII (1978).

[LO77] W.G. Love, Phys. Lett. 72B (1977) 4.

[MA78] Z. Majka, H.J. Gils and H. Rebel, Z. Phys. A288 (1978) 139.

[MA80] Z. Majka, H.J. Gils and H. Rebel,
Acta Phys. PolonicaB11 (1980) 227.

[PE77] F. Petrovitch, D. Stanley and J.J. Bevelacqua, Phys. Lett. 71B (1977) 259.

[PE80] R.E. Peierls and N. Vinh Mau, Nucl. Phys. A343 (1980) 1.

[SA69] S. Saito, Prog. Theor. Phys. 41 (1969) 705.

[SA79] G.R. Satchler and W.G. Love, Phys. Reports 55C (1979) 183.

[SH79] R. Shyam, G. Baur, F. Rösel and D. Trautmann,
Phys. Rev. C19 (1979) 1246 et références internes.

[SI75,a] B. Sinha, Phys. Reports 20C (1975) 1 ;
Phys. Rev. C11 (1975) 1546.

[SI75,b] P.P. Singh, P. Schwandt and G.C. Yang, Phys. Lett. 59B (1975) 113.

[TA78] Y.C. Tang, M. Lemere and D.R. Thompson, Phys. Rep. 47 (1978) 167.

[VDW78] J. Van de Wiele, E. Gerlic, H. Langevin-Joliot and
G. Duhamel, Nucl. Phys. A297(1978) 61, et références internes.

[VM77] N. Vinh Mau, Phys. Lett. 71B(1977) 5

[VM78] N. Vinh Mau, Proc. Second Louvain Cracow Seminar on the Alpha Nucleus Interaction, Louvain-la-Neuve, 1978, ed. G. Gregoire and K. Grotowski, p.243.

[WA78] N.S. Wall, A.A. Cowley and R.C. Johnson,
Phys. Rev. C17(1978) 1315.

[WI77] K. Wildermuth and Y.C Tang, A Unified Theory of the nucleus,
Vieweg Braunschweig, 1977.

[WU78] J.R. Wu, C.C. Chang and H.D. Holmgren,
Phys. Rev.Lett. 40 (1978) 1013

CHAPITRE I

INTERACTION α-NUCLEON A BASSE ENERGIE

La connaissance de l'interaction α-nucléon est essentielle dans le modèle que nous utilisons pour obtenir le potentiel optique α-noyau. Les premiers calculs théoriques [GL66, BR70], utilisaient le modèle de convolution où le potentiel α-nucléon est exprimé comme le produit de convolution de l'interaction nucléon-nucléon par la densité de la particule alpha. Les interactions ainsi calculées, locales et indépendantes de l'énergie, reproduisaient assez mal les données de la diffusion et en particulier leur comportement en énergie. En effet, un tel modèle néglige les effets d'échange entre le nucléon incident et les nucléons de l'alpha, effets dont Schaeffer a montré qu'ils sont importants [SC70].

Dans un premier travail qui a fait l'objet de notre thèse de troisième cycle [LA78], nous avons repris la dérivation du potentiel α-nucléon dans un modèle qui tient compte des effets d'échange. Pour des énergies dans le laboratoire inférieures à environ 25MeV pour le nucléon ou 100 MeV pour la particule alpha, les voies inélastiques du système α-nucléon sont fermées. Le potentiel effectif α-nucléon est donc purement réel et donné par le potentiel de Hartree-Fock :

$$
\begin{aligned}
V_{\alpha n}(\bar{r},\bar{r}') &= \delta(\bar{r}-\bar{r}')\int \rho_\alpha(r_1) V_{nn}(\bar{r}-\bar{r}_1;\rho)\,d\bar{r}_1 - \rho_\alpha(\bar{r},\bar{r}')V_{nn}(\bar{r}-\bar{r}';\rho) \\
&+ \frac{1}{2}\,\rho_\alpha(r)^{1/2}\,\delta(\bar{r}-\bar{r}')\int \rho_\alpha^{3/2}(r_1)\,\frac{\partial V_{nn}(\bar{r}-\bar{r}_1;\rho)}{\partial\rho}\,d\bar{r}_1 \qquad \text{(I.1)} \\
&- \frac{1}{2}\,\rho_\alpha(r)^{-1/2}\,\delta(\bar{r}-\bar{r}')\int |\rho_\alpha(\bar{r},\bar{r}_1)|^2 \rho_\alpha(r_1)^{1/2}\,\frac{\partial V_{nn}(\bar{r}-\bar{r}_1;\rho)}{\partial\rho}\,d\bar{r}_1
\end{aligned}
$$

où V_{nn} désigne l'interaction nucléon-nucléon, $\rho_\alpha(r)$ et $\rho_\alpha(\bar{r},\bar{r}')$ les densités Hartree-Fock locales et non locales. Le premier et le second termes de l'équation (I.1) sont respectivement le terme direct local et le terme d'échange non local habituels. Lorsque l'interaction nucléon-nucléon dépend de la densité, deux termes supplémentaires locaux apparaissent, les termes direct et d'échange de réarrangement qui sont respectivement les troisième et quatrième termes de l'équation (I.1). Ces termes sont absents dans le modèle de convolution antisymétrisé.

Le potentiel non local, eq.(I.1), a été calculé pour deux types d'interaction nucléon-nucléon.

1) Les interactions B_1 et C_1 de Brink et Boeker, indépendantes de la densité, comportant un terme attractif de longue portée et un terme répulsif de courte portée :

$$V_{nn}(x_1,x_2) = \sum_{i=1}^{2} Si(1-m_i+m_i P^r) e^{-\frac{(\bar{r}_1-\bar{r}_2)^2}{\mu_i^2}} \qquad (I.2)$$

où x désigne l'ensemble des variables d'espace, de spin et d'isospin $x = (\bar{r},\sigma,\tau)$ et P^r est l'opérateur d'échange de Majorana . Ces interactions ont été déterminées de manière à reproduire au mieux les énergies de liaison dans la matière nucléaire, ainsi que l'énergie de liaison et le rayon de la particule alpha. Supposant que l'état fondamental de l'alpha est un déterminant de Släter, Brink et Boeker [BR67] imposent aux états individuels d'être ceux d'un oscillateur harmonique et calculent alors les énergies et les fonctions d'onde par la méthode variationnelle, le paramètre variationnel étant b_0, celui de l'oscillateur harmonique. Les deux forces reproduisent bien l'énergie de liaison de l'alpha, mais B_1 surestime légèrement son rayon. Cependant, B_1 conduit aux meilleurs résultats lorsque l'on considère l'ensemble des trois noyaux : ^{4}He, ^{16}O et ^{40}Ca et de ce fait est la plus couramment utilisée.

2) L'interaction G-O de Banerjee-Campi-Sprung [CA72,SP71], dépendant de la densité, qui est déduite à l'approximation de densité locale de la matrice G calculée dans la matière nucléaire. Cette dépendance en densité de l'interaction effective nucléon-nucléon est essentielle pour reproduire simultanément, à l'approximation Hartree-Fock, les énergies de liaison, rayons carrés moyens des densités et dans une certaine mesure le spectre des énergies individuelles de l'ensemble des noyaux [NE70, CA72] . Cette interaction est paramétrisée, pour un état de spin et d'isospin donné, comme la superposition de cinq gaussiennes plus un terme correctif de portée nulle, traduisant le changement des dénominateurs d'énergie dans l'équation de Bethe-Goldstone lors du passage de la matière nucléaire aux noyaux finis :

$$V_{nn}(\bar{r}_1,\bar{r}_2,k_F) = \sum_{i=1}^{5} (a_i+b_i k_F^{1/2})\, e^{-\frac{(\bar{r}_1-\bar{r}_2)^2}{\mu_i^2}} + (W-W_0(k_F))A(k_F)\delta(\bar{r}_1-\bar{r}_2) \qquad (I.3)$$

où k_F désigne le moment de Fermi, W_0 représente l'énergie moyenne des deux nucléons en interaction dans la matière nucléaire et W l'énergie correspondante dans les noyaux finis. Les coefficients a_i et b_i, ainsi que les portées μ_i, ont été ajustés de manière à reproduire au mieux les éléments de matrice de G, calculés à partir du potentiel de Reid coeur mou.

A l'approximation de densité locale, le moment de Fermi k_F est relié à la densité nucléaire ρ aux points $\bar{r}_1$ et $\bar{r}_2$, caractérisant la position des deux nucléons en interaction. Les calculs Hartree-Fock de Campi, effectués pour l'interaction G-O [CA72], ont montré que les différentes expressions reliant la densité locale aux points 1 et 2 aux densités nucléaires en 1 et en 2, ou au centre de masse des deux nucléons en interaction, conduisent à des potentiels nucléon-noyau très voisins. Dans ce travail [LA78, LA80], nous avons utilisé la moyenne géométrique des densités nucléaires aux points $\bar{r}_1$ et $\bar{r}_2$:
$k_F^3 = \frac{3\pi^2}{2}(\rho(r_1)\rho(r_2))^{1/2}$ qui permet des calculs analytiques simples du potentiel α-nucléon.

Pour toutes les interactions nucléon-nucléon envisagées, nous avons calculé le potentiel α-nucléon avec les densités correspondant à la force utilisée. Ainsi, pour les forces B_1 et C_1, nous utilisons les fonctions d'onde de l'oscillateur harmonique avec la valeur b_0 obtenue par Brink et Boeker pour la force choisie. Pour l'interaction G-O, nous avons remplacé les densités locales et non locales de la particule alpha par des densités d'oscillateur et choisi la valeur de b_0 qui reproduit au mieux la densité Hartree-Fock de Campi pour la particule alpha avec la même interaction G-O.

Les potentiels α-nucléon peuvent alors s'écrire très généralement :

$$V_{\alpha n}(\bar{r},\bar{r}') = U_L(r)\,\delta(\bar{r}-\bar{r}') + U_{NL}(R,s) \qquad (I.4)$$

où :

$$U_L(r) = \begin{cases} \displaystyle\sum_{i=1}^{2} U_i\, e^{-r^2/\lambda_i^2} & \text{pour } B_1 \\ \displaystyle\sum_{i=1}^{5} U_i\, e^{-r^2/\lambda_i^2} + \sum_{i=1}^{5} U_{i\rho}\, e^{-r^2/\lambda_{i\rho}^2} + U^E(r) & \text{pour G-O} \end{cases} \qquad (I.5)$$

$$U_{NL}(R,s) = \begin{cases} e^{-R^2/b_0^2}\left(\displaystyle\sum_{i=i}^{2} U_{Ni}\; e^{-s^2/\beta_i^2}\right) & \text{pour } B_1 \\ e^{-R^2/b_0^2}\left(\displaystyle\sum_{i=1}^{5} U_{Ni}\; e^{-s^2/\beta_i^2}\right) + e^{-\frac{7}{6}\frac{R^2}{b_0^2}}\left(\displaystyle\sum_{i=1}^{5} U_{Ni\rho}\, e^{-s^2/\beta_{i\rho}^2}\right) & \text{pour G-} \end{cases} \qquad (I.6)$$

avec $\bar{R} = \frac{\bar{r}+\bar{r}'}{2}$; $\bar{s} = \bar{r}-\bar{r}'$ (I.7)

Les coefficients U, U_N et les portées λ, β dépendent analytiquement du paramètre b_0 de l'oscillateur harmonique pour la particule alpha et des paramètres de l'interaction nucléon-nucléon, les termes provenant de la partie dépendant de la densité de la force G-O étant étiquetés par le symbole ρ.

Dans l'équation (I.4), le potentiel U_L représente soit le terme direct pour la force B_1, soit la somme du terme direct, des termes de réarrangement et de la contribution U^E apportée par le terme de portée nulle dans l'équation (I.3) pour la force G-O tandis que le potentiel U_{NL} représente le terme d'échange habituel. Ce terme a été exprimé en fonction des coordonnnées R et s, eq.(I.7), qui sont particulièrement intéressantes à introduire pour l'étude du potentiel non local car elles permettent d'étudier directement la non localité du potentiel mesurée par sa variation en s alors que sa variation en R mesure sa portée.

Nous avons ensuite calculé le potentiel local équivalent au potentiel non local, eq.(I.4). A l'approximation de Perey-Saxon [PE64], ce potentiel local est donné par :

$$V_L(r) = U_L(r) + U_{LE}(r) \tag{I.8}$$

où :
$$U_{LE}(r) = \int e^{i\bar{k}.\bar{s}} \; U_{NL}(R,s) \; d\bar{s} \tag{I.9}$$

et :
$$k^2 = \frac{2\mu}{\hbar^2} (E - V_L(r)) \tag{I.10}$$

μ étant la masse réduite du système α-nucléon et E désignant l'énergie dans le centre de masse. La résolution par itération des équations (I.8-10) conduit à un potentiel local équivalent dépendant de l'énergie. Nous avons montré dans les Refs.[LA78, LA80] que cette dépendance en énergie est linéaire. D'autre part, à l'énergie E = 0MeV, le potentiel α-nucléon peut-être représenté par une gaussienne dans le cas des forces de Brink et Boeker. Nous avons donc écrit :

$$V_{\alpha n}(r,E_\alpha) = -U_0 \; e^{-r^2/a^2} \; (1-\gamma(r)E_\alpha) \tag{I.11}$$

où E_α représente l'énergie de la particule alpha incidente dans le laboratoire, la dépendance linéaire du potentiel α-nucléon étant caractérisée par le fac-

teur γ dépendant de la distance, et où les coefficients U_0 et a ont été ajustés sur ce potentiel calculé à l'énergie E_α = 0 MeV.

Cependant, une telle approche du potentiel α-nucléon non local par un potentiel local n'est pas très justifiée pour le potentiel α-nucléon dont le paramètre de non localité est du même ordre de grandeur que la portée [PE80]. Il est donc préférable de conserver l'interaction α-nucléon non locale pour calculer le potentiel optique α-noyau. Dans la suite de ce travail, nous utilisons effectivement l'interaction α-nucléon non locale pour obtenir la partie réelle de ce potentiel. Par contre, la dérivation du potentiel imaginaire devient très compliquée pour une interaction non locale. Etant donné l'absence de calculs théoriques de ce potentiel imaginaire, nous étions en premier lieu intéressés par ses propriétés moyennes et cherchions à comprendre les propriétés et le comportement des potentiels phénoménologiques. Nous nous sommes alors limités au cas le plus simple, où le potentiel α-nucléon est local et donné par l'équation (I.11).

REFERENCES

[BR67] D.M Brink and E. Boeker, Nucl. Phys. A91(1967) 1.

[BR70] I. Brissaud and B. Tatischeff, Nucl. Phys. A155(1970) 89.

[CA72] X. Campi and D.W.L. Sprung, Nucl. Phys. A194(1972) 401.

[GL66] N.K. Glendenning and M. Vénéroni, Phys. Rev. 144(1966) 839.

[LA78] M. Lassaut, Thèse de Troisième cycle, Université Paris VII,1978.

[LA80] M. Lassaut and N. Vinh Mau, Nucl. Phys. A349(1980) 372.

[NE70] J.W. Negele, Phys. Rev. C1(1970) 1260.

[PE64] F. Perey and D.S. Saxon, Phys. Lett. 10(1964) 107.

[PE80] R.E. Peierls and N. Vinh Mau, Nucl. Phys. A343(1980) 1.

[SC70] R. Schaeffer, Nucl. Phys. A158(1970) 321.

[SP71] D.W.L. Sprung and P.K. Banerjee, Nucl. Phys. A168(1971) 273.

CHAPITRE II

POTENTIEL OPTIQUE α-NOYAU

Connaissant l'interaction α-nucléon, nous dérivons le potentiel α-noyau en utilisant les mêmes techniques que pour la dérivation du potentiel nucléon-noyau à partir de l'interaction nucléon-nucléon. Dans un tel modèle, nous supposons que la particule alpha n'est pas modifiée au cours de la diffusion et qu'elle se comporte comme une particule élémentaire, donc est discernable des nucléons de la cible. A ce stade du calcul, nous ne devons pas tenir compte de l'antisymétrisation entre la particule incidente et le noyau cible. Toutefois, les effets d'échange entre un nucléon de la cible et un nucléon de la particule alpha sont inclus dans le potentiel α-nucléon du chapitre précédent. L'expression du potentiel optique α-noyau est alors donnée par la formule de Feshbach :

$$V_{\alpha N} = V^{(0)} + \Delta V \qquad \text{(II.1)}$$

$$= \langle\psi_0|\sum_{i=1}^{A} V_{\alpha n}(i)|\psi_0\rangle + \sum_{m\neq 0} \lim_{\varepsilon\to 0^+} \oint_a \frac{\langle\psi_0|\sum_{i=1}^{A} V_{\alpha n}(i)|\varphi_a\psi_m\rangle\langle\varphi_a\psi_m|\sum_{j=1}^{A} V_{\alpha n}(j)|\psi_0\rangle}{E-\varepsilon_a-E_m+i\varepsilon} \qquad \text{(II.2)}$$

où nous avons supposé que, dans son état intermédiaire, le système α-noyau est constitué de la particule alpha dans l'état a et du noyau cible dans l'état excité m. Dans l'équation (II.2), ψ_0 désigne la fonction d'onde de l'état fondamental du noyau cible, ψ_m et E_m la fonction d'onde et l'énergie du noyau cible dans l'état excité m, φ_a et ε_a la fonction d'onde et l'énergie de la particule alpha incidente dans l'état intermédiaire a, $V_{\alpha n}(i)$ est l'interaction entre

la particule alpha et le nucléon i dans le noyau, A désigne le nombre de nucléons du noyau et E l'énergie de la particule alpha incidente dans le système du centre de masse α-noyau.

Le potentiel α-nucléon calculé au chapitre I est réel, ce qui est en accord avec les analyses phénoménologiques de la diffusion α-nucléon à basse énergie. Par conséquent, le potentiel $V^{(0)}$, donné par le premier membre de l'équation (II.2), est réel et de plus non local puisque calculé dans le modèle de convolution à partir de l'interaction α-nucléon non locale. Le potentiel ΔV, donné par le second membre de l'équation (II.2), est dû aux processus en deux étapes donc non local quelle que soit l'interaction α-nucléon locale ou non locale. Sa partie réelle apporte une correction au potentiel du modèle de convolution tandis que sa partie imaginaire engendre le potentiel absorptif.

Etant non local, le potentiel α-noyau ne peut pas être comparé directement aux potentiels phénoménologiques déduits des analyses de diffusion, tous connus comme des potentiels locaux. Nous avons alors remplacé notre potentiel non local par un potentiel local équivalent, défini par l'équation (I.9). Le moment local k est ici celui de la particule alpha dans le champ du potentiel local α-noyau. Généralement, la partie imaginaire du potentiel est négligée dans la définition de ce moment local, qui est alors supposé réel. Ainsi, nos premiers travaux publiés portant sur l'étude de la partie réelle du potentiel α-noyau à l'approximation de convolution, la dérivation du potentiel absorptif α-^{40}Ca à basse énergie et l'analyse de la diffusion élastique (α,α) et de la réaction transfert (^{3}He,α) effectuée à partir de notre potentiel α-noyau calculé supposaient ce moment local réel. Ces premiers calculs montrent qu'effectivement le potentiel imaginaire est très faible à basse énergie, mais par contre nettement plus profond à haute énergie et dans ce cas l'approximation consistant à négliger le potentiel absorptif dans la définition du moment local n'est plus cohérente avec le résultat obtenu et doit être reconsidérée. Dans le même ordre d'idée, deux articles récents de Fantoni et al.[FA82] d'une part et Negele et al.[NE82]

d'autre part ont montré, pour le potentiel d'un nucléon dans la matière nucléaire, que l'approximation du moment local par sa partie réelle introduit des erreurs notables dans la détermination du potentiel absorptif. Nous avons alors repris entièrement le calcul du potentiel imaginaire à haute énergie à partir du moment local défini correctement pour le potentiel α-noyau complexe et étudié, formellement puis numériquement, les modifications apportées à notre premier calcul approché de la partie réelle et de la partie imaginaire du potentiel α-noyau.

Pour plus de cohérence dans la présentation de nos résultats, nous exposerons nos travaux dans un ordre différent de l'ordre chronologique. Notre travail est présenté en trois parties. En introduction aux trois articles regroupés dans ce chapitre, nous présentons, dans un cadre très général, la dérivation du potentiel local équivalent à un potentiel optique non local donné et examinons les effets sur la partie réelle et la partie imaginaire résultant de ce que le moment local a une composante imaginaire. Nous montrons ainsi que tenir compte de la partie imaginaire du moment local modifie peu la partie réelle du potentiel α-noyau, mais par contre modifie à la fois la profondeur et la forme de sa partie imaginaire.

La seconde partie de ce chapitre est constituée par notre article publié à Nuclear Physics, portant sur la partie réelle du potentiel à l'approximation de convolution. Précédant l'article, un court résumé retracera les points les plus importants et les plus originaux de ce travail.

Enfin la troisième partie du chapitre est consacrée à l'étude détaillée du potentiel imaginaire et simultanément aux corrections au potentiel réel calculé dans le modèle de convolution. Cette étude a fait l'objet de deux articles publiés à Physics Letters et Nuclear Physics qui sont présentés ici, précédés par quelques compléments sur notre calcul à basse énergie.

A Approximation locale du potentiel optique non local

Les potentiels optiques que nous calculons sont complexes,non locaux et dépendent de l'énergie. Le calcul des sections efficaces nécessite alors la résolution de l'équation de Schrödinger pour une particule soumise à un potentiel effectif non local,qui est une équation intégrodifférentielle. Une telle équation est moins aisée à résoudre que l'équation de Schrödinger pour un potentiel effectif local et,si nous voulons éviter cette difficulté,nous devons dériver un potentiel local équivalent au potentiel optique non local,qui de plus pourra être directement comparé aux potentiels phénoménologiques.

L'approximation couramment utilisée dans la littérature pour obtenir ce potentiel local équivalent est l'approximation de Perey-Saxon [PE64] à l'ordre le plus bas qui, dans le cas particulier des potentiels gaussiens, est identique à celle proposée par Perey et Buck [PE62]. Une telle approximation suppose que les termes d'ordre supérieur du développement de Perey-Saxon sont négligeables, ce qui a été vérifié par Fiedeldey [FI66] dans le cas particulier du potentiel n-^{40}Ca. Une étude,effectuée depuis par Peierls et Vinh Mau pour le problème à une dimension [PE80],a montré que ce potentiel local est également le premier terme d'un développement cohérent du potentiel non local en puissances de β/a (où β désigne la non localité du potentiel et a sa portée) et la validité de l'approximation qui consiste à n'en conserver que le premier terme repose alors sur l'hypothèse que la non localité du potentiel est faible comparée à sa portée. Entrent dans cette catégorie de potentiels non locaux,les potentiels nucléon-noyau ou α-noyau pour lesquels le noyau considéré a un nombre de masse A suffisamment élevé. En effet, alors que la non localité des potentiels optiques est en général de l'ordre de 1fm, la portée du potentiel, approximativement donnée par le rayon du noyau considéré, est d'autant plus élevée que A est grand.

Cette approximation à l'ordre le plus bas est par conséquent justifiée pour notre potentiel α-noyau que nous étudions principalement pour les noyaux $A \gtrsim 40$. Le potentiel local est alors simplement défini comme la transformée de Fourier du potentiel non local pour le moment local de la particule incidente dans le champ du potentiel local lui-même. Habituellement, ce moment local est supposé réel et défini à partir du seul potentiel réel. Toutefois, deux articles récents [FA82, NE82] ont montré, pour le potentiel d'un nucléon dans la matière nucléaire, que cette hypothèse est trop restrictive. Dans cette section, nous étudions l'implication d'une telle hypothèse dans le cas des noyaux finis, en reprenant la dérivation du potentiel local équivalent au potentiel optique non local pour le moment local défini correctement à partir du potentiel total.

Nous partons de l'expression la plus générale du potentiel optique non local :

$$V_N(\bar{r},\bar{r}') = U_N(R,s) + iW_N(R,s) \tag{II.3}$$

où : $$\bar{R} = \frac{\bar{r}+\bar{r}'}{2} \quad , \quad \bar{s} = \bar{r} - \bar{r}' \tag{II.4}$$

Nous supposerons que les potentiels non locaux réel U_N et imaginaire W_N ne dépendent pas de l'angle entre les vecteurs $\bar{R}$ et $\bar{s}$, ce qui est en général supposé dans les analyses phénoménologiques et bien vérifié théoriquement [VM76]. A l'ordre le plus bas du développement de Perey-Saxon, le potentiel local équivalent au potentiel V_N, eq.(II.3), s'écrit :

$$V(r) = U(r) + iW(r) \tag{II.5}$$

$$= \int e^{i\bar{k}.\bar{s}} \left[U_N(R,s) + iW_N(R,s) \right] d\bar{s} \tag{II.6}$$

ou, après intégration sur les variables angulaires :

$$V(r) = 4\pi \int_0^{+\infty} j_0(ks)[U_N(R,s) + iW_N(R,s)]\, s^2 ds \qquad (II.7)$$

Frahn [FR65] a montré que le meilleur choix de moment local est donné par l'expression :

$$k^2 = \frac{2\mu}{\hbar^2}(E - V) \qquad (II.8)$$

où V est le potentiel local, eq.(II.7), μ la masse réduite du système considéré et E l'énergie de la particule incidente dans le système du centre de masse. Notons que cette expression de k^2, eq.(II.8), découle naturellement du développement WKB du potentiel non local dans le problème à une dimension [PE80]. Habituellement, le potentiel W est supposé négligeable devant E - U, ce qui équivaut à approcher le moment k^2 par sa partie réelle :

$$k^2 \simeq \frac{2\mu}{\hbar^2}(E - U)$$

Cette approximation conduit à un potentiel approché dont la partie réelle et la partie imaginaire, désignées respectivement par U_0 et W_0, sont solutions de deux équations indépendantes obtenues en identifiant la partie réelle et la partie imaginaire de l'équation (II.7) :

$$U_0 = 4\pi \int_0^{+\infty} j_0(k_0 s) U_N(R,s)\, s^2 ds \qquad (II.9)$$

$$W_0 = 4\pi \int_0^{+\infty} j_0(k_0 s)\, W_N(R,s)\, s^2 ds \qquad (II.10)$$

où : $$k_0^2 = \frac{2\mu}{\hbar^2}(E - U_0) \qquad (II.11)$$

La première de ces équations, couplée à l'équation (II.11), permet d'obtenir le potentiel U_0 par itération. Le moment k_0 correspondant étant alors connu, W_0 peut être aisément calculé à partir de la seconde équation Si par contre nous ne supposons plus W négligeable devant E-U, alors le moment local k a une partie imaginaire. Nous écrivons alors :

$$k = k_r + ik_i \tag{II.12}$$

et d'après la définition de k^2 , eq.(II.8) , k_r et k_i sont respectivement donnés par le système d'équations :

$$\begin{cases} k_r^2 - k_i^2 = \frac{2\mu}{\hbar^2}(E - U) \\ 2k_r k_i = -\frac{2\mu}{\hbar^2} W \end{cases} \tag{II.13}$$

qui conduit aux expressions suivantes :

$$k_r^2 = \frac{2\mu}{\hbar^2}\left(\frac{E - U + \sqrt{(E - U)^2 + W^2}}{2}\right) \tag{II.14}$$

$$k_i = -\frac{\mu}{\hbar^2 k_r} \tag{II.15}$$

Si nous négligeons W^2 devant $(E - U)^2$, alors le moment k_r, eq.(II.14), peut s'écrire simplement :

$$k_r = \sqrt{\frac{2\mu}{\hbar^2}(E - U)} \tag{II.16}$$

La fonction de Bessel dans l'équation (II.7) est maintenant une fonction complexe dont l'argument dépend à la fois des potentiels U et W,et les équations déterminant les potentiels U et W deviennent des équations couplées:

$$U = 4\pi \int_0^{+\infty} s^2 ds \left(U_N(R,s)\,\mathrm{Re}(j_0(ks)) - W_N\,\mathrm{Im}(j_0(ks)) \right) \qquad \text{(II.17)}$$

$$W = 4\pi \int_0^{+\infty} s^2 ds \left(U_N(R,s)\,\mathrm{Im}(j_0(ks)) + W_N\,\mathrm{Re}(j_0(ks)) \right) \qquad \text{(II.18)}$$

Ce système d'équations (II.17-18) peut être résolu par itération à partir des valeurs initiales $U = U_0$, $W = W_0$. Cependant, il est intéressant de pouvoir comparer, du moins qualitativement, les potentiels exacts U et W aux potentiels approchés U_0 et W_0. Pour cela, nous effectuons un développement en série de Taylor du potentiel local V en fonction de la variable k^2, développement déjà utilisé par Fantoni et al. et Negele et al. pour le potentiel d'un nucléon dans la matière nucléaire. Le potentiel local, solution de l'équation (II.7), est une fonction de deux variables k^2 et r que nous supposerons indépendantes. Nous désignerons ce potentiel par $V(k^2,r)$. Lorsque $k^2 = k_0^2$, où k_0^2 est défini par l'équation (II.11), le potentiel correspondant $V(k_0^2,r)$ est alors le potentiel $U_0 + iW_0$, solution des équations (II.9-11). Si nous supposons que le potentiel V varie lentement en fonction de k^2 autour de la valeur $k^2 = k_0^2$, nous pouvons développer $V(k^2,r)$ autour de k_0^2 en ne retenant que les termes d'ordre un :

$$V(k^2,r) \simeq V(k_0^2,r) + (k^2-k_0^2) \left.\frac{\partial V}{\partial k^2}(k^2,r)\right|_{k^2=k_0^2} \qquad \text{(II.19)}$$

Reprenant la définition des différents termes de l'équation (II.19) en fonction des potentiels U, W et U_0, W_0, nous obtenons :

$$U + iW = U_0 + iW_0 + \frac{2\mu}{\hbar^2}(U_0-U-iW)\left.\left(\frac{\partial U}{\partial k^2} + i\frac{\partial W}{\partial k^2}\right)\right|_{k^2=k_0^2} \qquad \text{(II.20)}$$

Par définition, les potentiels U, eqs(II.5-6), et U_0, eq.(II.9), ont la même expression formelle en fonction des variables k^2 et k_0^2 respectivement donc la dérivée $\partial U/\partial k^2$, prise au point $k^2 = k_0^2$, n'est autre que $\partial U_0/\partial k_0^2$. De même, nous avons

$\left.\frac{\partial W}{\partial k^2}\right|_{k^2=k_0^2} = \frac{\partial W_0}{\partial k_0^2}$. L'équation (II.20) peut alors être écrite,en séparant partie réelle et partie imaginaire :

$$U = U_0 + \frac{2\mu}{\hbar^2}\left((U_0-U)\frac{\partial U_0}{\partial k_0^2} + W\frac{\partial W_0}{\partial k_0^2}\right) \qquad (II.21)$$

$$W = W_0 + \frac{2\mu}{\hbar^2}\left((U_0-U)\frac{\partial W_0}{\partial k_0^2} - W\frac{\partial U_0}{\partial k_0^2}\right) \qquad (II.22)$$

La première équation (II.21) nous permet d'obtenir $U-U_0$:

$$U-U_0 = \frac{\frac{2\mu}{\hbar^2} W \frac{\partial W_0}{\partial k_0^2}}{1+\frac{2\mu}{\hbar^2}\frac{\partial U_0}{\partial k_0^2}} \qquad (II.23)$$

$$= \frac{2\mu_K}{\hbar^2} W \frac{\partial W_0}{\partial k_0^2} \qquad (II.24)$$

où la masse effective μ_K est définie par :

$$\frac{\mu_K}{\mu} = \frac{1}{1+\frac{2\mu}{\hbar^2}\frac{\partial U_0}{\partial k_0^2}} \qquad (II.25)$$

Remplaçant alors,dans l'équation (II.22),$U-U_0$ par son expression donnée dans l'équation (II.23), nous obtenons :

$$W = \frac{\mu_K}{\mu}\left(1+\left(\frac{2\mu_K}{\hbar^2}\frac{\partial W_0}{\partial k_0^2}\right)^2\right)^{-1} W_0 \qquad (II.26)$$

Si l'on néglige alors le terme $\frac{2\mu_K}{\hbar^2}\frac{\partial W_0}{\partial k_0^2}$ dans les deux équations (II.24-26), nous retrouvons des résultats semblables à ceux obtenus par Fantoni et al. et Negele et al. pour le potentiel d'un nucléon dans la matière nucléaire mais avec un terme de masse effective qui,dans le cas des noyaux finis,dépend de

la distance :

$$U(r) \simeq U_0(r) \tag{II.27}$$

$$W(r) \simeq \frac{\mu_K(r)}{\mu} W_0(r) \tag{II.28}$$

La dérivation du potentiel W à partir du potentiel W_0 nécessite alors de connaître la variation de U_0 en fonction du moment k_0^2, donc demande une connaissance explicite de ce potentiel en fonction de k_0^2 . En pratique, le potentiel U_0 est calculé pour chaque énergie E. Comme le potentiel non local U_N est dominé par le potentiel de Hartree-Fock indépendant de l'énergie (sous réserve que l'interaction nucléon-nucléon ne dépende pas de l'énergie), la dérivée $\partial U_0/\partial k_0^2$ peut être transformée aisément en dérivée par rapport à l'énergie et l'on peut écrire la relation (II.28) comme :

$$W(r) = \frac{\mu^\star(r)}{\mu} W_0(r) \tag{II.29}$$

avec :
$$\frac{\mu^\star(r)}{\mu} = 1 - \frac{\partial U_0(E,r)}{\partial E} = \frac{\mu_K(r)}{\mu} \tag{II.30}$$

Ce facteur $\frac{\mu^\star}{\mu}$, eq.(II.30), traduit l'influence de la non localité du potentiel réel sur la détermination du potentiel absorptif. Dans le calcul du potentiel n-^{208}Pb effectué par V. Bernard et N.V Giai [BE79] avec l'interaction nucléon-nucléon de Skyrme, le facteur $\frac{\mu^\star}{\mu}$ apparaît naturellement et exactement et provient de la dépendance en moment du potentiel de Hartree-Fock correspondant.

Pour conclure, notre étude montre que, si la dépendance en moment du potentiel imaginaire est faible ($\partial W_0/\partial k_0^2 \ll 1$), le potentiel U_0 est une bonne approximation de la partie réelle du potentiel optique mais par contre

le potentiel W est différent du potentiel W_0. Dans le premier article présenté dans ce chapitre,consacré à la partie réelle du potentiel α-noyau,seul le potentiel U_0 a été calculé mais les résultats obtenus ne seraient pas modifiés par la résolution du système d'équations couplées (II.17-18). Par contre,nous devons reprendre notre étude du potentiel imaginaire α-^{40}Ca à basse énergie, qui fait l'objet du deuxième article présenté ici, où seul le potentiel W_0 a été calculé. Dans le troisième article présenté,qui est consacré à la partie imaginaire du potentiel α-noyau à plus haute énergie, W et W_0 sont calculés simultanément.

B Etude de la partie réelle du potentiel α-noyau à l'approximation de convolution

La partie réelle du potentiel optique α-noyau est dominée par le premier terme de l'équation (II.2). En effet,comme nous le verrons dans la suite de notre exposé,la correction due au second terme est très faible. Le premier article que nous présentons maintenant est ainsi consacré au calcul du premier terme de l'équation (II.2), c'est-à-dire au calcul du potentiel à l'approximation de convolution à partir de l'interaction α-nucléon calculée [LA78, LA80] comme nous l'avons exposé précédemment. Cette interaction est non locale. Les travaux précédents consacrés à la partie réelle du potentiel α-noyau utilisaient une interaction locale,soit phénoménologique,soit déduite à l'approximation de Perey-Saxon de l'interaction α-nucléon non locale, eq.(I.1). Toutefois, le fait de remplacer l'interaction α-nucléon non locale par une interaction locale peut être critiqué pour deux raisons : d'une part,l'approximation de Perey-Saxon n'est pas appropriée pour le potentiel α-nucléon dont la non localité est voisine de la portée [PE80] ; d'autre part, l'équivalence entre potentiel non local et potentiel local pour le problème de la diffusion α-nucléon n'implique pas nécessairement leur équivalence pour le problème de la diffusion α-noyau. Il nous a semblé alors préférable d'utiliser directement

l'interaction α-nucléon non locale. Le potentiel α-noyau ainsi obtenu est non local [JA74] et nous avons ensuite calculé son approximation locale par la méthode de Perey-Saxon qui, pour le problème α-noyau, est mieux appropriée que pour le problème α-nucléon [VM78]. Ceci explique les différences entre les potentiels α-noyau calculés avec des potentiels α-nucléon locaux on non locaux. En effet, nous verrons que l'utilisation de l'interaction α-nucléon sous sa forme non locale conduit à un potentiel α-noyau moins profond et plus proche de la phénoménologie et en outre est indispensable pour reproduire la dépendance en A de ce potentiel.

Nous calculons le potentiel α-noyau pour différentes interactions nucléon-nucléon : l'interaction B_1 de Brink et Boeker, indépendante de la densité, et les interactions G-O de Banerjee-Campi-Sprung et JLM de Jeukenne-Lejeune-Mahaux, dépendant de la densité. La dépendance en densité de l'interaction effective, essentielle pour que le modèle Hartree-Fock reproduise bien les propriétés des états liés, doit être traitée avec soin. Un calcul direct du potentiel α-noyau, effectué à partir de l'interaction α-nucléon calculée dans le chapitre précédent pour la force G-O, conduit à un potentiel trop profond comparé à la phénoménologie. En effet, la densité locale, présente dans l'interaction nucléon-nucléon, doit être définie pour deux nucléons en interaction dont l'un est dans la particule alpha et l'autre dans le noyau. Habituellement, cette densité locale est définie comme la somme des densités non perturbées du nucléon 1 dans l'alpha et du nucléon 2 dans le noyau. Toutefois, une telle définition conduit à des densités très élevées au centre pour lesquelles les interactions effectives n'ont pas été déterminées. Nous avons voulu éviter ces problèmes au centre et proposé une définition, suggérée par le modèle de convolution et les calculs Hartree-Fock pour nucléon-noyau, telle que la densité correspondante n'excède jamais la densité nucléaire et permette en outre une évaluation aisée du potentiel non local. Nous verrons que notre choix adopté dans la définition

de la densité locale, qui tient compte de la contribution en densité du noyau cible, augmente les effets de saturation du potentiel α-noyau à petites distances qui devient alors plus proche de la phénoménologie et permet en outre de mieux reproduire la dépendance en A de ce potentiel.

Pour conclure, notre étude a mis en évidence deux effets importants.Le premier est dû à la forte non localité de l'interaction α-nucléon. Le second provient de la dépendance en densité du noyau de l'interaction nucléon-nucléon effective. Ces deux effets sont en particulier indispensables pour reproduire la dépendance en A du potentiel α-noyau. Une analyse de la diffusion élastique $^{40}Ca(\alpha,\alpha)^{40}Ca$ à 104 MeV semble confirmer que les interactions nucléon-nucléon dépendant de la densité permettent une meilleure description des résultats expérimentaux.

Nuclear Physics **A355** (1981) 141–170; © *North-Holland Publishing Co., Amsterdam*
Not to be reproduced by photoprint or microfilm without written permission from the publisher

ANTISYMMETRIZATION AND DENSITY-DEPENDENT EFFECTS WITHIN THE FOLDING MODEL APPROACH TO α-NUCLEUS SCATTERING

F. DUGGAN †, M. LASSAUT, F. MICHEL †† and N. VINH MAU

Division de Physique Théorique †††, *Institut de Physique Nucléaire, F-91406 Orsay Cedex, France*

Received 9 June 1980

Abstract: The real α-nucleus interaction is investigated within the framework of the folding model. First the non-local α-nucleon interaction is calculated in the Hartree-Fock approximation and then folded in with the target matter density. The resulting α-nucleus potential is non-local but a local equivalent potential is obtained within the Perey-Saxon approximation. The calculations are performed both with density-independent and density-dependent forces. The rearrangement terms, arising from the density dependence of the force, which are usually neglected, are calculated and found to be significant at small distances. The local density appearing in the density-dependent part of the force is evaluated using a prescription which avoids explicit contradiction of the Pauli principle, in contrast to many earlier calculations where it is calculated as the sum of the densities of the colliding nuclei. However our prescription is expected to underestimate the density-dependent effects. The calculated potentials are used to fit elastic α-particle scattering from ^{40}Ca at 104 MeV incident energy. Good agreement with experimental data is obtained after renormalizing the theoretical potentials by a factor ranging from 0.6 to 0.9. Finally the E- and A-dependences of the volume integral per nucleon pair of the calculated potentials are investigated and found to be in good qualitative agreement with the available phenomenological results.

1. Introduction

Our knowledge of the phenomenological α-nucleus optical potential has been much improved [1]) during the last few years. Detailed analyses of elastic scattering data over a broad range of incident energies and scattering angles have reduced the ambiguities in the determination of the real part of the optical potential. The dependence of the real potential on the incident α-particle energy and, in some measure, its variation with the mass number of the target are much better known now. Therefore it is worth investigating the real α-nucleus interaction from microscopic considerations.

In this paper, we propose some improvements to the calculation of the real part of the α-nucleus potential within the framework of the folding model [2–4]) and we

† Present address: Nuclear Power Section, Dept. of Mechanical Engineering, Imperical College, Exhibition Road, London SW7 2AZ, UK.
†† Permanent address: Faculté des Sciences, Université de l'Etat, B-7000 MONS, Belgium.
††† Laboratoire associé au CNRS.

discuss their consequences against the experimental data. In our approach, it is assumed that the real part of the α-nucleus optical potential $V_{\alpha N}$ may be calculated by folding an effective α-nucleon interaction into the target matter density, i.e.:

$$V_{\alpha N} = \langle \varphi_T | \sum_{n=1}^{A} V_{\alpha n} | \varphi_T \rangle, \tag{1}$$

where φ_T and A denote respectively the ground state wave function and mass number of the target, and $V_{\alpha n}$ is the effective interaction between the incident α-particle and a target nucleon. Eq. (1) may be considered as the first-order term of the expansion of the real part of the optical in powers of $V_{\alpha n}$. The next term, involving intermediate excitations of the target nucleus, has been evaluated recently [5]) and found to be small. Therefore eq. (1) should provide a good approximation to the real α-nucleus potential.

In this simple folding-model approach, the calculation of $V_{\alpha N}$ requires the knowledge of the effective α-nucleon interaction $V_{\alpha n}$. Studies published so far can be classified into two groups according to the way $V_{\alpha n}$ is treated in the calculation:

(i) A direct calculation of the effective α-nucleon potential is avoided by using a phenomenological interaction derived from an analysis of scattering data. Most of the time, $V_{\alpha n}$ is taken as a local potential fitted to low-energy n-α scattering [6,7]). In this case the many-body effects of the nucleon-α system such as exchange effects are simulated only in the parametrization of $V_{\alpha n}$. The corresponding α-nucleus potential $V_{\alpha N}$ of eq. (1) is then renormalized by an energy-dependent constant fitted to the α-nucleus data. Alternatively, the parameters of $V_{\alpha n}$ can be fitted so that the α-nucleus potential of eq. (1) reproduces at best the experimental α-nucleus cross sections [8,9]). This fitted α-nucleon potential thus implicitly simulates the many-body effects contributing to the α-nucleus potential, such as exchange effects and higher-order terms which are neglected in eq. (1).

(ii) $V_{\alpha n}$ is calculated from the n-n interaction within the Hartree-Fock approximation [10]) or within the antisymmetrized folding model [2-4]). In the Hartree-Fock approximation the α-n interaction is

$$\begin{aligned} V_{\alpha n}(\boldsymbol{r}, \boldsymbol{r}'; \rho) = {} & \delta(\boldsymbol{r}-\boldsymbol{r}') \int \rho_\alpha(\boldsymbol{r}_1) V_{nn}(\boldsymbol{r}-\boldsymbol{r}_1; \rho) \mathrm{d}\boldsymbol{r}_1 - \rho_\alpha(\boldsymbol{r}, \boldsymbol{r}') V_{nn}(\boldsymbol{r}-\boldsymbol{r}'; \rho) \\ & + \tfrac{1}{2} \rho_\alpha(\boldsymbol{r})^{\frac{1}{3}} \delta(\boldsymbol{r}-\boldsymbol{r}') \int \rho_\alpha(\boldsymbol{r}_1)^{\frac{1}{3}} \frac{\partial V_{nn}(\boldsymbol{r}-\boldsymbol{r}_1; \rho)}{\partial \rho} \mathrm{d}\boldsymbol{r}_1 \\ & - \tfrac{1}{2} \rho_\alpha(\boldsymbol{r})^{-\frac{1}{3}} \delta(\boldsymbol{r}-\boldsymbol{r}') \int |\rho_\alpha(\boldsymbol{r}, \boldsymbol{r}_1)|^2 \rho_\alpha(\boldsymbol{r}_1)^{\frac{1}{3}} \frac{\partial V_{nn}(\boldsymbol{r}-\boldsymbol{r}_1; \rho)}{\partial \rho} \mathrm{d}\boldsymbol{r}_1, \end{aligned}$$

where $\rho_\alpha(\boldsymbol{r})$ and $\rho_\alpha(\boldsymbol{r}, \boldsymbol{r}')$ denote respectively the local and non-local Hartree-Fock α-particle densities and V_{nn} is the effective n-n interaction. The first and second

terms are respectively the local direct and non-local exchange terms. If V_{nn} is density dependent, then two further local terms arise: the direct and exchange rearrangement terms, which are respectively the third and fourth terms of eq. (2). In the antisymmetrized folding-model approximation these two terms are absent. Eq. (2) is a first-order approximation but corrections are expected to be negligible when the incident nucleon energy is lower than that of the first inelastic threshold, i.e. 25 MeV or equivalently when the incident α-particle energy is less than 100 MeV in the α-nucleus problem.

In the earliest works, the non-local exchange component of eq. (2) was neglected [11]), leading through eq. (1) to an α-nucleus potential which explicitly neglects all antisymmetrization effects. The α-nucleus scattering data were fitted by renormalizing the calculated potential with a constant which is energy dependent [12]) and simulates, among other effects, that of the exchange term.

More recent studies [5,13,14]) take the exchange term of eq. (2) into account. This term being non-local leads to somewhat complicated calculations when introduced into eq. (1) which also involves the mixed density of the target nucleus. The corresponding α-nucleus potential is itself non-local and a local equivalent potential must be derived [14]). A simpler treatment [5]) of the non-local component of V_{an} consists of first calculating the local equivalent α-nucleon potential and thereafter inserting this local potential into eq. (1) [5,15–17]). This latter method is certainly less reliable [14]) since the approximations used to derive a local equivalent potential are less appropriate when the non-locality range is similar to the range of the potential [18]), which is the case for the α-nucleon potential, while the range of non-locality for the α-nucleus potential is always much smaller [13,14]) than its range. To avoid the difficulties connected with the non-local exchange term, Love and Satchler have recently proposed [19]) a zero-range pseudo-potential simulating single-nucleon exchange in heavy-ion systems.

Most of the recent calculations of the second group have been carried out with effective nucleon-nucleon interactions derived from nuclear structure or nuclear matter calculations. The effective n-n interaction derived for finite nuclei from nuclear matter calculations in the local density approximation is density dependent. This density dependence of the effective n-n interaction is essential for a successful description of nuclear properties within the Hartree-Fock approximation [20–22]). One of the main difficulties encountered in extending the folding-model formalism to density-dependent forces is that of defining the local density in terms of the projectile and target densities. It has been proposed that the local density to be used in the density-dependent part of V_{nn} should be the sum of the densities of the undisturbed projectile and target [4,15,23–26]). This prescription obviously contradicts the Pauli principle, since it amounts to placing additional nucleons into already filled levels. Studies of the effect of antisymmetrization on the density distribution in nucleus-nucleus collisions [27,28]), taking into account the relative motion of the interacting nuclei, indicate that no appreciable compression builds

up in the overlap region, and that taking the sum of densities is only justified for very high incident energies. Moreover, taking a simple superposition of densities results in very high densities at complete overlap, for which currently available effective n-n interactions are not defined. In order to alleviate some of these problems, it has been suggested [16]) that the local density be defined allowing only a fraction of the α-particle density to be added to the target density. This is a phenomenological prescription for avoiding compression of the density in the overlap region.

An other problem that arises with density-dependent forces, that has so far not been investigated, is the calculation of the rearrangement terms. These terms arise from the variation of the density in the effective n-n interaction and contribute strongly to the saturation of the Hartree-Fock potential [20-22]) in the nuclear centre i.e. in the high-density region.

In the present investigation of the real part of the α-nucleus potential, we extend the recent calculations of Vinh Mau [14]) to density-dependent effective n-n interactions and propose a different treatment of the local density when both projectile and target densities are taken into account. In sect. 2, the details of the calculations for both density-independent and density-dependent forces are presented. In sect. 3, the results for the α-^{40}Ca elastic scattering are discussed and the energy and target dependence of the α-nucleus interaction are examined. We present our conclusions in sect. 4.

2. Calculation of the α-nucleus interaction

The α-nucleus optical potential is constructed by first calculating the α-nucleon interaction and then using eq. (1). In subsect. 2.1, details of the calculation are given for the density-independent interaction B1 of Brink and Boeker [29]) and in subsect. 2.2 for the density-dependent G-λ interactions of Sprung and Banerjee [30]) and that of Jeukenne *et al.* [31]) (JLM).

2.1. DENSITY-INDEPENDENT INTERACTION

The effective interaction B1 [29]) is expressed as a superposition of a long-range attractive and a short-range repulsive gaussian. Its parameters were obtained by fitting the binding energy and saturating momentum of nuclear matter and the binding energy and rms radius of ^{4}He. This force leads to qualitative agreement for the binding energies and densities of ^{16}O and ^{40}Ca.

The microscopic α-nucleon potential constructed with this force includes both a local direct potential and a non-local exchange potential [10]). The corresponding α-nucleus potential is calculated directly from eq. (1), leading to the sum of a local direct and non-local exchange components [13,14]):

$$V_{\alpha N}(R, R') = V_{L}(R)\delta(R-R') + V_{NL}(R, R'), \tag{3}$$

where

$$V_{\mathrm{L}}(R) = \sum_{j=1}^{2} V_j \int \rho_{\mathrm{T}}(r) \exp\left(-(\boldsymbol{R}-\boldsymbol{r})^2/\lambda_j^2\right) \mathrm{d}\boldsymbol{r}, \tag{4}$$

$$V_{\mathrm{NL}}(\boldsymbol{X}, \boldsymbol{s}) = a^3 \sum_{j=1}^{2} W_j H_j(as) \int \rho_{\mathrm{T}}(\boldsymbol{X}', b\boldsymbol{s}) \exp\left(-(\boldsymbol{X}-\boldsymbol{X}')^2/b_0^2\right) \mathrm{d}\boldsymbol{X}', \tag{4'}$$

with

$$\boldsymbol{X} = \tfrac{1}{2}(\boldsymbol{R}+\boldsymbol{R}'), \qquad \boldsymbol{s} = \boldsymbol{R}-\boldsymbol{R}', \tag{5}$$

$$a = 5A/(A+4), \qquad b = 4(A-1)/(A+4), \tag{5'}$$

$$H_i(s) = \exp\left(-s^2/\beta_j^2\right). \tag{5''}$$

$\rho_{\mathrm{T}}(\boldsymbol{R}, \boldsymbol{s})$ is the intrinsic mixed density of the target nucleus expressed as a function of c.m. and relative coordinates, and the parameters V_j, W_j, λ_j and β_j of the α-nucleon potential are given explicitly in ref. [10]). The harmonic oscillator parameter of the α-particle $b_0 = 1.40$ fm is taken from the original calculation of Brink and Boeker [29]). The mixed density of the target is calculated with a modified version of the Slater approximation proposed by Campi and Bouyssy [32]):

$$\rho_{\mathrm{T}}(\boldsymbol{R}, \boldsymbol{s}) \simeq \rho_{\mathrm{T}}(R) \hat{j}_1(s k_{\mathrm{A}}(R)), \tag{6}$$

where

$$\hat{j}_1(x) = 3j_1(x)/x, \tag{7}$$

and $k_{\mathrm{A}}(R)$ is given by:

$$k_{\mathrm{A}}(R) = \left(\frac{5}{3\rho_{\mathrm{T}}(R)}\left(\tau(R) - \tfrac{1}{4}\nabla^2 \rho_{\mathrm{T}}(R)\right)\right)^{\frac{1}{2}}, \tag{8}$$

involving the kinetic energy density $\tau(R)$.

The local equivalent potential of V_{NL} of eq. (4') is obtained in the Perey-Saxon approximation [33]) as:

$$V_{\mathrm{LE}}(R) = 4\pi \int_0^{+\infty} j_0(ks) V_{\mathrm{NL}}(R, s) s^2 \mathrm{d}s, \tag{9}$$

where

$$k^2(R) = \frac{2\mu}{\hbar^2}\left(E_{\mathrm{c.m.}} - V_{\mathrm{L}}(R) - V_{\mathrm{LE}}(R)\right), \tag{10}$$

μ being the reduced mass of the system and $E_{\mathrm{c.m.}}$ the c.m. energy of the projectile. V_{LE} is obtained by solving eqs. (9) and (10) by iteration.

2.2. DENSITY-DEPENDENT INTERACTIONS

The density-dependent interactions [30,31]) we consider in this work are derived from n-n potentials fitted to very similar sets of phase shifts. However, the effective interactions are constructed in different ways.

The G-λ interactions [30]) are derived from a nuclear matter calculation using the Reid soft-core potential. They are parametrized as a sum of five gaussians, each having a density-independent and a density-dependent part, the latter appearing as a power of the local Fermi momentum k_F. The forces are classified according to the power λ of k_F and are denoted by G-0, G-1 and G-3 respectively for $\lambda = \frac{1}{2}$, 1 and 3. They also include a zero-range energy-dependent term that takes into account the difference between the energy denominators of the Bethe-Goldstone equation for nuclear matter and finite nuclei. Hartree-Fock calculations [20]), in the local density approximation, have been performed with these three forces. The best results were obtained with the G-0 force.

Jeukenne *et al.* [31]) (JLM) started with the Reid hard-core n-n interaction and calculated the nucleon optical potential in nuclear matter. The optical potential for a nucleon interacting with a finite nucleus is then constructed in the local density approximation. JLM proposed a density- and energy-dependent effective interaction which is parametrized so that the Hartree term alone is able to reproduce the entire nucleon-nucleus optical potential. Therefore this effective interaction should be used in a double folding model calculation without the exchange term. This effective interaction reads:

$$V_{\text{eff}}(|\boldsymbol{r}-\boldsymbol{r}'|;\rho,E) = \frac{1}{(t\sqrt{\pi})^3}\,\mathrm{e}^{-|\boldsymbol{r}-\boldsymbol{r}'|^2/t^2}\sum_{i,j=1}^{3} a_{ij}\rho^{i-1}E^{j-1}, \tag{11}$$

where the gaussian factor of range $t = 1.20$ fm was introduced to correct the local density approximation which systematically yielded too small radii as compared to the phenomenological potentials because of the neglect of surface corrections [31]).

In subsect. 2.2.1 we calculate the α-nucleus optical potential with the G-λ interactions starting from the α-nucleon interaction derived in ref. [34]). Therefore the local density, appearing in the effective n-n interaction does not include the effect of the target density. In subsection 2.2.2 we attempt to include this effect in an approximate way for the G-λ forces with and without rearrangement terms. In subsect. 2.2.3 we calculate the α-nucleus potential with the JLM force.

2.2.1. No target density dependence for the G-λ forces. For density-dependent forces like G-λ, the Hartree-Fock approximation of the α-nucleon potential involves not only local direct and non-local exchange parts but also the local rearrangement terms as given by eq. (2). We use here the potential derived by Lassaut and Vinh Mau [34]) for the G-0 force. The generalization to the other G-λ forces is straightforward and the component parts of $V_{\alpha n}$ are given explicitly in appendix

A.1. These forces have a zero-range term depending on the energy of the two interacting nucleons. The results of ref. [34]) show that the calculated α-n potential does not depend much upon this energy and in the present work, it is taken as twice the nucleon energy inside the α-particle.

The α-nucleus potential denoted by $V^{R}_{\alpha N}$, is constructed from eq. (1) by using the local and non-local parts of this α-nucleon interaction. It is given by

$$V^{R}_{\alpha N}(R, R') = V_{L}(R)\delta(R-R') + V_{NL}(R, R'). \tag{12}$$

The local term $V_{L}(R)$ is given by

$$V_{L}(R) = V_{LI}(R) + V_{LD}(R) + V_{W}(R), \tag{13}$$

where

$$V_{LI}(R) = \sum_{j=1}^{5} U_{j} \int \exp[-(r-R)^2/\lambda_j^{0}]\rho_{T}(r)\mathrm{d}r,$$

$$V_{LD}(R) = \sum_{j=1}^{5} U_{j\rho} \int \exp[-(r-R)^2/\lambda_j'^{2}]\rho_{T}(r)\mathrm{d}r,$$

$$V_{W}(R) = \int U_{W}(R-r)\rho_{T}(r)\mathrm{d}r. \tag{14}$$

V_{LI}, V_{LD} and V_{W} come respectively from the direct density-independent term of $V_{\alpha n}$, U_{LI} [eq. (A.3)], its direct density-dependent term plus its rearrangement terms, U_{LD} [eqs. (A.6)], and from the term U_{W} [eq. (A.11)] arising from the zero-range part of the G-λ forces. The coefficients U_j, $U_{j\rho}$, λ_j, λ_j' are given in appendix A.1 in terms of the parameters of the G-λ forces.

The non-local term V_{NL} of eq. (12) is written as

$$V_{NL}(X, s) = V_{NI}(X, s) + V_{ND}(X, s),$$

$$V_{NI}(X, s) = a^3 \sum_{j=1}^{5} U_{Nj} \exp(-a^2 s^2/\beta_j^2) \int \exp[-(X-X')^2/b_0^2]\rho_{T}(X', bs)\mathrm{d}X',$$

$$V_{ND}(X, s) = a^3 \sum_{j=1}^{5} U'_{Nj} \exp(-a^2 s^2/\beta_j'^{2}) \int \exp[-(X-X')^2(\lambda+3)/3b_0^2]\rho_{T}(X', bs)\mathrm{d}X'. \tag{15}$$

V_{NI} and V_{ND} arise respectively from the density-independent and density-dependent exchange terms of the α-n interaction [U_{NI} of eq. (A.14) and U_{ND} of eq. (A.18)]. The coefficients U_{Nj}, U'_{Nj}, β_j and β'_j are given in appendix A.1 and s, X, a and b are defined by eqs. (5) and (5').

The local potential $V^{R}_{\alpha N}(R)$ is calculated by taking the local equivalent of the non-local potential of eq. (15) in the Perey-Saxon approximation as explained in subsect. 2.1.

2.2.2. Target density dependence for the G-λ forces. In the previous subsection

the α-nucleon and α-nucleus potentials were constructed in two completely independent states: namely, the local density in the effective G-λ interactions was defined for the α-n system disregarding the fact that, in the second step of the calculation of the α-nucleus potential, the nucleon is a target nucleon. Since the contribution to the α-nucleus potential of the density-dependent part of the effective n-n interaction is large, as we shall see later on, it is important to define the local density at points 1 and 2 which are the position coordinates of the interacting nucleons so as to include the effects of both target and projectile densities. There is no unique way to relate the local density to the densities ρ_α and ρ_T of the alpha-particle and the target and therefore only approximate relations can be proposed. Our choice was guided by two considerations. Our calculation relies on the validity of the folding model where the two interacting nuclei are assumed to keep their identity and to stay in their ground state throughout the scattering process. Furthermore we know that in Hartree-Fock calculations of bound states there is some freedom in the choice of the local density and that taking $\rho(1, 2) = \frac{1}{2}(\rho_N(1)+\rho_N(2))$ or $\sqrt{\rho_N(1)\rho_N(2)}$ or $\rho(G)$ (where G is the c.m. of nucleons 1 and 2 and ρ_N the density of the nucleus) leads to very similar results [35]). In the α-n potential calculation of ref. [34]), the second of these prescriptions was used where ρ_N stands for the α-particle density. One can then think of a possible definition of the local density for the α-nucleus potential when nucleon 1 is in the α-particle and nucleon 2 in the target as:

$$\rho(1, 2) = \sqrt{\rho_\alpha(1)\rho_T(2)}, \tag{16}$$

which is a direct extrapolation of our choice of $\rho(1, 2)$ for the α-n system.

It is clear that we are not able to justify this choice more deeply. It is also clear that this suggested relation is very different from the prescription used in similar studies where one assumes [19]) that:

$$\rho(1, 2) \simeq \rho_\alpha(1)+\rho_T(2), \tag{17}$$

or

$$\rho(1, 2) \simeq \rho(G) \simeq \rho_\alpha(G)+\rho_T(G), \tag{17'}$$

where G is the c.m. of nucleons 1 and 2.

This latter choice does not seem very realistic, since it yields, when the two nuclei are strongly overlapping, very high and unphysical densities. Furthermore in this case it implies that the effective n-n interaction involved in the calculation of the α-nucleus potential is taken for very high values of k_F for which it has not been determined. In this sense our prescription of eq. (16) looks more satisfactory because our density $\rho(1, 2)$ never exceeds the normal density. Nevertheless the point of view

presented here can be criticized on many points. Indeed if one goes back to the initial problem of finding an effective interaction for the $\alpha + {}^{40}Ca$ system and calculates it as the potential energy of the total system within the energy-density formalism [36]), the local density $\rho(1, 2)$ in the effective interaction should be related to the antisymmetrized density $\rho_{\mathscr{A}}$ of the whole system. Following references [28, 36]), this density is much weaker than the sum of densities for strong overlap but close to this sum for weak overlap of the α-particle and the target nucleus. Comparing with the densities of eqs. (16) and (17) it is clear that the density of eq. (16) is a better approximation to $\rho_{\mathscr{A}}$ for small distances but that it underestimates $\rho_{\mathscr{A}}$ at large distances.

The rearrangement terms of eq. (2) give a large contribution to the α-n potential [34]) and should therefore be included in our calculation. Again they are related to the density-dependent part of the force and we have in a folding model picture no direct way to introduce them in our calculation. Therefore in a first step we drop these terms as has been done up to now in similar calculations. In a second step they will be included in an approximate way.

The density-independent parts of the α-nucleus potential, V_{LI} of eq. (14) and V_{NI} of eq. (15) remain unchanged. However our local density prescription of eq. (16) modifies the density-dependent parts of both the α-n and α-nucleus potentials. This leads to an effective α-n interaction $V_{\alpha n}^{\mathrm{T}}$ which depends on the internal coordinates of both the α-particle and the target nucleus. The prescription of eq. (16) is not easy to use in the derivation of the non-local part of the potential and we have modified it in order to simplify numerical calculations. To do so eq. (16) has to be symmetrized and we have taken the following relation:

$$\rho(1, 2) \simeq \bar{\rho}(G) = \sqrt{\rho_{\alpha}(G)\rho_{\mathrm{T}}(G)}, \tag{16'}$$

where G is the c.m. of nucleons 1 and 2. By replacing eq. (16) by eq. (16') we certainly weaken the effect of density dependence mainly when the two nuclei have weak overlap. Therefore we should remember in the discussion of our potentials that we certainly underestimate the effects of density-dependent terms while previous calculations [4, 15, 23–26]) most likely overestimate them. In appendix A.2, the explicit form of $V_{\alpha n}^{\mathrm{T}}$ is given. The corresponding α-nucleus potential $V_{\alpha \mathrm{N}}^{\mathrm{T}}$ becomes

$$V_{\alpha \mathrm{N}}^{\mathrm{T}}(\boldsymbol{R}, \boldsymbol{R}') = V'_{\mathrm{L}}(R)\delta(\boldsymbol{R}-\boldsymbol{R}') + V'_{\mathrm{NL}}(\boldsymbol{R}, \boldsymbol{R}'), \tag{18}$$

with

$$V'_{\mathrm{L}}(R) = V_{\mathrm{LI}}(R) + V'_{\mathrm{LD}}(R) + V'_{W}(R), \tag{19}$$

$$V'_{\mathrm{NL}}(\boldsymbol{R}, \boldsymbol{R}') = V_{\mathrm{NI}}(\boldsymbol{R}, \boldsymbol{R}') + V'_{\mathrm{ND}}(\boldsymbol{R}, \boldsymbol{R}'). \tag{20}$$

V_{LI} and V_{NI} are unchanged and given by eqs. (14) and (15). The density-dependent

terms are

$$V'_{\mathrm{LD}}(R) = \sum_{j=1}^{5} U'_{j\rho}\rho_{\mathrm{T}}^{\lambda/12}(R)\int \rho_{\mathrm{T}}(r)^{1+\lambda/12}\exp\left[-(\boldsymbol{R}-\boldsymbol{r})^2/\lambda''^2_j\right]\mathrm{d}\boldsymbol{r},$$

$$V'_{W}(R) = \int \rho_{\mathrm{T}}(r)U'_{W}(\boldsymbol{R}-\boldsymbol{r})\mathrm{d}\boldsymbol{r}, \tag{21}$$

$$V'_{\mathrm{ND}}(\boldsymbol{R},\boldsymbol{R}') = a^3\rho_{\mathrm{T}}^{\lambda/12}(X)\sum_{j=1}^{5} U''_{\mathrm{N}j}\exp\left[-(as)^2/\beta_j^2\right]\int \rho_{\mathrm{T}}(\boldsymbol{X}',b\boldsymbol{s})\rho_{\mathrm{T}}^{\lambda/12}(X')$$

$$\times \exp\left[-(\boldsymbol{X}-\boldsymbol{X}')^2(\lambda+6)/6b_0^2\right]\mathrm{d}\boldsymbol{X}'.$$

V'_{LD}, V'_{ND} are respectively the density-dependent direct and exchange terms and V'_{W} comes from the zero-range part of the G-λ forces. All coefficients of eqs. (21) and the function U'_{W} are given explicitly by eqs. (A.24–A.29) of appendix A.2.

This potential neglects the rearrangement terms of $V_{\alpha\mathrm{n}}$ which are expected to give a sizeable contribution to the α-nucleus potential. In the particular case of the α-nucleon potential they have the same structure as the direct density-dependent term [34]). This is not a general result but a consequence of the gaussian 1s harmonic oscillator α-particle wave function. If we make the approximation that this property still holds in the α-nucleus case, we can calculate the α-nucleus rearrangement terms by replacing the α-particle local density by the local density ρ given by eqs. (16) or (16′). The detailed calculation is performed in appendix A.2 and the corresponding α-nucleus potential $V^{\mathrm{RT}}_{\alpha\mathrm{N}}$ is then given by

$$V^{\mathrm{RT}}_{\alpha\mathrm{N}}(\boldsymbol{R},\boldsymbol{R}') = V''_{\mathrm{L}}(R)\delta(\boldsymbol{R}-\boldsymbol{R}') + V'_{\mathrm{NL}}(\boldsymbol{R},\boldsymbol{R}'). \tag{22}$$

V'_{NL} is the same as before and defined by eq. (20) and V''_{L} is given by eq. (19) where the coefficients $U'_{j\rho}$ and the function U'_{W} are now replaced by $U''_{j\rho}$ and U''_{W} respectively calculated in eqs. (A.34) and (A.35) of appendix A.2.

2.2.3. JLM force. As mentioned earlier in this section the JLM force [31]) is parametrized so that the nucleon-nucleus optical potential is reproduced by the Hartree term only. Therefore we can directly use the local density prescription of eq. (16) and get:

$$V_{\alpha\mathrm{N}}(R) = \sum_{i,j=1}^{3} a_{ij}E^{j-1}\left(\frac{4}{\pi^{\frac{3}{2}}b_0^3}\right)^{(i+1)/2}\left(\frac{2}{i+1}\right)^{\frac{3}{2}}\left(\frac{b_0}{\sigma_i}\right)^3\int \rho_{\mathrm{T}}(r)^{(i+1)/2}$$

$$\times \exp\left(-(\boldsymbol{R}-\boldsymbol{r})^2/\sigma_i^2\right)\mathrm{d}\boldsymbol{r}, \tag{23}$$

where

$$\sigma_i^2 = \frac{2b_0^2}{i+1} + t^2. \tag{24}$$

On the other hand we can calculate the α-nucleus interaction in the same way as

for G-λ forces, namely using prescription (16′) for the local density and the approximations explained in appendix A.2. The α-nucleus potential is now given by:

$$V_{\alpha N}(R) = \sum_{i,j=1}^{3} a_{ij} E^{j-1} \rho_T(R)^{(i-1)/4} \left(\frac{4}{\pi^{\frac{3}{2}} b_0^3}\right)^{(i+1)/2} \left(\frac{4}{i+3}\right)^{\frac{3}{2}} \left(\frac{b_0}{\eta_i}\right)^3 \int \rho_T(r)^{(i+3)/4} \times \exp[-(\boldsymbol{R}-\boldsymbol{r})^2/\sigma_i'^2] \mathrm{d}\boldsymbol{r} \quad (25)$$

with

$$\eta_i^2 = \frac{4b_0^2}{i+3} + t^2, \qquad \sigma_i'^{-2} = \eta_i^{-2} + \frac{i-1}{4b_0^2}. \quad (26)$$

Comparison of potentials calculated from eqs. (23) and (25) (which will be denoted respectively by JLMI and JLMII) will measure the underestimation of density-dependent effects introduced by the use of eq. (16′).

3. Results

In subsect. 3.1, the results for the α-^{40}Ca elastic scattering are examined in detail. Then the target dependence of the α-nucleus interaction is discussed in subsect. 3.2.

All the calculations are performed using the target density distributions deduced by Alkhazov *et al.* [37]) from high-energy (p, p) scattering. These densities include the finite size of the nucleon, which is unfolded to get the point nucleon distribution required in our calculations. This unfolding is performed in an approximate way by modifying the radius of the 3-parameter Fermi distributions of ref. [37]) so that the rms radii of the modified densities differ from the original ones by 0.8 fm [ref. [38])]. The local Fermi momentum k_A defined by eq. (8), which enters into the calculation of the non-local target density, is evaluated approximately using harmonic oscillator densities with an oscillator parameter determined to yield the same rms radii as the unfolded matter densities defined above. On the other hand, for the α-particle the harmonic oscillator density is used throughout. For the B1 interaction, $b_0 = 1.40$ fm is taken from the original calculation of Brink and Boeker [29]) and for the other interactions, we used $b_0 = 1.20$ fm, which reproduces the empirical rms radius of the α-particle [39]).

3.1. α-^{40}Ca SCATTERING

3.1.1. Calculated potentials at 30 MeV c.m. energy. For the G-λ interactions we have considered three cases: (i) The α-nucleus potential $V_{\alpha N}^{R}$ defined in subsect. 2.2.1 where the target contribution to the local density is neglected, but the HF rearrangement terms are included in the α-nucleon potential. (ii) the α-nucleus potential $V_{\alpha N}^{T}$ defined in subsect. 2.2.2 where the target density-dependence is included via eq. (16′), but the rearrangement terms are omitted.

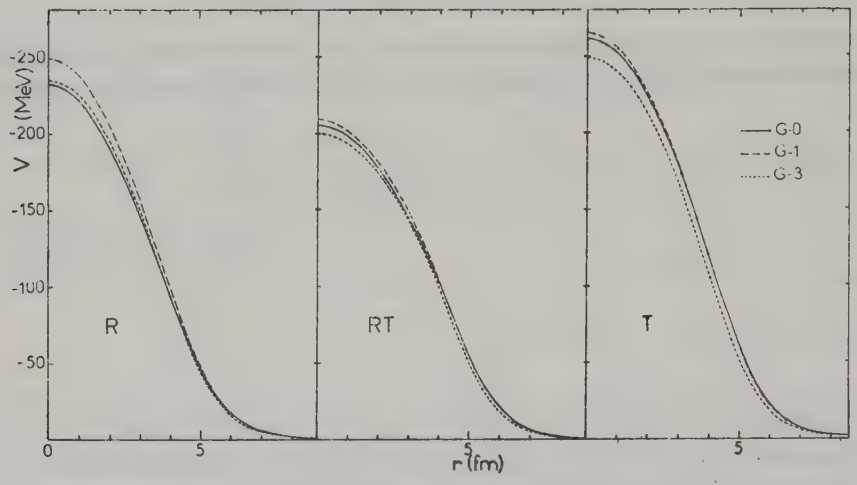

Fig. 1. Potentials calculated for ^{40}Ca(α, α) at 30 MeV c.m. energy with the G-λ forces within approximations R, T and RT (see text).

(iii) The α-nucleus potential $V^{RT}_{\alpha N}$ including both the target contribution to the local density and rearrangement terms as discussed in subsect. 2.2.2.

In fig. 1, we compare the potentials $V^{R}_{\alpha N}$, $V^{T}_{\alpha N}$ and $V^{RT}_{\alpha N}$ calculated at 30 MeV c.m. energy for all the G-λ forces. For each case, all the G-λ forces yield potentials which are very similar in shape and magnitude (G-3 gives potentials that are in general slightly shallower in the tail). Therefore the discussion of the results of calculations performed with the G-λ forces will be restricted to the G-0 case, which was found to be the best in nuclear structure calculations [20].

In fig. 2 are displayed the component parts of the potentials calculated with G-0. All the terms are attractive, except the rearrangement contributions which are strongly repulsive. It can be seen that the direct potentials (excluding rearrangement contributions) for cases T and RT are shallower than for case R, as is expected since in cases T and RT the inclusion of the target density leads to an increased repulsion of the density-dependent part of the interaction. There is very little difference between the rearrangement contributions in the cases R and RT, the latter being slightly more repulsive at the center of the nucleus. The energy-corrective terms V_W, V'_W and V''_W have the shortest range of all the components because they arise from the zero-range term in the force. V_W and W''_W are shallower than V'_W because they include a repulsive rearrangement term which is absent in V'_W. The local equivalent of the non-local exchange potentials are very similar for $V^{R}_{\alpha N}$ and $V^{RT}_{\alpha N}$ and both are somewhat deeper than for $V^{T}_{\alpha N}$. In all cases the exchange component is deeper than the direct part, but has a shorter range. The essential difference between the three cases arises in the ratio of the exchange component to the direct one. Finally it is worth remarking that near the strong absorption radius R_1, which in this case is about 7.4 fm [ref. [40])], the rearrangement and energy-

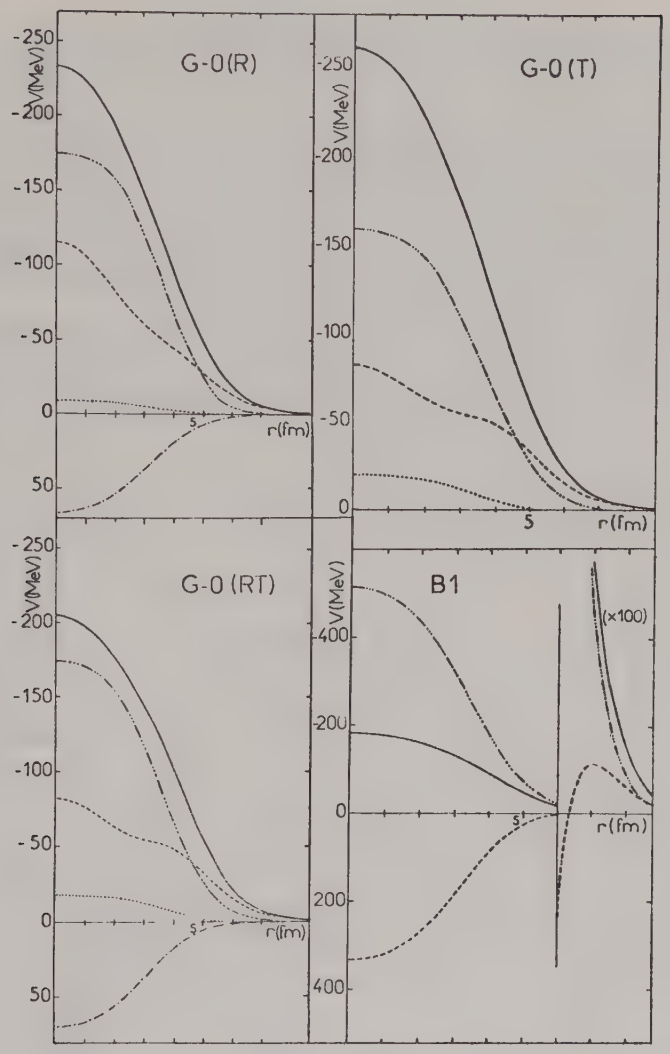

Fig. 2. Component parts of the α-^{40}Ca potentials calculated at 30 MeV c.m. energy with G-0 within approximations R, T and RT, and with the B1 forces: dashed line: direct term; dot-dashed line: rearrangement term; dotted line: energy corrective term; triple dot-dashed line: local approximation to the exchange term, and their sum: solid line.

corrective terms give very small contributions to the calculated potential, the latter being mainly due to the direct term with some small contribution from the exchange term. Therefore the double folding model with antisymmetrization but without inclusion of the rearrangement terms seems to be a valid approach in the vicinity of the strong absorption radius even when density-dependent interactions are considered.

In fig. 2, we also display the different contributions to the α-nucleus potential constructed from the B1 interaction. The local direct potential of eq. (4) is mainly repulsive and only becomes attractive beyond 6 fm. The local equivalent exchange potential of eqs. (9) and (10) is attractive everywhere. In the extreme tail, both components are attractive and comparable. This was not the case for the G-λ potentials and some earlier results [17,19]) where the exchange contribution to the potential was found to be negligible near the strong absorption radius. Thus it illustrates the fact that the relative contributions of the direct and exchange components are dependent on the particular n-n interaction considered.

In fig. 3, we compare the potentials constructed with the G-0 interaction for cases T and RT at 30 MeV c.m. energy, together with the potential C obtained by dropping the rearrangement terms in potential R. Comparison of potentials C and T gives directly the effect of taking the target density into account in the effective n-n force and shows a reduction of the depth at small distances. On the other hand, comparison of potentials T and RT reveals the importance of the rearrangement terms (see also fig. 2), which lead to an additional reduction of the

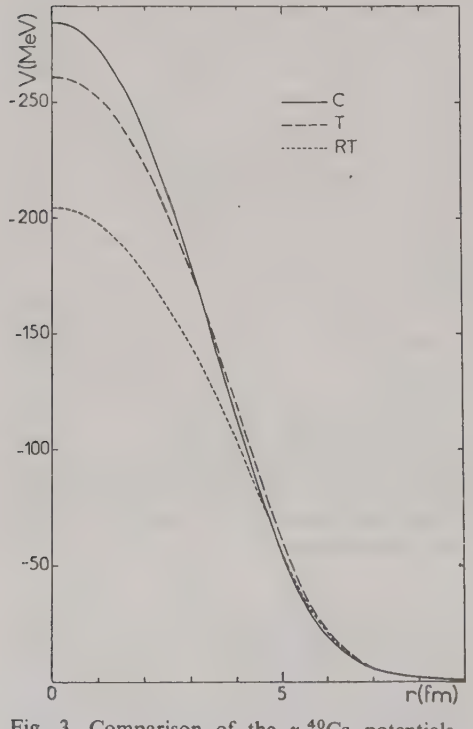

Fig. 3. Comparison of the α-^{40}Ca potentials calculated at 30 MeV c.m. energy with G-0 within approximations C, T and RT.

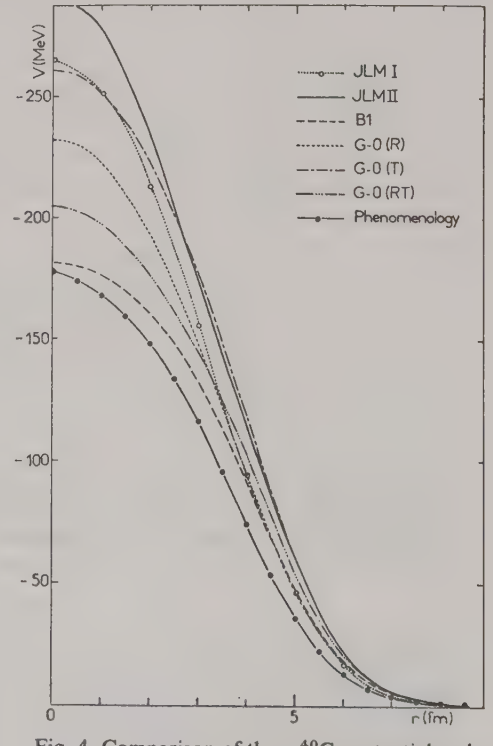

Fig. 4. Comparison of the α-^{40}Ca potentials calculated at 30 MeV c.m. energy with the G-0, JLM and B1 interactions with the phenomenological potential of ref. [41]) eq. (27) at the same energy.

potential depth. These results point to the importance of taking into account *both* the target density dependence and the HF rearrangement terms when using density-dependent forces.

In fig. 4, we compare the potentials constructed with the B1, JLMI and JLMII forces with those built from G-0 within approximations R, T and RT. The potential calculated with B1 is the shallowest obtained in this work. For the G-0 force, $V_{\alpha N}^{RT}$ is more diffuse than $V_{\alpha N}^{R}$ and $V_{\alpha N}^{T}$. The potential JLMI is shallower than JLMII which explicitly illustrates the underestimation of the density-dependence effects when eq. (16′) is used. We have plotted in the same figure a phenomenological potential recently extracted by Delbar *et al.* [41]) in a global analysis of ^{40}Ca(α, α) scattering data extending over the whole angular range between 24 and 166 MeV incident energy. This potential has a form factor of the squared Woods-Saxon type:

$$V(R) = -U_0(1+e^{(R-R_0)/2a})^{-2}, \tag{27}$$

with

$$U_0 = 198.6(1-0.00168\,E_\alpha)\ \text{MeV}, \quad R_0 = 4.685\ \text{fm}, \quad a = 0.645\ \text{fm}, \tag{28}$$

where E_α denotes the incident laboratory energy. It can be seen that all the calculated potentials are deeper than the phenomenological potentials at all distances.

The volume integrals per nucleon pair $J_V/4A$ and the rms radii $\langle r^2\rangle^{\frac{1}{2}}$ of all the potentials represented in fig. 4 are listed in table 1. The volume integrals of the calculated potentials are larger than the phenomenological value by a factor ranging from 1.2 to 1.6. The potential calculated with B1 gives the volume integral closest to phenomenology, but leads to a slight overestimation of the rms radius due to the oscillator parameter b_0 of Brink and Boeker, which is used in the present calculation and which leads to a too large r.m.s. radius for the α-particle [39]). The r.m.s. radii of the potentials calculated with the other interactions are very similar and turn out to be in better agreement with phenomenology, except in the G-0 (RT) case where $\langle r^2\rangle^{\frac{1}{2}}$ is overestimated by 0.2 fm.

TABLE 1

Volume integrals per nucleon pair and rms radii of the α-^{40}Ca potentials displayed in fig. 4 at $E_{c.m.} = 30$ MeV

Potential	$-J_V/4A$ (MeV · fm^3)	$\langle r^2\rangle^{1/2}$ (fm)
G-0(R)	477.4	4.383
G-0(T)	581.6	4.389
G-0(RT)	508.3	4.488
B1	450.3	4.433
JLMI	478.5	4.228
JLMII	570.4	4.285
phenom. [41])	364.8	4.290

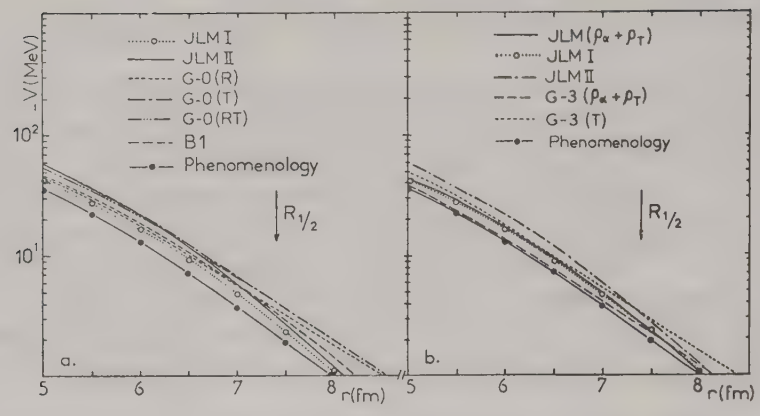

Fig. 5. α-^{40}Ca potentials calculated at 30 MeV c.m. energy compared to the phenomenological potential of ref. [41]) eq. (27) near the strong absorption radius; (a) for the G-0, JLM and B1 interactions and ρ given by eqs. (16) or (16′), (b) for G-3 and JLM, $\rho = \rho_\alpha + \rho_T$ and ρ given by eqs. (16) or (16′).

We have also examined the depth of our theoretical potentials in the vicinity of the strong absorption radius $R_{\frac{1}{2}}$, since this depth is a well-defined quantity phenomenologically for strongly absorbed projectiles [42]). The phenomenological potential of eqs. (27) and (28) gives a depth of 2.21 MeV at $r = 7.4$ fm whereas Fernandez and Blair's potential [40]) is 2.23 MeV deep at the same radius. In fig. 5a we have represented the tail of all the calculated potentials in the neighbourhood of the strong absorption radius together with phenomenology. All the calculated potentials are too deep by a factor ranging from 1.45 to 1.90 except for JLMI which is closer to the phenomenological potential. For density-dependent forces, one can inquire if the systematic overestimation of the depth we observe is not related to our approximate treatment of the target density dependence in the effective n-n interaction. In the vicinity of the strong absorption radius, the overlap densities are of the order of one tenth to one hundredth of the central nuclear density. Therefore we expect that the simple sum of densities gives a better approximation to the total antisymmetrized [36]) density in this low-density region than taking into account the projectile density only (cf. subsect. 2.2.1) or using our ansatz of eq. (16′) (cf. subsect. 2.2.2). We have used the simple sum of densities taken at the c.m. of the two nucleons to calculate the α-nucleus potential with the G-3 and JLM interactions. The density-dependent part of the G-3 interaction is linear in ρ, which makes the evaluation of the non-local part of the potential easy. In fig. 5b the results of the calculations, using both the simple sum of densities and prescription of eqs. (16) and (16′) for the local density are compared with the phenomenological potential. For the radial range considered in fig. 5 the overlap densities do not exceed the limiting value above which the effective interactions we use are no longer defined [i.e., $\rho = 0.332$ fm^{-3} for G-3, ref. [30]), and 0.185 fm^{-3} for JLM, ref. [31]), corresponding to $k_F = 1.7$ fm^{-1} and 1.4 fm^{-1} respectively].

The calculated potentials are now much closer to phenomenology for large values of R for both JLM and G-3 interactions (the overestimation of the depth has been reduced to 20 % at 7.4 fm). For large values of R the potential calculated with the G-3 interaction is now closer to phenomenology than JLM. On the other hand in this domain of R the potential calculated with JLM is nearly identical to the previous potential JLMI and both are close to phenomenology. At small distances, the simple sum of densities prescription gives very high densities for which the effective interactions we use become undefined, leading as expected to unphysical depths for the calculated potentials. This is shown in fig. 6 where the potentials calculated with G-3 and JLM and the sum of densities are displayed for illustrative purposes on the whole radial range. For each interaction, the dotted portion of the curve corresponds to distances for which the local density exceeds the limits given above where the effective n-n interaction is no longer defined. For large distances both these potentials are similar but they are completely different for smaller distances which shows the difficulties mentioned above when the sum of densities is used.

As a conclusion, it seems that prescription (16′) leads to results similar to the sum of densities prescription at large distances but more reasonable at small distances. However by replacing (16) by (16′) one weakens the effects of density dependence.

3.1.2. Energy dependence of the α-nucleus interaction. In this subsection, we consider the dependence of the α-^{40}Ca optical potential on the incident energy of the projec-

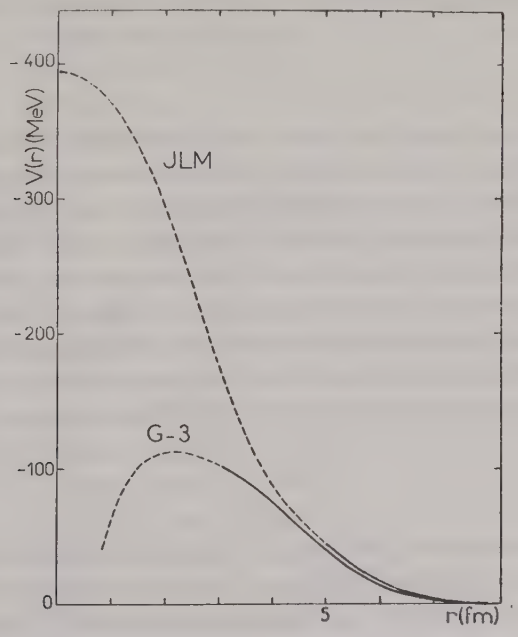

Fig. 6. α-^{40}Ca potentials calculated over all distances at 30 MeV with the G-3 and JLM interactions using the sum of densities for the total density of the system.

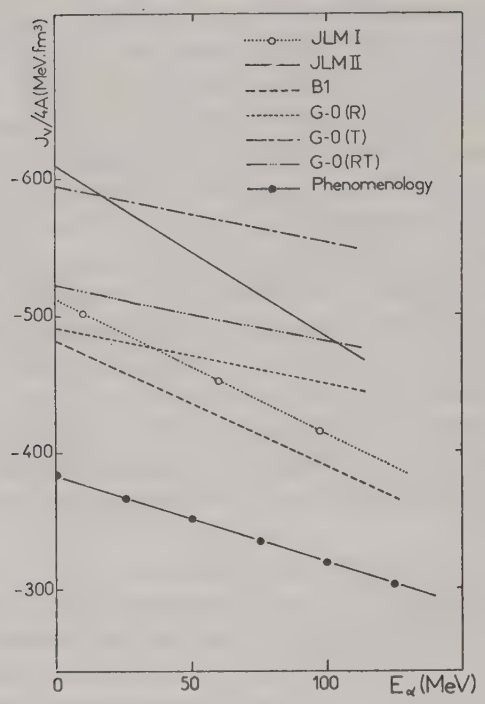

Fig. 7. Energy dependence of the volume integrals per nucleon pair $J_V/4A$ for the various calculated potentials as compared to phenomenology [41]).

tile. In our calculations, the terms that determine the energy dependence of the potential depend on the particular effective n-n interaction considered. In the case of the B1 and G-λ interactions, it arises solely from the energy dependence of the local equivalent exchange potential. The energy dependence of the JLM potential arises from the energy dependence of the parametrized effective interaction which in fact is partly due to the simulation of the exchange term [43]).

In fig. 7, we have plotted the volume integrals per nucleon pair for the various calculated potentials as a function of the incident lab energy. This dependence is linear to a very good approximation and can be written as:

$$J_V/4A = (J_V^{(0)}/4A)(1 - aE_\alpha), \tag{29}$$

which has the same form as the energy dependence derived from phenomenological analyses of α-nucleus scattering data [13]). In table 2, we have listed the values of the parameter a of eq. (29) for the potentials constructed with the B1, JLM and G-0 interactions (the energy dependence obtained with G-1 and G-3 is very close to that obtained with G-0). They may be compared with the phenomenological value [41])

TABLE 2

Values of the parameters a [eq. (29)] for the α-^{40}Ca and α-n potentials described in the text

Potential	$a \times 10^3$ (MeV^{-1})
G-0(R)	0.84
G-0(T)	0.69
G-0(RT)	0.80
B1	1.91
JLMI	1.90
JLMII	2.05
phenom. [41])	1.68
α-n (B1) [34])	2.0
α-n (G-0) [34])	0.8

$a = 0.00168$ MeV^{-1} [see eq. (26)] which is typical of those quoted in the literature, which range between 0.001 and 0.003 MeV^{-1} [refs. [12,13,44])]. Table 2 shows that the energy dependence of the calculated potentials is on the whole compatible with phenomenology.

The JLMII potential has the strongest energy dependence while the JLMI potential has an energy dependence similar to B1 but stronger than that of the G-λ interactions. For the JLM force the energy dependence comes from both the energy dependence of the G-matrix and the simulation of the exchange term. Although the B1 interaction is energy-independent, it gives also rise to a strong energy dependence in the α-nucleus potential because it has a large non-local exchange term as shown in fig. 2. The potentials calculated with G-λ yield particularly low values of a. The same feature was observed for the α-n potentials derived in ref. [34]) with the same interaction. In fact, it has been shown [13,14]) that the energy dependence of the α-nucleus potential constructed from the non-local α-nucleon interaction is very close to that of the potential derived from the α-nucleon local equivalent interaction. (In the latter case, the energy dependence of the α-nucleus potential is of course identical to that of the input α-nucleon interaction.) This is indeed the case for both the B1 and G-0 interactions as can be seen in table 2 where we also give the energy dependence of the volume integral of the α-nucleon potentials derived in ref. [34]) expressed as a function of the α-particle lab energy.

Our results are obtained within the framework of folding models. However Fliessbach [45]) going beyond this model has approximately taken into account the Pauli distortion of the incident α-particle. This effect gives a repulsive contribution but decreases with incident energy. Combined with the energy dependence calculated above it leads to a non-linear dependence of the real well depth [45]) at low energy as is suggested by a recent "model-independent" analysis of ^{40}Ca(α, α) scattering data from 18 to 166 MeV incident energy [46]). However above $E_\alpha \approx 60$ MeV this effect disappears [45]) and the energy dependence is approximately that of the folding model.

3.1.3. Optical-model analysis. In this subsection, we examine the ability of the potentials calculated in sect. 2 with the B1, G-0 and JLM interactions to reproduce the experimental elastic cross sections. In our analysis, we use the above real α-nucleus potentials multiplied by an adjustable renormalization constant λ, and for the imaginary potential a Woods-Saxon squared form factor [cf. eq. (27)]. The four parameters λ, W_0, R_W, a_W are varied in an automatic search program to yield a minimum of chi-square per degree of freedom χ^2/F. It is clear that the introduction of the renormalization constant λ and that of a phenomenological imaginary potential will in some measure lessen the sensitivity of the analysis to distinguish between the calculated potentials. This may not be a serious restriction since the absorption is relatively weak in the α-nucleus case [47]).

Our analysis was carried out using the high-precision cross sections recently measured by Gils *et al.* [48]) at 104 MeV incident lab energy. These data extend up to 120° in the c.m., i.e. beyond the rainbow angle θ_r which is about 100° at this energy. They should provide our calculations with a good test since it has been shown that the discrete ambiguities are resolved at these energies when using data extending beyond the rainbow angle [49]). Another reason for not testing our calculated potentials against lower-energy data lies in the fact that at low energies there are three active semi-classical turning points [50]). The corresponding angular distributions then result from the interference of the so-called barrier wave and internal wave amplitudes [50]), making the cross sections extremely sensitive to very minor modifications of the real part of the potential. This is no more the case at the energy we are considering, which is about twice the critical energy $\varepsilon_{\text{crit}}^{(1)}$ [ref. [50])] for which the effective potential loses its internal "pocket" for the grazing angular momentum. Thus there is only one important turning point left for each partial wave at this energy [50]), making the cross section less sensitively dependent on fine details of the interaction potential.

In fig. 8, we have displayed the resulting fits to the data and the corresponding parameters are listed in table 3. The fits obtained for the G-0 interaction (within both approximations R and T) and for the JLM interaction are visually almost indistinguishable and lead to very similar values of χ^2/F. Their quality is comparable to that obtained with the phenomenological potential of ref. [16]) which gives $\chi^2/F = 2.7$.

The fits obtained with B1 and G-0 in approximation RT are somewhat poorer: the value of χ^2/F is about five times that for JLM or G-0 (R and T) and the calculated cross sections are slightly shifted with respect to experiment for angles less than 40°. This is probably due to the too large ranges of these potentials (see table 1).

Our fitting procedure leaves unchanged the ranges of the form factors of the real potentials. Therefore comparison of the calculated cross sections with experiment is a direct test of these form factors. It seems then that density-dependent forces yield better form factors than B1. However the too large radius of our potential calculated with B1 which explains in a large measure these discrepancies is a

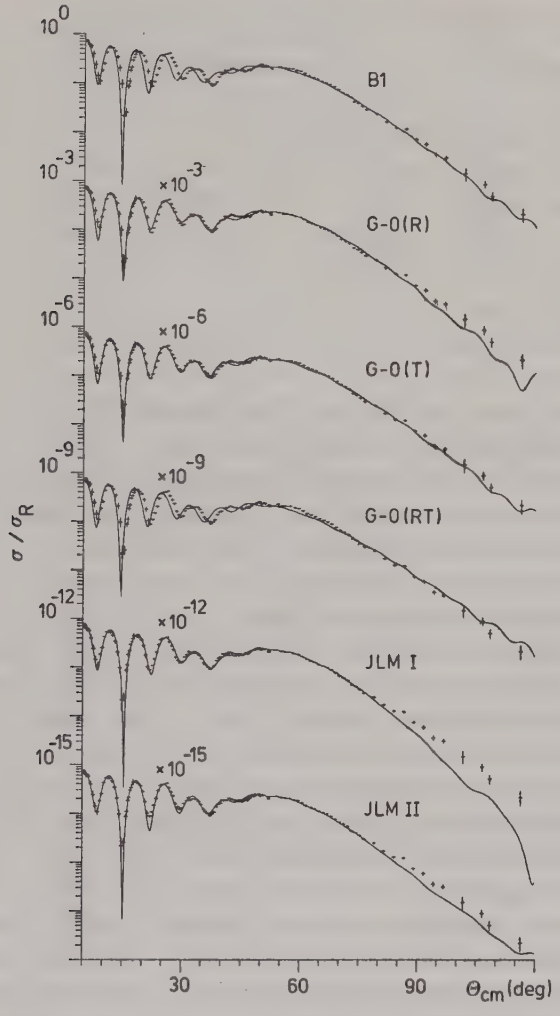

Fig. 8. Fits to the 104 MeV ^{40}Ca(α, α) data of ref. [48]) using the various calculated potentials. The corresponding adjusted parameters are listed in table 3.

consequence of our choice of b_0, which we have taken, to be consistent with the Brink and Boeker calculation, as $b_0 = 1.40$ fm. This value gives too large a radius for the α-particle and therefore gives also too large a radius for the potential. For all the other forces we have used $b_0 = 1.20$ fm and thus it is not surprising that the corresponding potentials have smaller radii. We certainly could get a better fit for B1 by lowering the value of b_0. The approximation RT for G-0 leads to a too large range of the form factor. This is certainly due to the underestimation at large distances of the repulsive rearrangements terms which are strongly dependent on the local density. On the other hand the value of the renormalization constant λ

TABLE 3

Parameters corresponding to the fits of ^{40}Ca(α, α) scattering data at E_α = 104 MeV displayed in fig. 8 (lengths in fm, energies in MeV)

Potential	λ	W_0	R_W	a_W	$\langle r^2\rangle^{1/2}$	$\lambda J_V/4A$	$\lambda V(R_{1/2})$	χ^2/F
G-0(R)	0.73	−21.4	6.23	0.55	4.41	325.9	2.58	7.0
G-0(T)	0.59	−21.3	6.28	0.51	4.41	326.9	2.39	6.2
G-0(RT)	0.73	−22.3	6.38	0.54	4.51	350.5	2.89	34.5
B1	0.89	−22.7	6.34	0.61	4.47	343.2	2.74	46.5
JLMI	0.72	−21.1	6.11	0.54	4.21	295.6	1.62	8.0
JLMII	0.63	−23.7	6.08	0.58	4.25	311.1	1.64	8.0
phenom. [16])		[a])	[a])	[a])	4.32	326.8	1.78	2.7

[a]) Saxon-Woods form factor different from that used in our analysis.

is expected to test the strength of the potential. The best value is obtained for B1 with $\lambda = 0.9$, while λ takes quite small values for all the density-dependent forces. The value $\lambda = 0.9$ for B1 seems reasonable, in the sense that its deviation from unity may be interpreted as due to our neglect of higher-order contributions to the potential of eq. (1). Indeed such corrections become repulsive at large enough distances [5]) and they contribute to lower the strength of the potential. For density-dependent forces, λ lies between about 0.5 and 0.7 and cannot be entirely explained by such effects. It is more likely that it indicates the sensitivity of the calculation to the prescription used for the local density. As mentioned above, we expect our prescription to underestimate the effect of such terms. As they are of repulsive character, we then get an overestimation of the total strength. Comparison of the potentials calculated in subsect. 3.1.1 with $\rho = \rho_\alpha + \rho_T$ and with our prescription of eq. (16′) for G-3 and JLM forces shows that the α-nucleus potential is very sensitive to the definition of the local density even at large distances. This is also clear from the comparison of potentials JLMI and JLMII, which have, respectively, $\lambda = 0.72$ and $\lambda = 0.63$. We believe that this problem is an important one for all calculations using a density-dependent force. Obviously there are other sources of uncertainty in our calculations. The main one is inherent in the folding model where only one-nucleon exchange is taken into account. However resonating group calculations show that at least at this energy, other types of exchanges are small for systems like α-^{40}Ca [ref. [51])]. Finally, introduction of rearrangement terms in the α-nucleus potential has a quite large effect on the strength of the potential. This can be seen from the renormalization constant λ which changes from 0.59 to 0.73 when these terms are added to the potential $V^T_{\alpha N}$.

3.2. TARGET DEPENDENCE OF THE α-NUCLEUS POTENTIAL

We finally examine the dependence of the volume integral per nucleon pair of the real potential upon the nucleon number A of the target nucleus. Simple folding

model calculations of the α-nucleus potential starting from a purely local α-nucleon interaction, obtained either by neglecting the exchange term or by approximating the non-local exchange term by a local equivalent one, would lead to volume integrals per nucleon pair which are independent of A if the effective nucleon-nucleon interaction used is density-independent. The phenomenological potentials recently extracted by Goldberg at 140 MeV incident energy [52]) exhibit a decrease of $J_V/4A$ from light to medium-weight nuclei followed by some saturation for heavier nuclei. The empirical potentials retained in this analysis have a Woods-Saxon shape [other form factors were investigated in ref. [52]) but they lead to a closely similar A-dependence]. For the first four nuclei considered (i.e., ^{12}C, ^{40}Ca, ^{58}Ni and ^{90}Zr), they are unique at the energy considered ($E_\alpha = 141.7$ MeV) in the sense that the data are sufficient to resolve the discrete ambiguity in the strength of the potential and they have volume integrals per nucleon pair of the order of 300 MeV · fm^3. The discrete ambiguity is not resolved for the ^{208}Pb data ($E_\alpha = 139$ MeV): there are four potentials families fitting the data, whose volume integrals range from 283 to 532 MeV · fm^3; we decided to retain the family giving the value nearest to that obtained for the other nuclei, i.e. $J_V/4A = 283$ MeV · fm^3.

In fig. 9, we present our results for the B1, JLM and G-0 interactions at $E_\alpha = 140$ MeV for nuclei ranging from ^{28}Si to ^{208}Pb. The small fluctuations seen in the volume integrals of the calculated potentials at low A are related to corresponding variations of the geometries of the input matter distributions. This has been checked by repeating the calculations in the JLM case with the average matter distributions of Negele [53]) which give a smooth A-dependence. All the forces considered predict a target dependence qualitatively similar to that of the phenomenological potentials. However the slope at low A sensitively depends on the particular interaction considered. For the B1 and G-0 (R) case, the entire A-dependence comes from the use of the non-local α-nucleon potential. The results show clearly that this non-locality is very important to reproduce the general behaviour of the α-nucleus potential for a wide range of nuclei. However the predicted decrease is too weak at low A in these two cases. For the G-0 (T) and G-0 (RT) cases both non-locality of the exchange term and target density-dependence in the interaction contribute to the A-dependence. The results show a faster decrease at low A and a better agreement with Goldberg's empirical potentials. For the JLM interaction there is no explicit exchange term and the A-dependence results only from its density-dependence. The predicted target dependence is identical for JLMI and JLMII potentials but is weaker than in the G-0 (T) and G-0 (RT) cases. These calculations indicate that both the exact treatment of the non-locality of the exchange term and the target density-dependence of the effective n-n interaction are necessary to explain the A-dependence of the volume integral per nucleon pair of the phenomenological α-nucleus optical potentials.

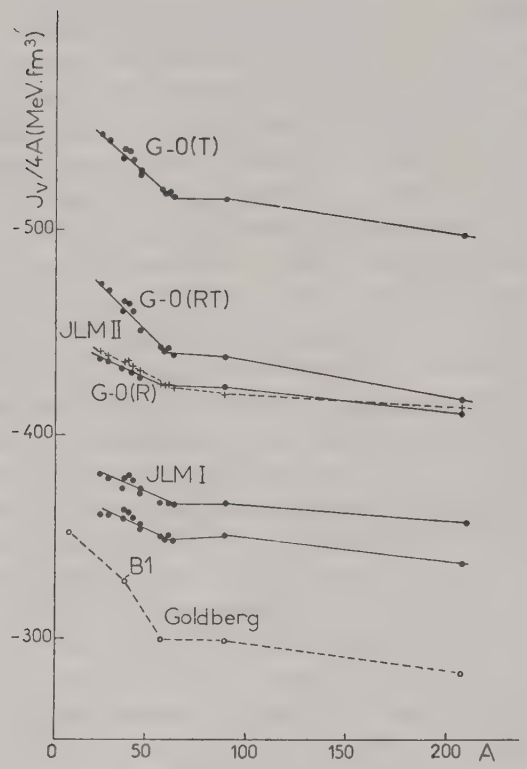

Fig. 9. Dependence of the volume integrals per nucleon pair $J_V/4A$ of the various calculated potentials on the mass number of the target A as compared to phenomenological results of Goldberg [52]) (curves are drawn to guide the eye).

4. Conclusions

The real part of the α-nucleus optical potential was calculated by folding the α-nucleon interaction with the target matter density distribution. This non-local α-n interaction was calculated in the Hartree-Fock approximation using several effective n-n interactions. In contrast with most previous studies, the α-nucleus potential was derived with this non-local interaction instead of calculating first a local equivalent potential. It is therefore non-local, with a very small non-locality range compared to the range of the potential unlike the α-nucleon case. Then the Perey-Saxon approximation is more reliable and was used to derive the local equivalent potential.

Both density-independent and density-dependent effective interactions were considered. Initially the local density in the density-dependent effective interaction was assumed to be that of the α-n system, thereafter the target nucleus density contribution was taken into account. A relation between the local density and the

α and target densities was proposed which never exceeds the nuclear density of finite nuclei in contrast with previous prescriptions of taking the sum of α and target densities. Thus we have avoided the problem of using an effective interaction for high densities for which it has not been defined. However our prescription (16′) underestimates the contribution of the density-dependent terms and can be considered as the other extreme compared to the prescription of taking the sum. The Hartree-Fock rearrangement terms, neglected in previous studies, were included in an approximate way for the Sprung-Banerjee interactions. They give a sizeable contribution mainly at small distances.

Our potentials were tested on the 104 MeV ^{40}Ca(α, α) data of Gils *et al.* [48]) over the whole angular range. The calculated real potentials were multiplied by an adjustable constant λ and a phenomenological imaginary potential was added, all parameters being fitted to the scattering data. The angular distribution is best reproduced with density-dependent interactions showing that the shape of the optical potential is best reproduced by these interactions. The renormalization factor λ is closer to 1 for B1 than for density-dependent interactions. For the latter we believe that the small values of λ come partly from our treatment of the local density which underestimates the density-dependent effects and therefore overestimates the strength of the potential. The ambiguity in the definition of the local density in the derivation of the nucleus-nucleus potential in the framework of the folding models leads to uncertainties in the results which are far more important than in Hartree-Fock calculations of nuclear ground-state properties.

We have also investigated the energy dependence of the calculated potentials. All the forces predict a linear decrease of the volume integral per nucleon pair as a function of the incident energy, with a slope compatible with the phenomenological values. For the JLM interaction the energy dependence arises entirely from the explicit energy dependence parameterized in the force, but for the G-λ and B1 interactions it arises from the energy dependence of the equivalent local single-nucleon exchange potential. The B1 case displays a stronger energy dependence than the G-λ case because for the former the exchange contribution is very large.

Finally, the α-nucleus potential was calculated at 140 MeV incident energy for various targets ranging from ^{28}Si to ^{208}Pb. The volume integral per nucleon pair of the theoretical potentials show a decrease with the target mass in the low-A region, followed by saturation for heavier nuclei, in qualitative agreement with the phenomenological results of Goldberg *et al.* [52]) at the same energy. The best agreement is obtained when both the non-locality of the exchange term and the target density dependence of the effective n-n interaction are taken into account in the calculations, suggesting the importance of a proper treatment of both these effects.

It is a pleasure to thank Dr. X. Campi for stimulating discussions. One of us (N.VM) is very grateful to Prof. P. Benoist-Gueutal for helpful comments at the

early stage of this work. Two of the authors (F.D and F.M) gratefully acknowledge the hospitality extended to them by the Division de Physique Théorique de l'IPN d'Orsay, as well as financial support from the CNRS.

Appendix

CALCULATION OF THE EFFECTIVE α-NUCLEON INTERACTION WITH THE DENSITY-DEPENDENT INTERACTIONS G-λ

We give the explicit expressions of the effective α-n interaction calculated with the G-λ forces for the various approximations defined in the text. The α-particle is described as four particles in a 1s harmonic oscillator state of parameter b_0. The G-λ effective interactions for a given (S, T) state are the sum of two terms V^{ST} and V_W^{ST}:

$$V^{ST}(\boldsymbol{r}, \boldsymbol{r}'; k_F) = \sum_{j=1}^{5} (a_j^{ST} + b_j^{ST} k_F^{\lambda}(\boldsymbol{r}, \boldsymbol{r}')) \exp[-(\boldsymbol{r}-\boldsymbol{r}')^2/\mu_j^2], \tag{A.1}$$

which is derived directly from a nuclear matter calculation and

$$V_W^{ST}(\boldsymbol{r}, \boldsymbol{r}'; k_F) = (W - W_0(k_F)) A^{ST}(k_F) \delta(\boldsymbol{r}-\boldsymbol{r}'), \tag{A.2}$$

which simulates the fact that the single-particle energies are different in nuclear matter and finite nuclei. W is the binding energy of the two interacting nucleons in the α-particle and $W_0(k_F)$ twice the average one-nucleon binding energy in nuclear matter. The coefficients a_j^{ST}, b_j^{ST} and A^{ST} are given in ref. [30]).

A.1. EFFECTIVE α-n INTERACTION $V_{\alpha n}^{R}$ WITH G-λ FORCES FOR A FREE NUCLEON

The formulae given in this subsection are a generalization of those given in ref. [34]) for the G-0 interaction. The various contributions to the α-nucleon interaction, calculated from eq. (2), are listed below:

The direct, density-independent term U_{LI} corresponding to the potential eq. (A.1):

$$U_{LI}(r) = \sum_{j=1}^{5} U_j \exp[-r^2/\lambda_j^2], \tag{A.3}$$

where

$$U_j = \tfrac{1}{4}(a_j^{11} + 3a_j^{13} + 3a_j^{31} + 9a_j^{33})(\mu_j/\lambda_j)^3, \tag{A.4}$$

$$\lambda_j^2 = b_0^2 + \mu_j^2. \tag{A.5}$$

The direct density-dependent term plus the rearrangement terms U_{LD} corresponding to the potential of eq. (A.1):

$$U_{LD}(r) = \sum_{j=1}^{5} U_{j\rho} \exp[-r^2/\lambda_j'^2], \tag{A.6}$$

where

$$U_{j\rho} = \tfrac{1}{4}(b_j^{11} + (\lambda+3)(b_j^{13} + b_j^{31}) + 9b_j^{33})(\mu_j/\nu_j)^3 b_0^{-\lambda}\kappa_\lambda, \tag{A.7}$$

$$\nu_j^2 = \frac{6}{\lambda+6}\, b_0^2 + \mu_j^2, \tag{A.8}$$

$$\lambda_j'^{-2} = \frac{\lambda}{6b_0^2} + \nu_j^{-2}, \tag{A.9}$$

$$\kappa_\lambda = (6\sqrt{\pi})^{\lambda/3}\left(\frac{6}{\lambda+6}\right)^{\frac{3}{2}}. \tag{A.10}$$

The energy corrective term U_W which is the sum of direct, exchange and rearrangement components for the potential of eq. (A.2):

$$U_W(r) = \tfrac{1}{16}\rho_\alpha(r)\left(6S(k_F) + k_F \frac{\partial S}{\partial k_F}(k_F)\right), \tag{A.11}$$

where

$$k_F^3 = \tfrac{3}{2}\pi^2(\rho_\alpha(r)\rho_\alpha(r'))^{\frac{1}{2}}, \tag{A.12}$$

$$S(k_F) = (W - W_0(k_F))(A^{13}(k_F) + A^{31}(k_F)). \tag{A.13}$$

As mentioned in subsect. 2.2.1 the weak energy dependence of W has been neglected in the present calculation.

The non-local, density-independent term U_{NI} corresponding to the potential of eq. (A.1):

$$U_{NI}(\boldsymbol{X}, \boldsymbol{x}) = \sum_{j=1}^{5} U_{Nj} \exp[-x^2/\beta_j^2] \exp[-X^2/b_0^2], \tag{A.14}$$

where

$$\boldsymbol{X} = \tfrac{1}{2}(\boldsymbol{r}+\boldsymbol{r}'), \qquad \boldsymbol{x} = \boldsymbol{r}-\boldsymbol{r}', \tag{A.15}$$

$$U_{Nj} = \frac{1}{4\pi^{\frac{3}{2}} b_0^3}(-a_j^{11} + 3a_j^{13} + 3a_j^{31} - 9a_j^{33}), \tag{A.16}$$

$$\beta_j^{-2} = (2b_0)^{-2} + \mu_j^{-2}. \tag{A.17}$$

The non-local, density-dependent term U_{ND} corresponding to the potential of eq. (A.1):

$$U_{ND}(\boldsymbol{X}, \boldsymbol{x}) = \sum_{j=1}^{5} U'_{Nj} \exp[-x^2/\beta_j'^2] \exp[-X^2/b_0'^2], \tag{A.18}$$

where

$$U'_{Nj} = \frac{1}{4\pi^{\frac{3}{2}} b_0^3}(-b_j^{11} + 3b_j^{13} + 3b_j^{31} - 9b_j^{33})(6\sqrt{\pi})^{\lambda/3} b_0^{-\lambda}, \tag{A.19}$$

$$b'_0 = \left(\frac{3}{\lambda+3}\right)^{\frac{1}{2}} b_0, \tag{A.20}$$

$$\beta'^{-2}_j = (2b'_0)^{-2} + \mu_j^{-2}. \tag{A.21}$$

A.2. EFFECTIVE α-n INTERACTION FOR THE G-λ FORCES TAKING INTO ACCOUNT THE TARGET DENSITY

The density-independent contributions of the G-λ forces to both the local and the non-local terms remain unchanged and are those of appendix A.1. For the density-dependent terms we use the symmetrical relation eq. (16′) for the local density. However these terms are complicated functions of the variables defined in fig. 10. Indeed this relation (16′) introduces in some of them an angular dependence in the integrals which would require very long computer time, so that, when necessary, we use simplified but still symmetrical relations:

$$\rho_{\alpha(T)}(G) \simeq \sqrt{\rho_{\alpha(T)}(1)\rho_{\alpha(T)}(2)}, \tag{A.22}$$

where G is the c.m. of nucleons 1 and 2.

Furthermore we neglect the size of the α-particle compared to the distance R and write:

$$\boldsymbol{s} = \boldsymbol{R} + \boldsymbol{r}_1 \simeq \boldsymbol{R}. \tag{A.23}$$

We calculate first the potential $V^{\mathrm{T}}_{\alpha n}$ corresponding to the usual direct and exchange terms, then we give the potential $V^{\mathrm{RT}}_{\alpha n}$ including rearrangement terms.

(*a*) *Potential* $V^{\mathrm{T}}_{\alpha n}$. The density-dependent terms U_{LD}, U_W and U_{ND} are modified and replaced by the new quantities U'_{LD}, U'_W and U'_{ND} which now depend also on the coordinate of the nucleon inside the target nucleus and on the distance R between the centers of mass of both nuclei. The new expressions are:

$$\text{(i)}\quad U'_{\mathrm{LD}}(r; r_2, R) = (\rho_{\mathrm{T}}(r_2)\rho_{\mathrm{T}}(R))^{\lambda/12} \sum_{j=1}^{5} U'_{j\rho} \exp\left[-r^2/\lambda''^2_j\right], \tag{A.24}$$

where

$$U'_{j\rho} = \tfrac{1}{4}(b_j^{11} + 3b_j^{13} + 3b_j^{31} + 9b_j^{33})(\mu_j/\nu'_j)^3 b_0^{-\lambda/2}\kappa'_\lambda, \tag{A.25}$$

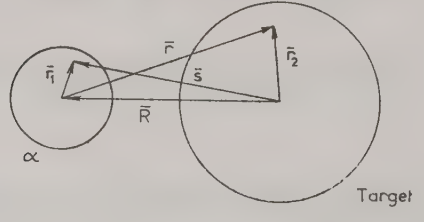

Fig. 10. Definition of the system of coordinates used in the calculation of the various α-nucleon interactions.

$$\nu_j'^2 = \frac{12}{\lambda+12} b_0^2 + \mu_j^2, \tag{A.26}$$

$$\lambda_j''^{-2} = \frac{\lambda}{12 b_0^2} + \nu_j'^{-2}, \tag{A.27}$$

$$\kappa_\lambda' = (9\pi^{\frac{5}{2}})^{\lambda/6} \left(\frac{12}{\lambda+12}\right)^{\frac{3}{2}}. \tag{A.28}$$

$$\text{(ii)}\quad U_W'(r; r_2) = \tfrac{3}{8}\rho_\alpha(r) S(\hat{k}_F), \tag{A.29}$$

where the function S is defined by eq. (A.13) and:

$$\hat{k}_F^3 = \tfrac{3}{2}\pi^2(\rho_T(r_2)\rho_\alpha(r))^{\frac{1}{2}}. \tag{A.30}$$

$$\text{(iii)}\quad U_{ND}'(X, x; r_2, R) = (\rho_T(r_2)\rho_T(R))^{\lambda/12} \sum_{j=1}^{5} U_{Nj}'' \exp[-x^2/\beta_j^2] \exp[-X^2/b_0''^2], \tag{A.31}$$

where β_j is defined by eq. (A.17) and:

$$U_{Nj}'' = \frac{1}{4\pi^{\frac{3}{2}} b_0^3}(-b_j^{11} + 3b_j^{13} + 3b_j^{31} - 9b_j^{33})(9\pi^{\frac{5}{2}})^{\lambda/6} b_0^{-\lambda/2}, \tag{A.32}$$

$$b_0'' = \left(\frac{6}{\lambda+6}\right)^{\frac{1}{2}} b_0. \tag{A.33}$$

(*b*) *Potential* $V_{\alpha n}^{RT}$. All the expressions given in the above subsection remain valid except:

(i) The coefficients $U_{j\rho}'$ of eq. (A.25) which are replaced by:

$$U_{j\rho}'' = \tfrac{1}{4}(b_j^{11} + (\lambda+3)(b_j^{13} + b_j^{31}) + 9b_j^{33})(\mu_j/\nu_j')^3 b_0^{-\lambda/2} \kappa_\lambda', \tag{A.34}$$

where the coefficients ν_j' and κ_λ' are given by eqs. (A.26) and (A.28).

(ii) Making the assumption that the energy corrective term including rearrangement has the same structure as in the R case but where k_F is now replaced by $\hat{k}_F$ of eq. (A.30), we get:

$$U_W''(r; r_2) = U_W(\hat{k}_F), \tag{A.35}$$

with U_W as defined by eq. (A.11).

References

1) Proc. Second Louvain-Cracow Seminar on the alpha-nucleus interaction, Louvain-la-Neuve, 1978, ed. G. Grégoire and K. Grotowski, unpublished
2) B. Sinha, Phys. Reports **20C** (1975) 1
3) R. C. Barrett and D. F. Jackson, Nuclear sizes and structure (Clarendon, Oxford, 1977)
4) G. R. Satchler and W. G. Love, Phys. Reports **55C** (1979) 183
5) N. Vinh Mau, Phys. Lett. **71B** (1977) 5

6) J. S. Lilley, Phys. Rev. **C3** (1971) 2229
7) P. Mailandt, J. S. Lilley and G. W. Greenlees, Phys. Rev. **C8** (1973) 2189
8) A. M. Bernstein, Advances in nuclear physics, ed. M. Baranger and E. Vogt, vol. 3 (Plenum, New York, 1969) p. 325
9) C. J. Batty, E. Friedman and D. J. Jackson, Nucl. Phys. **A175** (1971) 1
10) M. Lassaut and N. Vinh Mau, Phys. Lett. **70B** (1977) 14
11) A. Budzanowski, A. Dudek, K. Grotowski and A. Strzalkowski, Phys. Lett. **32B** (1970) 431
12) G. M. Lerner, J. C. Hiebert, L. L. Rutledge and A. M. Bernstein, Phys. Rev. **C6** (1972) 1254
13) D. F. Jackson and R. C. Johnson, Phys. Lett. **49B** (1974) 249
14) N. Vinh Mau, ref. [1]), p. 243
15) B. Sinha, Phys. Rev. **C11** (1975) 1546
16) Z. Majka, H. J. Gils and H. Rebel, Z. Phys. **A288** (1978) 139
17) Y. Eisen and B. Day, Phys. Lett. **63B** (1976) 253
18) R. E. Peierls and N. Vinh Mau, Nucl. Phys. **A343** (1980) 1
19) G. R. Satchler and W. G. Love, Phys. Lett. **65B** (1976) 415
20) X. Campi and D. W. L. Sprung, Nucl. Phys. **A194** (1972) 401
21) J. W. Negele, Phys. Rev. **C1** (1970) 1260
22) D. Vautherin and D. M. Brink, Phys. Rev. **C5** (1972) 626
23) W. G. Love, Phys. Lett. **72B** (1977) 4
24) M. D. Cohler, B. Sinha, R. J. Griffiths and N. M. Clarke, Phys. Lett. **63B** (1976) 377
25) F. Petrovich, D. Stanley and J. J. Bevelacqua, Phys. Lett. **71B** (1977) 259
26) S. K. Gupta and S. Kailas, Phys. Lett. **73B** (1978) 398
27) T. Fliessbach, Z. Phys. **238** (1970) 329
28) T. Fliessbach, Z. Phys. **242** (1970) 287
29) D. M. Brink and E. Boeker, Nucl. Phys. **A91** (1967) 1
30) D. W. L. Sprung and P. K. Banerjee, Nucl. Phys. **A168** (1971) 273
31) J. P. Jeukenne, A. Lejeune and C. Mahaux, Phys. Rev. **C16** (1977) 80
32) X. Campi and A. Bouyssy, Phys. Lett. **73B** (1978) 263
33) F. Perey and D. S. Saxon, Phys. Lett. **10** (1964) 107
34) M. Lassaut and N. Vinh Mau, Nucl. Phys. **A349** (1980) 372
35) C. W. Wong and S. A. Moszkowski, Nucl. Phys. **A239** (1975) 209
36) D. M. Brink and Fl. Stancu, Nucl. Phys. **A243** (1975) 175
37) G. D. Alkhazov, S. L. Belostotsky and A. A. Vorobyov, Phys. Reports **42C** (1978) 89
38) H. R. Collard, L. R. B. Elton and R. Hofstadter, Nuclear Radii, ed. H. Schopper (Springer; Berlin, 1967)
39) J. S. McCarthy, I. Sick and R. R. Whitney, Phys. Rev. **C15** (1977) 1396
40) B. Fernandez and J. S. Blair, Phys. Rev. **C1** (1970) 523
41) T. Delbar, G. Grégoire, G. Paic, R. Ceuleneer, F. Michel, R. Vanderpoorten, A. Budzanowski, H. Dabrowski, L. Freindl, K. Grotowski, S. Micek, R. Planeta, A. Strzalkowski and K. A. Eberhard, Phys. Rev. **C18** (1978) 1237
42) D. F. Jackson and C. G. Morgan, Phys. Rev. **175** (1968) 1402
43) C. Mahaux, Proc. Hamburg Topical Workshop on nuclear physics, Hamburg, 1978, ed. H. V. Von Geramb (Springer, Berlin, 1979)
44) P. P. Singh, P. Schwandt and G. C. Yang, Phys. Lett. **59B** (1975) 113
45) T. Fliessbach, Nucl. Phys. **A315** (1979) 109
46) H. P. Gubler, G. R. Plattner and I. Sick, Proc. Conf. What do we know about the radial shape of nuclei in the Ca region?, Karlsruhe, 1979, ed. H. Rebel, H. J. Gils and G. Schatz, unpublished
47) D. A. Goldberg, ref. [1]), p. 41
48) H. J. Gils, H. Rebel, E. Friedman and Z. Majka, Phys. Rev. **C21** (1980) 1245
49) D. A. Goldberg and S. M. Smith, Phys. Rev. Lett. **29** (1972) 500
50) D. M. Brink and N. Takigawa, Nucl. Phys. **A279** (1977) 159;
N. Takigawa and L. W. Put, Phys. Lett. **84B** (1979) 371
51) M. Lemere, D. J. Studeba, H. Horiuchi and Y. C. Tang, Nucl. Phys. **A320** (1979) 449
52) D. A. Goldberg, Phys. Lett. **55B** (1975) 59;
D. A. Goldberg, S. M. Smith, H. G. Pugh, P. G. Roos and N. S. Wall, Phys. Rev. **C7** (1973) 1938
53) J. W. Negele, Phys. Rev. **C1** (1970) 1260

C Etude de la correction au modèle de convolution et de la partie imaginaire du potentiel α-noyau

La correction au potentiel réel calculé dans le modèle de convolution et le potentiel absorptif sont respectivement donnés par la partie réelle et la partie imaginaire du second terme ΔV de l'équation (II.2). Pour calculer ΔV, nous avons supposé l'interaction α-nucléon locale et utilisé l'interaction gaussienne $V_{\alpha n}(r) = -U_0 e^{-r^2/a^2}$, où $U_0 = 47.3$ MeV et $a = 1.97$fm, qui a été ajustée sur le potentiel α-nucléon local calculé pour la force B_1 de Brink et Boeker. Une telle interaction est proche de l'interaction effective de Bimbot et al., dont on sait qu'elle reproduit correctement les sections efficaces des états collectifs les plus bas du ^{40}Ca [BI73], donc devrait particulièrement convenir pour notre calcul du potentiel α-^{40}Ca. Reprenant les mêmes notations que celles introduites pour l'équation (II.2), le potentiel $\Delta V(\bar{r},\bar{r}')$ s'écrit simplement ;

$$\Delta V(\bar{r},\bar{r}') = \sum_{m\neq 0} \langle \psi_0 | \sum_{i=1}^{A} V_{\alpha n}(\bar{r},\bar{x}_i) | \psi_m \rangle \langle \psi_m | \sum_{i=1}^{A} V_{\alpha n}(\bar{r}',\bar{x}_i') | \psi_0 \rangle f_{\alpha n}(E-E_m,\bar{r},\bar{r}') \tag{II.31}$$

en fonction de l'interaction $V_{\alpha n}(\bar{r},\bar{x}_i)$ entre la particule alpha au point $\bar{r}$ et le nucléon i dans la cible au point $\bar{x}_i$, et du propagateur $f_{\alpha n}$ de la particule alpha :

$$f_{\alpha n}(E-E_m;\bar{r},\bar{r}') = \lim_{\varepsilon\to 0^+} \sum\!\!\!\!\!\!\int_a \frac{\varphi_a^*(\bar{r}')\varphi_a(\bar{r})}{E-E_m-\varepsilon_a+i\varepsilon} \tag{II.32}$$

Nous avons calculé ce propagateur à l'approximation eikonale qui, d'après les travaux de Bouyssy et al. [BO81,a], conduit à des résultats très proches de ceux obtenus à partir d'un calcul exact pour les énergies que nous considérons ici. Avec cette approximation, le propagateur $f_{\alpha n}$ s'écrit simplement comme le propagateur d'une onde plane de moment local k_m défini par :

$$k_m^2 = \frac{2\mu}{\hbar^2} (E - E_m - V_L(r)) \qquad (II.33)$$

où μ désigne la masse réduite du système α-noyau et V_L est le potentiel local équivalent au potentiel α-noyau non local donné par l'équation (II.2).

D'après l'équation (II.32), il est clair que la sommation sur les états m, eq.(II.31), doit être restreinte aux états d'énergie $E_m < E$ pour le calcul du potentiel imaginaire. Ainsi, à basse énergie peu d'états m peuvent contribuer au potentiel absorptif et nous en avons tenu compte explicitement. Par contre, à plus haute énergie le nombre de voies ouvertes est très important et nous avons appliqué la relation de fermeture sur les états excités du noyau, ce qui permet d'obtenir simplement, pour un grand nombre de noyaux, le potentiel ΔV partie réelle et partie imaginaire.

Le premier article que nous présentons ici, publié dans Physics Letters, relate brièvement notre calcul du potentiel absorptif α-^{40}Ca effectué à basse énergie dans le modèle RPA. Nous le développerons plus en détail dans ce chapitre. En outre, cet article supposant le moment local réel dans la dérivation du potentiel local équivalent, nous le compléterons ici par le calcul du potentiel local W comme nous l'avons expliqué précédemment. Le second article, publié dans Nuclear Physics, est consacré au calcul du potentiel ΔV à plus haute énergie et à l'étude détaillée de sa partie imaginaire.

1-Calcul du potentiel absorptif α-^{40}Ca à basse énergie

Les états excités ψ_m du calcium sont décrits dans le modèle RPA. Nous avons utilisé les états impairs calculés par Gillet et Sanderson [GI67] à partir de leur interaction nucléon-nucléon effective et les états pairs calculés par Bouyssy et al. [BO81,b] avec la même interaction résiduelle. Si nous appelons $\chi_{pt}^{(m)}$ et $\chi_{tp}^{(m)}$ les amplitudes RPA telles que l'indice p représente un état inoccupé dans l'état fondamental de Hartree-Fock et

t un état occupé, nous pouvons écrire schématiquement :

$$\langle\psi_m|V_{\alpha n}|\psi_0\rangle = \sum_{pt,m} (\chi^{(m)}_{pt} \langle(pt)|V_{\alpha n}|0\rangle + \chi^{(m)}_{tp} \langle(tp)|V_{\alpha n}|0\rangle)$$

Les fonctions d'onde individuelles sont celles d'un oscillateur harmonique dont le paramètre $b_0 = 1.93$fm est celui donné par Brink et Boeker,qui ont montré que cette valeur reproduit correctement l'énergie de liaison et le rayon du ^{40}Ca pour la force B_1 [BR67] .

Le potentiel imaginaire $W_N = Im\Delta V$, ainsi calculé,dépend des coordonnées $\bar{r}$ et $\bar{r}'$, distances entre les centres de masse de la particule alpha et du noyau cible. Pour le calcul du potentiel local aussi bien que pour dériver les propriétés globales du potentiel non local (paramètre de non localité, rayon),il est plus pratique de connaître W_N en fonction des coordonnées $\bar{R}$ et $\bar{s}$ telles que $\bar{R} = \frac{\bar{r}+\bar{r}'}{2}$, $\bar{s} = \bar{r}-\bar{r}'$. En utilisant la transformation de Moshinsky,nous avons ainsi écrit W_N en fonction de ces nouvelles coordonnées et obtenu le développement multipolaire du potentiel imaginaire non local sous la forme :

$$W_N(\bar{R},\bar{s}) = \sum_L W_{NL}(R,s)\, PL(\cos\Theta) \qquad (II.34)$$

où Θ désigne l'angle entre les deux vecteurs $\bar{R}$ et $\bar{s}$. Le potentiel $W_N(\bar{R},\bar{s})$ dépend de l'angle entre les deux vecteurs $\bar{R}$ et $\bar{s}$. Toutefois, une étude similaire du potentiel nucléon-^{40}Ca a montré que le terme $L = 0$ du développement, eq.(II.34), est dominant [VM76] . La structure des équations étant la même dans les deux études n-^{40}Ca et α-^{40}Ca, cette propriété doit se retrouver ici et nous pouvons alors écrire :

$$W_N(\bar{R},\bar{s}) \simeq W_{NO}(R,s) \equiv W_N(R,s)$$

$$= -\frac{\mu}{\pi\hbar^2} \sum_{\substack{m\neq 0 \\ E_m<E}} \frac{\sin k_m s}{s} \sum_{\substack{J \\ pt \\ p't'}} (\chi^{(m)}_{pt} + \chi^{(m)}_{tp})(\chi^{(m)}_{p't'} + \chi^{(m)}_{t'p'})$$

$$(-)^{\ell_p+\ell_{p'}+J} \hat{J}_p\hat{j}_t\hat{j}_{p'}\hat{j}_{t'}\hat{J}^2 \begin{Bmatrix} \ell_p & j_p & 1/2 \\ j_t & \ell_t & J \end{Bmatrix} \begin{Bmatrix} \ell_{p'} & j_{p'} & 1/2 \\ j_{t'} & \ell_{t'} & J \end{Bmatrix}$$

$$\sum_{\substack{n_1\ell N_1 L \\ n_1' N_1' L}} (-)^{\ell+L+\lambda} \hat{\lambda}^2 \begin{Bmatrix} \ell_p & \ell_{p'} & \lambda \\ \ell_{t'} & \ell_t & J \end{Bmatrix} F_{N_1N_1'L}(R) G_{n_1n_1'\ell}(s)$$

$$\langle n_1 \ell N_1 L\lambda | n_p\ell_p n_{p'}\ell_{p'}\lambda\rangle\langle n_1'\ell N_1' L\lambda | n_t\ell_t n_{t'}\ell_{t'}\lambda\rangle \qquad \text{(II.35)}$$

Dans cette équation, les symboles { } et < > désignent respectivement les coefficients 6-j de Wigner et les coefficients de Moshinsky, $\hat{j}$ est défini comme étant $\sqrt{2j+1}$ et les fonctions F et G sont données par les intégrales :

$$F_{N_1N_1'L}(R) = \frac{U_0a^2}{4R} \int_0^{+\infty} R'dR' e^{-\frac{2}{a^2}(R^2+R'^2)} \operatorname{sh}\left(\frac{4RR'}{a^2}\right) R_{N_1L}(R'\sqrt{2}) R_{N_1'L}(R'\sqrt{2})$$

$$G_{n_1n_1'\ell}(s) = \frac{U_0a^2}{s} \int_0^{+\infty} s'ds' e^{-\frac{1}{2a^2}(s^2+s'^2)} \operatorname{sh}\left(\frac{ss'}{a^2}\right) R_{n_1\ell}\left(\frac{s'}{\sqrt{2}}\right) R_{n_1'\ell}\left(\frac{s'}{\sqrt{2}}\right)$$

où U_0 et a sont les profondeur et portée de l'interaction α-nucléon gaussienne utilisée et les fonctions radiales $R_{n\ell}$ sont celles de l'oscillateur harmonique.

Alors que pour un nucléon incident, tous les états du noyau cible peuvent contribuer, la particule alpha ayant un spin et un isospin nuls, seuls les états excités de parité naturelle et d'isospin nul contribuent au potentiel α-^{40}Ca. Nous devons par conséquent nous attendre à une absorption

très faible et principalement concentrée à la surface,puisque les études portant sur le potentiel nucléon-^{40}Ca ont montré que les états excités RPA T=0 contribuent principalement à la surface.

Dans notre lettre à Physics Letters présentée ici, nous avons calculé le potentiel non local, eq.(II.35), pour le moment local k_m, eq.(II.33), supposé réel et déterminé à partir du potentiel réel approché par le premier terme $V^{(0)}$ de l'équation (II.2), de telles approximations étant utilisées couramment pour l'étude du potentiel nucléon-noyau. Dans ces premiers calculs, le potentiel $V^{(0)}$ était remplacé par la partie réelle du potentiel phénoménologique A de Delbar et al.[DE78],qui est très proche du potentiel calculé dans notre article précédent pour l''interaction B_1 de Brink et Boeker. Nous avons montré que la contribution au potentiel non local $W_N(R,s)$, s = 0fm, calculé à l'énergie de la particule alpha incidente E = 30MeV, est principalement engendrée par les états $J = 0^+$ pour la partie interne et les états $J = 3^-$ à la surface. Ces résultats sont en accord avec ceux obtenus récemment par Dermawan et al [DE82,a] dans le même modèle que le nôtre et à la même énergie. Toutefois,leur potentiel non local est moins profond,en particulier pour l'état $J = 0^+$. Notre absorption très élevée à petites distances peut être expliquée par le fait que le potentiel $V^{(0)}$ est très profond au voisinage de l'origine, en particulier comparé au potentiel nucléon-noyau ou au potentiel α-noyau utilisé par Dermawan et al. En effet, le potentiel absorptif est,aux faibles valeurs de s,très sensible au potentiel réel puisque,pour s = 0fm,W_m se comporte comme k_m donc une réduction importante du potentiel réel diminuerait probablement la profondeur du potentiel absorptif.

Nous avons examiné l'influence du potentiel réel sur nos résultats en reprenant le calcul du potentiel non local pour le potentiel $V^{(0)}$, résultant de la convolution de l'interaction α-nucléon gaussienne utilisée ici par la densité d'oscillateur harmonique du ^{40}Ca. Ce nouveau potentiel,appelé $V'^{(0)}$, est nettement plus profond au voisinage de zéro que le potentiel utilisé dans notre lettre à Physics Letters (environ 300 MeV à l'origine au lieu

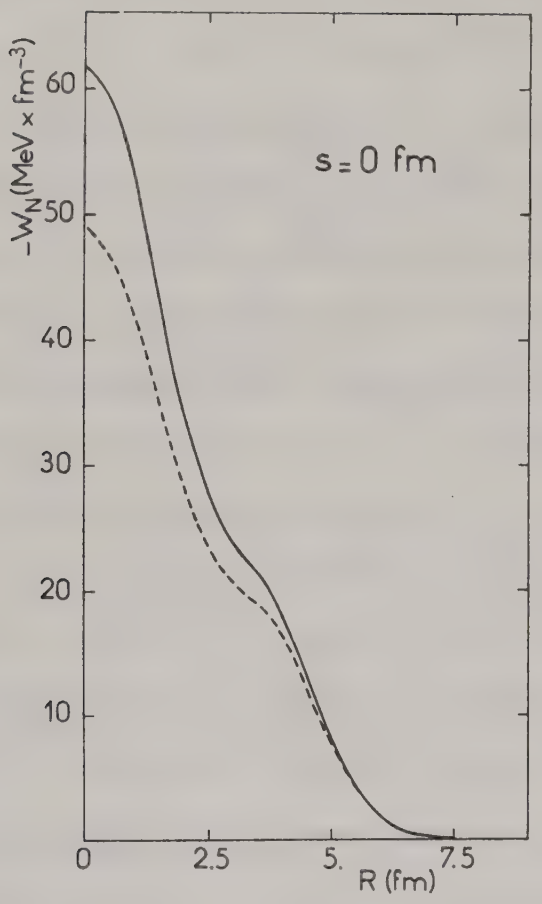

Fig.1 : Potentiel non local $W_N(R,s)$, s = 0fm à 30MeV calculé pour les potentiels réels $V'^{(0)}$(—) et $V^{(0)}$(--).

de 200 MeV) et, d'après la figure 1 où nous comparons les potentiels $W_N(R,s)$, s = 0fm obtenus à 30 MeV pour $V^{(0)}$ et $V'^{(0)}$, rend le potentiel non local W_N plus profond à petites distances, les résultats étant proches à la surface.

D'autre part, notre première étude montre que le potentiel non local W_N présente de nombreuses oscillations en fonction de la variable s. Ces oscillations, engendrées par la fonction de Green du propagateur de la particule alpha, ont également été mises en évidence dans les travaux de Dermawan et al. Bien que la partie non oscillante du potentiel puisse, pour chaque valeur de R, être représentée par une gaussienne dont la non localité est faible comparée à la portée du potentiel, il n'est pas clair que l'approximation du Perey-Saxon convienne à notre potentiel non local, en particulier aux faibles valeurs de R où les amplitudes des oscillations en fonction de

s sont les plus fortes. En particulier, l'étude récente de Dermawan et al. [DE82,b] semble indiquer que l'approximation du potentiel imaginaire non local par un potentiel local conduit à une surestimation des sections efficaces aux angles arrières, donc à une absorption sous-estimée, mais, du fait que leur potentiel local a été déterminé à partir du potentiel non local sous sa représentation gaussienne, les divergences observées entre les sections efficaces calculées à 30 MeV peuvent provenir en partie de la troncation de la partie oscillante du potentiel. Toutefois, notre première étude du potentiel non local supposait le moment local k_m réel et si nous travaillons par contre avec le moment local complexe défini à partir du potentiel α-noyau total V_L, chaque terme $-\frac{\sin k_m s}{s}$ de la sommation sur m, eq.(II.35), devient $\frac{\sin \mathrm{Re} k_m s}{s} e^{-\mathrm{Im} k_m s}$. Le potentiel non local ainsi obtenu W'_N a la même structure que W_N au terme exponentiel près donc présente également des oscillations en fonction de s, mais plus atténuées du fait de la présence du facteur amortissant $e^{-\mathrm{Im} k_m s}$. L'effet de cet amortissement devrait principalement jouer pour les états 3^-, qui engendrent un potentiel non local dont les oscillations s'étendent jusqu'à des valeurs de s élevées, et nous pouvons alors espérer des résultats plus réalistes en reprenant le calcul du potentiel local équivalent au potentiel α-noyau non local, eq.(II.2), pour le moment local k défini également à partir du potentiel α-noyau complexe V_L. Reprenant les notations introduites au début du chapitre, nous désignerons par U et W la partie réelle et la partie imaginaire du potentiel α-noyau à son approximation locale V_L. D'après notre étude précédente, les potentiels U et W sont solutions du système d'équations couplées (II.17-18), écrites pour les potentiels non locaux réel U_N et imaginaire W'_N et où le moment k est donné par la relation :

$$k^2 = \frac{2\mu}{\hbar^2} (E - U - iW) \qquad \text{(II.36)}$$

Dans toute l'étude qui suit, nous avons remplacé le potentiel U_N par le premier terme de l'équation (II.2) (indépendant de k_m), calculé comme

précédemment pour la force B_1 mais où la densité du ^{40}Ca est maintenant une densité d'oscillateur harmonique de paramètre $b_0 = 1.93fm$. Cette approximation est justifiée dans la suite de notre exposé où nous montrerons que le terme négligé $Re\Delta V$ est très faible. Nous avons calculé les potentiels U et W simultanément par itération à partir du système de solutions initiales $U = U_0$, $W = W_0$, où U_0 et W_0 désignent respectivement les potentiels réel et imaginaire obtenus en supposant les moments locaux k_m et k, eqs.(II.33-36), réels. Les résultats obtenus montrent que le potentiel U est proche de U_0, mais par contre le potentiel W est différent de W_0. Les potentiels W et W_0, calculés

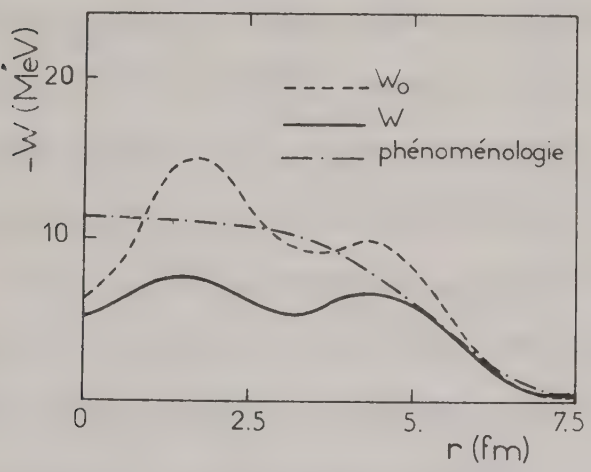

Fig.2 : Comparaison des potentiels locaux W et W_0 calculés à 30 MeV à la phénoménologie.

à l'énergie E = 30 MeV, sont présentés dans la figure 2 et comparés à la partie imaginaire du potentiel phénoménologique A de Delbar et al. à la même énergie. Le potentiel appelé ici W_0 est celui présenté dans notre lettre à Physics Letters. Nous observons, pour nos deux potentiels W et W_0, une forte absorption en volume due à la forte profondeur du potentiel réel U, cependant la validité de nos approximations étant douteuse, nous n'attachons pas une grande crédibilité aux résultats obtenus pour $r \leqslant 2fm$. A la surface où le potentiel non local a un comportement en s plus régulier, W est nettement plus faible que W_0 et en meilleur accord avec la phénoménologie.

Nous avons examiné la dépendance en énergie de notre potentiel qui, d'après l'équation (II.35), résulte à la fois de l'ouverture progressive des canaux inélastiques, soumise à la condition $E_m<E$, de la dépendance en moment k_m et de la non localité du potentiel W_N. Le potentiel W, calculé

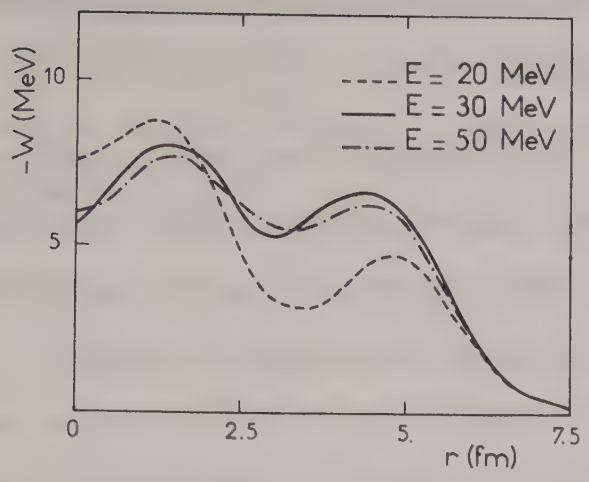

Fig.3 : Potentiel local W calculé pour différentes énergies

aux énergies E= 20, 30 et 50 MeV,est présenté dans la figure 3. Nous observons une forte croissance de l'absorption à la surface du noyau jusqu'à 30 MeV, suivie d'une dépendance en énergie plus douce au-delà de cette valeur pour laquelle les états RPA les plus collectifs peuvent contribuer au potentiel imaginaire. Nous retrouvons la même tendance pour l'intégrale de volume par paires de nucléon : J_W = 27, 35 et 35 MeV fm^3, que nous pouvons directement comparer aux intégrales de volume phénoménologiques : J_W=36, 46 et 71 MeV fm^3, déduites du potentiel A de Delbar et al. (ou du potentiel de Michel et Vanderpoorten [MI77] qui conduit aux mêmes valeurs de J_W). Nos intégrales de volume, bien que plus faibles, sont en relativement bon accord avec la phénoménologie jusqu'à 30 MeV puis l'accord se détériore au-delà de cette énergie, comme nous l'avions déjà constaté dans notre première étude du potentiel W_0. En effet,nos intégrales de volume se stabilisent au-delà de 30 MeV, alors que la phénoménologie prévoit une forte croissance de J_W jusqu'à l'énergie E = 100 MeV. Ce désaccord au-delà de 30 MeV est dû probablement à notre troncation de la base particule-trou,ainsi qu'à notre modèle qui néglige les voies de break-up de la particule alpha ou du noyau cible qui deviennent importantes à ces énergies.

2-Calcul du potentiel absorptif α-noyau et de la correction au modèle de convolution aux énergies intermédiaires

Un calcul analogue à celui effectué précédemment reste en principe possible,mais devient vite inextricable étant donné le grand nombre de voies de réaction ouvertes. Dans l'article que nous présentons maintenant, nous nous intéressons principalement aux propriétés globales du potentiel ΔV, second membre de l'équation (II.2), et avons évité une sommation explicite sur les voies ouvertes en faisant des approximations nous permettant d'utiliser la relation de fermeture sur les états m du noyau cible. Nous devons alors supposer que l'énergie de la particule alpha incidente est suffisamment élevée pour que toutes les voies ayant une forte contribution soient physiquement ouvertes. Le potentiel ΔV peut être alors calculé très simplement pour tous les noyaux,puisque son expression finale ne dépend que des densités locales et non locales à un corps du noyau cible et du paramètre $\overline{E_m}$, représentant l'énergie moyenne des états fortement excités du noyau, paramètre que nous avons fait varier en fonction du noyau considéré. Dans cet article,le calcul du potentiel local équivalent est effectué selon la méthode exposée au début de ce chapitre.

Nous avons pu ainsi dériver un grand nombre de propriétés du potentiel imaginaire, sa variation en fonction de l'énergie et du noyau cible,et montrer que les corrections au potentiel réel du modèle de convolution n'excèdent jamais 5%. Nous avons pu ainsi reproduire les propriétés globales des potentiels phénoménologiques au-delà de 80-100 MeV, notamment leur forme, leur dépendance en énergie et en nombre de nucléons A du noyau, en particulier en ce qui concerne les fluctuations entre noyaux à couches fermées et noyaux adjacents à couches ouvertes. Toutefois, nos potentiels manquent d'absorption à la surface, ce qui pourrait être expliqué, du moins partiellement, par le fait que notre modèle néglige les voies correspondant au break-up de la particule alpha qui sont importantes à ces énergies et

qui contribueraient principalement dans la région de surface. En effet, nous verrons, dans le chapitre suivant, qu'ajouter un terme de surface très faible à notre potentiel absorptif suffit pour bien reproduire la diffusion élastique (α,α).

REFERENCES

[BE79] V. Bernard and Nguyen Van Giai, Nucl. Phys. A327(1979) 397

[BI73] L. Bimbot, B. Tatischeff, I. Brissaud, Y. Le Bornec, N. Frascaria and A. Willis, Nucl. Phys. A210(1973) 397.

[BO81,a] A. Bouyssy, N. Vinh Mau and D.M. Brink, Phys. Lett. 102B(1981) 109.

[BO81,b] A. Bouyssy, H. Ngô and N. Vinh Mau, Nucl. Phys. A371(1981) 173.

[BR67] D.M. Brink and E. Boeker, Nucl. Phys. A91(1967) 1.

[DE78] T. Delbar, G. Grégoire, G. Paic, R. Ceuleneer, F. Michel, R. Vanderpoorten, A. Budzanowski, H. Dabrowski, L. Freindl, K. Grotowksi, S. Micek, R. Planeta, A. Strzalkowski and K.A. Eberhard, Phys. Rev C18(1978) 1237.

[DE82,a] H. Dermawan, F. Osterfeld and V.A. Madsen Phys. Rev. C25(1982) 180.

[DE82,b] H. Dermawan, F. Osterfeld and V.A. Madsen, preprint Jülich.

[FA82] S. Fantoni, B.L. Friman and V.R. Pandharipande Phys. Lett. 104B(1981) 89.

[FI66] H. Fiedeldey, Nucl. Phys. 77(1966) 149.

[FR65] W.E. Frahn, Nucl. Phys. 66(1965) 358.

[GI67] V. Gillet and E.A. Sanderson, Nucl. Phys. A91(1967) 292.

[JA74] D.F. Jackson and R.C. Johnson, Phys. Lett. 49B(1974) 249.

[LA78] M. Lassaut, Thèse de troisième cycle, Université Paris VII (1978).

[LA80] M. Lassaut and N. Vinh Mau, Nucl. Phys. A349(1980) 372.

[MI77] F. Michel and R. Vanderpoorten, Phys. Rev. C16(1977) 142.

[NE82] J.W. Negele and K. Yasaki, Phys. Rev. Lett. 47(1981) 71.

[PE82] F. Perey and B. Buck, Nucl. Phys. 32(1962) 353.

[PE64] F. Perey and D.S. Saxon, Phys. Lett. 10(1964) 107.

[PE80] R.E. Peierls and N. Vinh Mau, Nucl. Phys. A343(1980) 1.

[VM76] N. Vinh Mau and A. Bouyssy, Nucl. Phys. A257(1976) 189.

[VM78] N. Vinh Mau, Proc. Second Louvain Cracow Seminar on the Alpha Nucleus Interaction, Louvain-la-Neuve, 1978, ed. G. Gregoire and K. Grotowksi, p. 243.

Volume 105B, number 4 PHYSICS LETTERS 8 October 1981

A MICROSCOPIC CALCULATION OF ABSORPTION IN LOW-ENERGY ALPHA–^{40}Ca SCATTERING

M. LASSAUT

Division de Physique Théorique[1], *Institut de Physique Nucléaire, F-91406 Orsay Cédex, France*

Received 17 December 1981
Revised manuscript received 20 July 1981

The effective α–^{40}Ca imaginary potential is calculated for incident energies $20 < E_\alpha < 50$ MeV from a microscopic α–nucleon interaction. The excited states of the ^{40}Ca are described in the RPA model. The resulting local equivalent potential, calculated from the non-local one in the Perey–Saxon approximation, is compared to phenomenology.

Most of the theoretical calculations of the α–nucleus optical potential are carried out by folding an α–nucleon interaction into the target density [1–3]. This latter interaction is either deduced from phenomenological analyses [4–7] or is derived by folding a nucleon–nucleon interaction into the α-particle density [8–10], which is equivalent to a double folding calculation of the α–nucleus potential. However, at low energy the α–nucleon interaction is real so that this model leads to a real α–nucleus potential only and is unable to explain the absorptive part of the potential. Recently, Vinh Mau [11] has derived both the real and the imaginary part of the α–nucleus interaction in a model where the folding term is the lowest-order approximation. Nevertheless, using a closure relation for the intermediate states of the target nucleus, this work cannot be applied at low energy where only a few inelastic channels are opened. In the present work, we report a microscopic calculation of the α–^{40}Ca imaginary potential, following the model of Vinh Mau [11] but evaluating explicitly the contribution of each RPA excited states involved in our calculation.

As in ref. [11], the derivation of the α–^{40}Ca imaginary potential relies on the assumption that the α-particle is an elementary particle. This hypothesis is reasonable since the α-particle has a large binding energy and a small radius and allows us to make a formal identification of the α–^{40}Ca potential with the nucleon–^{40}Ca one when the nucleon–nucleon interaction in the latter is replaced by the α–nucleon potential. Nevertheless, as the α-particle is considered as a particle it is distinguishable from the nucleons of the target and there is no exchange term between target and projectile arising in the calculation. Therefore, following Feshbach [12], we write:

$$
\begin{aligned}
V_{\alpha-^{40}\mathrm{Ca}} &= V_{\alpha\mathrm{N}} = V^{(0)}_{\alpha\mathrm{N}} + \Delta V_{\alpha\mathrm{N}} \\
&= \langle\Psi_0| \sum_i V_{\alpha\mathrm{n}}(i) |\Psi_0\rangle \\
&+ \sum_{M\neq 0} \lim_{\epsilon\to 0^+} \sum\!\!\!\!\!\!\int_a \langle\Psi_0| \sum_i V_{\alpha\mathrm{n}}(i) |\Psi_M \varphi_a\rangle \\
&\times \langle\varphi_a \Psi_M| \sum_j V_{\alpha\mathrm{n}}(j) |\Psi_0\rangle (E_\alpha + \mathrm{i}\epsilon - \epsilon_a - E_M)^{-1},
\end{aligned}
\tag{1}
$$

where $V_{\alpha\mathrm{n}}(i)$ represents the interaction between the α-particle and the nucleon i in the ^{40}Ca, Ψ_0 is the ground-state wavefunction of the ^{40}Ca, Ψ_M and E_M the wavefunction and energy of its excited states M, φ_a and ϵ_a the wavefunction and energy of the α-particle in the intermediate state a and E_α represents the c.m.-energy of the incident α-particle. The first term of eq. (1) $V^{(0)}_{\alpha\mathrm{N}}$ is real for incident energies E_α below 100 MeV and corresponds to the usual folding-

[1] Laboratoire associé au CNRS.

0 031-9163/81/0000--0000/$ 02.75 © 1981 North-Holland

model potential. The second-order term $\Delta V_{\alpha N}$ is complex: its real part constitutes a small correction to $V^{(0)}_{\alpha N}$ and its imaginary part generates the absorptive term of the α–^{40}Ca potential. In our derivation of the imaginary potential $W = \mathrm{Im}\,\Delta V_{\alpha N}$ we have made the additive assumptions:

(i) φ_a, wavefunction of the α-particle in the field of the nucleus therefore the solution of the Schrödinger equation for a potential assumed to be $V^{(0)}_{\alpha N}$, is calculated in the eikonal approximation which here is not reduced to its lowest-order term as it was in refs. [11,13].

(ii) The α–nucleon interaction is the local potential derived in a previous work [14] from the B_1 and C_1 forces of Brink and Boeker [15] and parametrized as a gaussian

$$V_{\alpha N} = -V_0 \exp[-(r/a_0)^2], \qquad (2)$$

with $V_0 = 47.3$ MeV, $a_0 = 1.97$ fm for B_1 and $V_0 = 55.6$ MeV, $a_0 = 1.71$ fm for C_1.

Now, if we restrict the summation over the excited states M of the ^{40}Ca to the RPA excited states, the function W is expressed in terms of χ^M_{ph} and χ^M_{hp} the particle–hole and hole–particle amplitudes which have been calculated with harmonic oscillator wavefunctions. A product of two such harmonic oscillator wavefunctions for two particles situated at r and r' can be expanded, via the Moshinsky transformation, as a sum of products of two harmonic oscillator wavefunctions expressed in terms of the coordinates R and s defined as

$$R = \tfrac{1}{2}(r + r'), \quad s = r - r'. \qquad (3)$$

Using the approximations (i) and (ii) quoted above, we are led to the following form for W:

$$W(R,s) = \sum_L W_L(R,s) P_L(\cos\theta), \qquad (4)$$

where θ denotes the angle between the two vectors R and s.

The potential $W(R,s)$ depends on the angle between the vectors R and s. However, it has been shown [16] in the neutron–^{40}Ca case that the terms $L > 0$ in the summation are much smaller than the first term $L = 0$, due to the properties of the angular-momentum coupling coefficients involved in the term $W_L(R,s)$. Assuming that the same property still holds in the α–^{40}Ca case as well, we have restricted our calculation to the first term W_0 and written: $W(R,s) \approx W_0(R,s)$.

The potential W includes the momentum k_M:

$$k^2_M = (2\mu/\hbar^2)[E_\alpha - V^{(0)}_{\alpha N}(R) - E_M], \qquad (5)$$

where μ is the reduced mass of the α–^{40}Ca system. The potential $V^{(0)}_{\alpha N}$ used here is the real part of the phenomenological potential of Delbar et al., labelled A in ref. [17].

The explicit calculation of W shows that the imaginary potential is non-local and energy dependent. Moreover the summation over the excited states M, see eq. (1), is for the imaginary potential restricted to the state $E_M \leqslant E_\alpha$. Therefore the energy dependence of W results from the superposition of two effects: (1) the progressive opening of the inelastic channels due to the condition $E_M \leqslant E_\alpha$ which makes the potential more absorptive as E_α increases and (2) the variation of k_M, eq. (5), with the energy which is much smoother than the previous one. We thus expect a large energy dependence at low energy, followed by a flattened energy dependence above 35–40 MeV when all the RPA excited states are included in the summation.

We report first some results about the α–^{40}Ca imaginary potential calculated at 29 MeV laboratory energy. The RPA energies E_M and amplitudes χ^M_{ph}, χ^M_{hp} are taken from the work of Gillet and Sanderson [18] for the odd-parity states and for the even-parity states we have used the energies and amplitudes calculated with the same Gillet–Sanderson nucleon–nucleon interaction. The α–nucleon interaction used here is this one derived from the B_1 force. It is close to the effective α–nucleon interaction derived by Bimbot et al. [19] which yields a good reproduction of inelastic cross sections for the low-lying collective states of the ^{40}Ca. The evaluation of W requires also the knowledge of the harmonic oscillator parameter for the ^{40}Ca. We have taken $b = 1.93$ fm from the work of Brink and Boeker [15] who have shown that this value reproduces correctly the binding energy and the radius of the ^{40}Ca when the B_1 force is used [15].

We have examined the contributions to the non-local potential arising from the different multipoles. Since the α-particle has spin and isospin zero, only the natural parity $T = 0$ RPA states have to be taken into account. In the RPA spectrum, we have omitted the lowest 1^- $T = 0$ state which is the spurious state

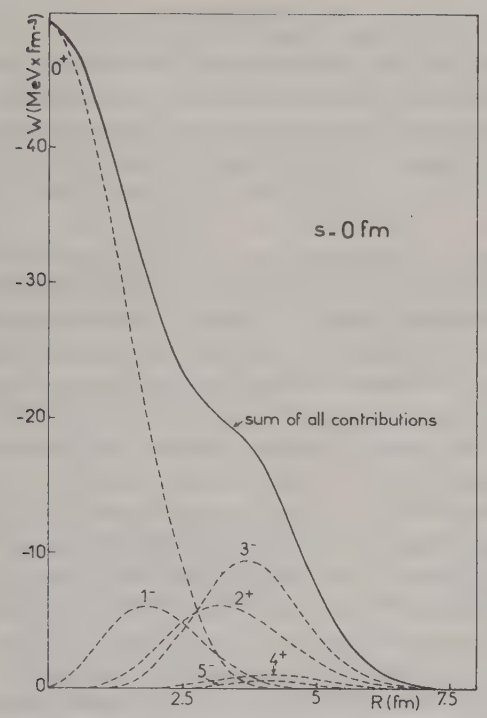

Fig. 1. Non-local potential $W(R,s)$ at $s = 0$ fm calculated at 29 MeV laboratory energy (solid line) and its component parts due to the different multipoles J^{π} (dashed lines).

due to center of mass motion. The non-local potential $W(R,s)$ calculated at $s = 0$ fm and at 29 MeV laboratory energy is displayed in fig. 1 with its component parts generated by the different multipoles. Fig. 1 shows that the major contribution to the optical potential is carried by the states $J = 0^+$ in the interior and by the states $J = 3^-$ at the surface. The two multipoles $J = 1^-$ and $J = 2^+$ give a weaker but sizeable contribution to the non-local potential while the remaining multipoles $J = 4^+$ and $J = 5^-$ lead to an almost negligible contribution.

These results are similar to those recently acquired by Dermawan et al. [20] who have calculated the α–^{40}Ca imaginary potential at 31 and 100 MeV laboratory energy in the same model as we. Nevertheless they get a lower potential mainly for the $J = 0^+$ state. It could be explained by the fact that the potential $V_{\alpha N}^{(0)}$ is very deep. Indeed, we have checked numerically that the imaginary potential W is very sensitive to $V_{\alpha N}^{(0)}$ and is the more absorptive as $V_{\alpha N}^{(0)}$ is deep.

We have examined the s-dependence of the non-local potential $W(R,s)$. In fig. 2 we have drawn the calculated potentials for, respectively, $R = 0$, 2 and 4 fm. One sees that for all values of R the potential W presents many oscillations which are more important at small R. Consequently defining a non-locality range for the potential according to the relation [16]

$$W(R,s) = W(R,s = 0 \text{ fm}) \exp(-s^2/\beta_R^2), \qquad (6)$$

is somewhat ambiguous. Nevertheless for the non-oscillating part of the potential, we get, respectively, $\beta = 0.37$, 0.40 and 0.54 fm for $R = 0$, 2 and 4 fm. Although this non-locality range is weak as compared to the range of the potential we cannot conclude, referring to the work of Peierls and Vinh Mau [21], that the Perey–Saxon approximation [22] constitutes a good approach to the non-local potential because of the oscillations which extend to quite large values of s. The presence of such oscillations makes the use of the Perey–Saxon method questionable,

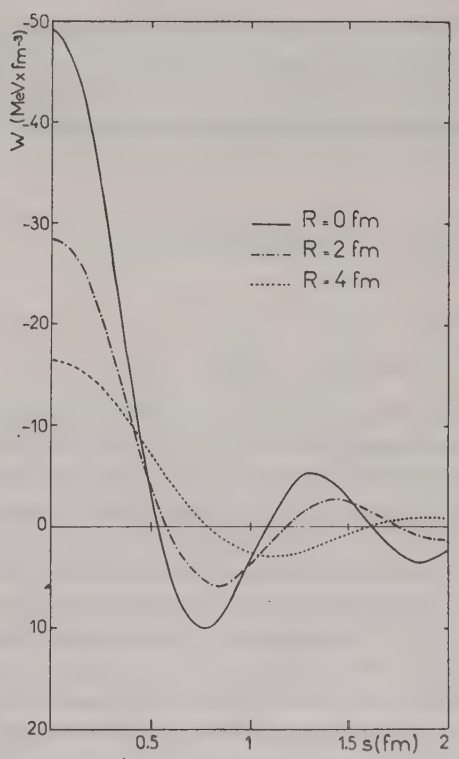

Fig. 2. Non-local potential $W(R,s)$ calculated at $E_{\alpha}^{\text{lab}} = 29$ MeV as a function of s for different values of R.

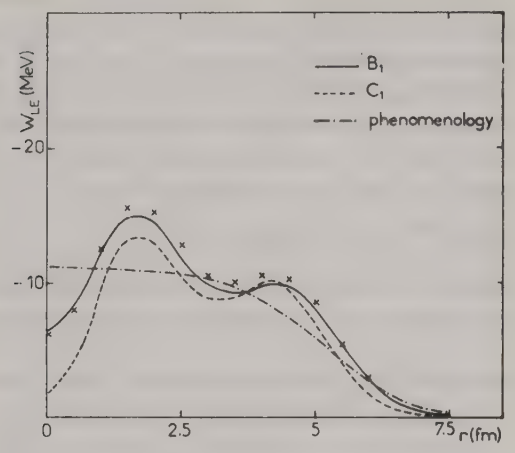

Fig. 3. Comparison of the local potentials W_{LE} calculated at 29 MeV laboratory energy with the α–nucleon interactions derived from the B_1 and C_1 forces with the imaginary part of the phenomenological potential A of ref. [17] at the same energy. The crosses correspond to a calculation including the Coulomb potential (see text).

at least at low values of R where their amplitudes are the largest relatively to the depth of the potential at $s = 0$ fm. This is illustrated by studying the non-local potential W' generated by the multipole $J = 3^-$ and its local equivalent potential defined by

$$W_{LE}(r) = 4\pi \int_0^{+\infty} j_0(kr) W(r, s) s^2 \, ds, \tag{7}$$

where

$$k^2 = (2\mu/\hbar^2)[E_\alpha - V_{\alpha N}^{(0)}(r)]. \tag{8}$$

At small values of R ($R < 1$ fm) W' is very weak (it represents 0.5% of the total potential W) and oscillates for large values of s but, unlike the total non-local potential, it is vanishingly small between $s = 0$ and $s = 2.5$ fm. However, for such a non-local potential the Perey–Saxon approximation induces a strongly repulsive local equivalent potential (9.7 MeV deep) when $R < 1$ fm which does not seem very realistic to us. Nevertheless at large R the oscillations of the total non-local potential have a weak amplitude as compared to the strength of $W(R, s)$ at $s = 0$ fm and one can expect that in this case the Perey–Saxon approximation is more adequate.

The total potential W_{LE} calculated at 29 MeV laboratory energy is displayed in fig. 3, with, for comparison, the imaginary part of the potential A of Delbar et al. [17]. The crosses refer to a calculation where the Coulomb potential, which is the potential due to an uniformly charged sphere of radius $1.4 \times A^{1/3}$ fm ($A = 40$), is added to the potential $V_{\alpha N}^{(0)}$ in eqs. (5) and (8). One sees that the introduction of the Coulomb potential does not affect the results which has been observed also for the non-local potential W. To test the influence of the α–nucleon interaction on the imaginary potential, we have also reported in fig. 3 the results arising when the C_1 force (with the corresponding harmonic-oscillator parameter for the ^{40}Ca) is used throughout the whole calculation instead of the B_1 force. We observe for both microscopic potentials a dip at the origin, which we think to be a spurious effect due to the contribution of 3^- states as discussed above, and an important surface effect generated by the strongly collective 3^- states and the 2^+ giant quadrupole resonance. The C_1 force leads to a shallower potential than B_1 in the interior but the potentials are very close to each other at the surface. At the energy considered, both potentials are in relatively good agreement with the phenomenology. However, our potentials are deeper than the microscopic potential derived by Dermawan et al. [20]. It could be explained as previously by our choice of the potential $V_{\alpha N}^{(0)}$. Moreover, our local potential W_{LE} is overestimated due to the approximation used in the derivation of the local equivalent potential, which consists in neglecting the imaginary part of the local momentum [23,24].

We have looked at the energy dependence of the potential by studying the variation with the energy of its volume integral. The volume integral per nucleon pair J of our microscopic potential derived from the B_1 force is compared to that of the phenomenological potential A of Delbar et al. [17] or equivalently the phenomenological potential of Michel and Vanderpoorten [25], both predicting the same volume integral. We get $J = 39$ and 51 MeV fm^3 at laboratory energies 20 and 29 MeV, respectively, which is in agreement with the phenomenological values $J = 36$ and 46 MeV fm^3. However, this agreement deteriorates at higher energies since J saturates ($J = 50$ and 49 MeV fm^3 at laboratory energies 40 and 50 MeV) due to the fact that at 29 MeV the most collective RPA channels are opened while phenomenol-

ogy predicts an increase of J until $E_{\alpha}^{\mathrm{lab}} = 100$ MeV ($J = 59$ and 71 MeV fm^3 at 40 and 50 MeV). This disagreement above 29 MeV is certainly due to our truncation of the particle–hole basis as well as our neglect of all the channels corresponding to a break-up of the projectile or target which become important at those energies.

I am very grateful to N. Vinh Mau for many suggestions and discussions and for her critical reading of the manuscript. I am also thankful to H. Ngô for communicating to me the energies and amplitudes of the even-parity RPA states.

References

[1] B. Sinha, Phys. Rep. 20C (1975) 1.
[2] R.C. Barrett and D.F. Jackson, Nuclear sizes and structure (Clarendon, Oxford, 1977).
[3] G.R. Satchler and W.G. Love, Phys. Rep. 55C (1979) 183.
[4] J.S. Lilley, Phys. Rev. C3 (1971) 2229.
[5] P. Mailandt, J.S. Lilley and G.W. Greenlees, Phys. Rev. C8 (1973) 2189.
[6] A.M. Bernstein, Advances in nuclear physics, eds. M. Baranger and E. Vogt, Vol. 3 (Plenum, New York, 1969) p. 325.
[7] C.J. Batty, E. Friedman and D.F. Jackson, Nucl. Phys. A175 (1971) 1.
[8] I. Brissaud and B. Tatischeff, Nucl. Phys. A155 (1970) 89.
[9] A. Budzanowski, A. Dudek, K. Grotowski and A. Strzalkowski, Phys. Lett. 32B (1970) 431.
[10] G.M. Lerner, J.C. Hiebert, L.L. Rutledge and A.M. Bernstein, Phys. Rev. C6 (1972) 1254.
[11] N. Vinh Mau, Phys. Lett. 71B (1977) 5;
N. Vinh Mau, Proc. Second Louvain–Cracow Seminar on the Alpha–nucleus interaction (Louvain-la-Neuve, 1978), eds. G. Gregoire and K. Grotowski, unpublished, p. 243.
[12] H. Feshbach, Ann. Phys. 5 (1958) 357.
[13] A. Bouyssy and N. Vinh Mau, private communication.
[14] M. Lassaut and N. Vinh May, Phys. Lett. 70B (1977) 14; Nucl. Phys. A349 (1980) 372.
[15] D.M. Brink and E. Boeker, Nucl. Phys. A91 (1967) 1.
[16] N. Vinh Mau and A. Bouyssy, Nucl. Phys. A257 (1976) 189.
[17] T. Delbar et al., Phys. Rev. C18 (1978) 1237.
[18] V. Gillet and E.A. Sanderson, Nucl. Phys. A91 (1967) 292.
[19] L. Bimbot et al., Nucl. Phys. A210 (1973) 397.
[20] H. Dermawan, F. Osterfeld and V.A. Madsen, Phys. Rev. C, to be published.
[21] R.E. Peierls and N. Vinh Mau, Nucl. Phys. A343 (1980) 1.
[22] F. Perey and D.S. Saxon, Phys. Lett. 10 (1964) 107.
[23] J.W. Negele and K. Yazaki, Phys. Rev. Lett. 47 (1981) 71.
[24] S. Fantoni, B.L. Friman and V.R. Pandharipande, preprint Urbana.
[25] F. Michel and R. Vanderpoorten, Phys. Rev. C16 (1977) 142.

Nuclear Physics **A391** (1982) 118–136
© North-Holland Publishing Company

THE IMAGINARY PART OF THE LOCAL POTENTIAL EQUIVALENT TO THE NON-LOCAL α-NUCLEUS OPTICAL POTENTIAL

M. LASSAUT and N. VINH MAU

Division de Physique Théorique †, *Institut de Physique Nucléaire, F-91406, Orsay Cedex, France*

Received 1 June 1982

Abstract: A simple expression of the α-nucleus optical potential has been derived from the Feshbach formula by using a closure approximation for summing over the excited states of the target nucleus. It has been shown that the correction to the real folding model potential is small. The imaginary local potential equivalent to the non-local Feshbach potential has been studied in detail for Ca nuclei and shown to reproduce quite well the gross properties of empirical potentials above 100 MeV with, however, a lack of absorption in the surface region. The A-dependence of the imaginary potential volume integral has also been investigated.

1. Introduction

Even though a great effort has been put into microscopic calculations of the real part of α-nucleus potentials – or in general nucleus-nucleus potentials – very few attempts to investigate its imaginary part have been carried out. Most works on the real part rely on the double folding model with or without one-nucleon exchange, few use the resonating group method or Hartree-Fock-like model, with all of these models leading to a purely real potential. Recently simplified models have been proposed to derive the imaginary part of the α-nucleus potential. The first one, is based on Feshbach's formula simplified by several assumptions [1]: the α-particle intermediate-state wave function was approximated by the first-order term of an eikonal expansion, closure relation was used to sum over intermediate states of the nucleus, the α-nucleon interaction was assumed to be local and gaussian, and an equivalent local potential was calculated with the Perey-Saxon approximation with a purely real local momentum. Another model has been proposed for the heavy ion potential [2] based on Feynman's path integral method and applied recently to the α-nucleus potential. In the latter paper this model is shown to be equivalent to a semi-classical approximation of Feshbach's formula and therefore is conceptually close to the former model that we are using in the present paper. For heavy ions, the imaginary potential has been recently studied in a nuclear matter approach [3] but this derivation is not very suitable for a light nucleus like the α-particle.

In the present paper, we follow the model of ref. [1]. The α-nucleus potential is a sum of

† Laboratoire associé au CNRS.

two terms, the antisymmetrized double folding real term which has been studied in details in a previous paper [4]) and a second term correcting the real first-order term and generating the imaginary potential. The correction to the real potentials is weak [1]) and will be studied only briefly while the imaginary potential will be discussed in detail. Two of the approximations used in ref. [1]) are reconsidered. As shown in ref. [5]) the assumption that the eikonal expansion of the α-particle wave function can be reduced to its first-order term is unnecessary and in the Feshbach formula the α-particle propagator can be replaced directly by the most general eikonal propagator, avoiding any expansion of the wave function. This α-particle eikonal propagator was shown to be a very good approximation to the exact one for energies considered in this work. On the other hand, the α-particle local momentum which is related to the α-nucleus potential was assumed to be real and defined by the double folding model term alone. This local momentum appears in the α-particle eikonal propagator, and therefore in the calculation of the non-local potential and in the derivation of the local equivalent potential. It has already been pointed out [5]) that the imaginary potential calculated with a real momentum was strongly absorptive and therefore inconsistent with the starting assumption. In the case of the nuclear matter nucleon-nucleus potential, the effect of taking a complex local momentum has been recently studied in two papers [6,7]) and shown to reduce the nucleon imaginary potential by a factor m^*/m, where m^* and m are respectively the effective and free nucleon-mass. Therefore we take into account the imaginary part of the local momentum and study the modification of the imaginary local potential.

In sect. 2, we briefly recall the calculation of the second term of Feshbach's formula. In sect. 3 we discuss the derivation of a local potential equivalent to the non-local real and imaginary potentials. The potentials obtained for alpha-calcium scattering at energies higher than 50 MeV are presented in sect. 4. At the end of this section we discuss the variation of our imaginary potential as a function of A, the mass number of target nucleus.

2. Derivation of the non-local potential

Let us write the Feshbach potential as:

$$V = V^{(0)} + \Delta V. \tag{1}$$

$V^{(0)}$ is the antisymmetrized double folding potential with a local and a non-local term. If in intermediate states the system is formed of the α-particle in a state a and the target nucleus in an excited state n, ΔV can be written:

$$\Delta V(\boldsymbol{r}, \boldsymbol{r}') = \sum_{n \neq 0} \langle 0| \sum_{i=1}^{A} v(\boldsymbol{r}, \boldsymbol{x}_i)|n\rangle\langle n| \sum_{i=1}^{A} v(\boldsymbol{r}', \boldsymbol{x}_i')|0\rangle f_{an}(E - E_n; \boldsymbol{r}, \boldsymbol{r}'). \tag{2}$$

$|0\rangle$ and $|n\rangle$ are respectively the wave functions of the nucleus in its ground state and in an excited state of excitation energy E_n. E is the incident α-particle energy, $v(\boldsymbol{r}, \boldsymbol{x}_i)$ is the local interaction between the α-particle at position $\boldsymbol{r}$ and a nucleon i at position $\boldsymbol{x}_i$ in the target nucleus and $f_{\alpha n}(E-E_n; \boldsymbol{r}, \boldsymbol{r}')$ is the α-particle propagator:

$$f_{\alpha n}(E-E_n; \boldsymbol{r}, \boldsymbol{r}') = \lim_{\varepsilon \to 0^+} \sum_a \frac{\varphi_a^*(\boldsymbol{r}')\varphi_a(\boldsymbol{r})}{E-E_n-E_a+i\varepsilon}. \tag{3}$$

The φ_a are the α-particle intermediate-state wave functions at energy E_a in the potential V of eq. (1). In the eikonal approximation $f_{\alpha n}$ can be written [5]) as a modified plane wave propagator:

$$f_{\alpha n}(E-E_n; \boldsymbol{r}, \boldsymbol{r}') = -\frac{\mu}{2\pi\hbar^2} \frac{\exp(ik_n(R)s)}{s}, \tag{4}$$

$$\boldsymbol{s} = \boldsymbol{r}-\boldsymbol{r}', \qquad \boldsymbol{R} = \tfrac{1}{2}(\boldsymbol{r}+\boldsymbol{r}'), \tag{5}$$

$$k_n^2 = \frac{2\mu}{\hbar^2}(E-E_n-V_{\mathrm{L}}(R)). \tag{6}$$

$V_{\mathrm{L}}(R)$ is the local optical potential equivalent to the non-local potential of eq. (1). We note that the propagator of eq. (4) is different from that used in ref. [1]). Indeed, as recalled above and explained in ref. [5]), the propagator of eq. (3) was calculated with wave functions φ_a expanded in powers of V_{L}/E and restricted to first-order terms. This approximation has been shown to be unsatisfactory at the energies where we are working mainly for small values of R. To calculate ΔV we need V_{L}, the α-nucleus local potential and therefore the local potential equivalent to $V^{(0)}+\Delta V$. Previously this difficulty was turned over by replacing V_{L} by the local approximation of $V^{(0)}$. We will come back to this question in the next section where we derive the local potential.

In the eikonal approximation for a given intermediate state n, the propagator $f_{\alpha n}$ depends on n via the quantity $(E-E_n-V_{\mathrm{L}}(R))$. If E is high enough, all strongly excited states will contribute to both the real and the imaginary parts of ΔV and because E is large and $\mathrm{Re}V_{\mathrm{L}}$ a very deep potential we can replace E_n by an average value $\bar{E}_n$ determined as the average excitation energy of the most collective states. With this assumption the function $f_{\alpha n}$, eqs. (3)–(6), does not depend on the state n and the summation over n states in eq. (2) can be performed by closure relation. In this approximation the calculation of ΔV implies the knowledge of the target nucleus ground-state wave function only. Taking an independent-particle model wave function we can write eq. (2) as:

$$\Delta V(\boldsymbol{r}, \boldsymbol{r}') = f_\alpha(s)\left\{ \int d\boldsymbol{r}_1 \rho(\boldsymbol{r}_1) v(\boldsymbol{r}', \boldsymbol{r}_1) v(\boldsymbol{r}, \boldsymbol{r}_1) \right.$$

$$\left. -\frac{1}{4}\iint d\boldsymbol{r}_1 d\boldsymbol{r}_2 [\rho(\boldsymbol{r}_1, \boldsymbol{r}_2)]^2 v(\boldsymbol{r}, \boldsymbol{r}_1) v(\boldsymbol{r}', \boldsymbol{r}_2) \right\}. \tag{7}$$

The function $f_\alpha(s)$ is defined by eqs. (4)–(6) where k_n is replaced by k such that:

$$k^2 = \frac{2\mu}{\hbar^2}[E - \bar{E}_n - V_L(R)]. \tag{8}$$

The functions $\rho(r)$ and $\rho(r, r')$ are the local and non-local ground-state densities of the target nucleus.

The nucleon–α-particle interaction v has been calculated [8]) with the B1 nucleon-nucleon interaction of Brink and Boeker in the folding model with one nucleon exchange term. The α-particle was described as four nucleons in a harmonic oscillator 1s state. This n-α potential which has a non-local part was converted with the Perey-Saxon lowest-order approximation into a local potential which happens to be very close to a gaussian function. In the present work we use this gaussian potential parametrized as

$$v(r) = -v_0 \exp(-r^2/a^2), \tag{9}$$

with $v_0 = 47.3$ MeV and $a = 1.97$ fm. These parameters deduced from a calculation of v are very close to the phenomenological ones used by Bonaccorso and Brink [2]).

With the interaction of eq. (9), the calculation of ΔV, eq. (7), is much simplified and can be written explicitly as a function of the R- and s-variables defined in eq. (5). We get:

$$\Delta V(R, s) = v_0^2 f_\alpha(s)\left[e^{-s^2/2a^2}\int d\boldsymbol{R}' \exp\left(-\frac{2}{a^2}(\boldsymbol{R}-\boldsymbol{R}')^2\right)\rho(\boldsymbol{R}')\right.$$

$$\left. - \frac{1}{4}\iint d\boldsymbol{R}' ds' \exp\left(-\frac{1}{2a^2}(s-s')^2 - \frac{2}{a^2}(\boldsymbol{R}-\boldsymbol{R}')^2\right)\rho^2(\boldsymbol{R}', s')\right]. \tag{10}$$

The density $\rho(R)$ is calculated with harmonic oscillator wave functions and $\rho(R, s)$ is either calculated exactly in the same model for closed-shell nuclei or for open-shell nuclei approximated by the relation [9]):

$$\rho(R, s) = \rho(R)[3j_1(sk_A(R))/(sk_A(R))],$$

$$k_A(R) = \left[\frac{5}{3\rho(R)}(\tau(R) - \tfrac{1}{4}\nabla^2\rho(R))\right]^{\frac{1}{2}}. \tag{11}$$

The kinetic energy $\tau(R)$ and the derivatives of $\rho(R)$ are easily and analytically calculable for a harmonic oscillator density $\rho(R)$.

Our approximations imply that our study of ΔV, and therefore of the imaginary α-nucleus potential, concerns only α-particle energies higher than the excitation energy of all strongly excited states. This threshold energy is not precisely defined and we have

tried the lower value $E_m' = 50$ MeV. For $E > E_m$, the equation (7) or (10) tells us that the variation of ΔV as a function of A, the mass number of the target nucleus, comes from the variation of the density and that of the average energy $\bar{E}_n$. Both are smooth functions of A with however a rapid increase of $\bar{E}_n$ for closed-shell nuclei. However, we have assumed $E \gg \bar{E}_n$ so that this effect should not produce a large modification of ΔV and our imaginary potential is expected to show little variation with A. This property is in agreement with phenomenological analyses of α-scattering in the domain of energies where our approximations should be valid, contrary to low-energy scattering where the enhancement of the angular distributions at backward angles observed for closed-shell nuclei only indicates a discontinuity in the imaginary potential when one crosses a closed-shell nucleus [10]).

3. Derivation of the local equivalent potential

To calculate the Green function of eq. (4) we need the local potential equivalent to V. Furthermore, phenomenological analyses of α-particle scattering data are always performed with local optical potentials which we want to compare with our potential. Therefore we need the local potential equivalent to V. In this section we study the derivation of the local potential equivalent to our non-local potential in the lowest-order Perey-Saxon approximation [11]). Indeed this local potential can be considered as the first term of an expansion of the non-local one in powers of b/a where b is its non-locality range and a its radius. For α-nucleus scattering [1]) b/a is very small, of the order of $\frac{1}{10}$, and this lowest approximation should be valid. The local potential is then defined as the Wigner transform of the non-local one taken for the momentum K of a particle in the local potential itself. This local momentum is generally assumed to be real and determined by the local equivalent of the first term $V^{(0)}$ of eq. (1) (plus the Coulomb potential). In this case the local potential V_L is determined by two independent equations. The first one determines the potential $V_L^{(0)}$ equivalent to $V^{(0)}$ and therefore the local momentum K_0 which is then introduced into the second one defining the local potential equivalent to ΔV as the Wigner transform of ΔV at momentum K_0. However, two recent papers [6, 7]) have shown that this approximation of a real local momentum induces quite large errors in the calculation of the nuclear matter nucleon-nucleus local imaginary potential. Taking into account the imaginary part of the local momentum reduces the calculated imaginary potential by the K-mass ratio m_K/m which is at low energy of the order of 0.7. For our α-nucleus potential the local absorptive potential calculated with K_0 is very strong and we expect an even larger modification as was briefly noticed previously [5]).

The two terms of eq. (1) can be written as follows:

$$V^{(0)}(R, s) = V^{d}(R)\delta(s) + V^{e}(R, s),$$
$$V(R, s) = e^{iks} g(R, s), \tag{12}$$

$V^{d}(R)$ and $V^{e}(R, s)$ being respectively [4]) the local direct and non-local exchange terms of the antisymmetrized double folding model potential. In ΔV the factor depending on k, the WKB α-particle momentum, has been separated. The real function $g(R, s)$, independent of k, contains all other factors given in eq. (10).

In the lowest order of the Perey-Saxon expansion, the local potential equivalent to V is given by

$$V_{L}(R) \equiv U(R)+iW(R)$$

$$= V^{d}(R)+4\pi \int_{0}^{\infty} j_{0}(Ks)[V^{e}(R, s)+e^{iks}g(R, s)]s^{2}\,ds. \qquad (13)$$

The best choice of the local momentum has been shown [12]) to be such that:

$$K^{2}(R) = \frac{2\mu}{\hbar^{2}}(E-V_{L}(R)). \qquad (14)$$

In fact the expression (14) of K^{2} happens naturally in a WKB expansion of the non-local potential in the one-dimensional problem [13]).

Generally one assumes that W is negligible compared to $E-U$ so that K^{2} of eq. (14) and k^{2} of eq. (8) can be replaced by

$$K^{2} \simeq K_{0}^{2} = \frac{2\mu}{\hbar^{2}}(E-U),$$

$$k^{2} \simeq k_{0}^{2} = \frac{2\mu}{\hbar^{2}}(E-\bar{E}_{n}-U). \qquad (15)$$

With this approximation eq. (13) leads to two independent equations determining the real and the imaginary parts of V_{L}. Let us call these two approximate solutions of eq. (13) U_{0} and W_{0}. They are determined from the following equations:

$$U_{0}(R) = V^{d}(R)+4\pi \int_{0}^{\infty} j_{0}(K_{0}s)[V^{e}(R, s)+\cos(k_{0}s)g(R, s)]s^{2}ds, \qquad (16a)$$

$$W_{0}(R) = 4\pi \int_{0}^{\infty} j_{0}(K_{0}s)\sin(k_{0}s)g(R, s)s^{2}\,ds. \qquad (16b)$$

The first equation (16a) together with eqs. (15) determine U_{0}. Once U_{0} is known, and therefore k_{0} and K_{0}, W_{0} is easily obtained from the imaginary part of ΔV. These two equations have been extensively used in the literature and in particular in derivations of the α-particle optical potential. In practice, a further simplification is added which

where U_0 and W_0 are defined by eqs. (16). Assuming that V_L is a smooth function of K^2 and that $K_I^2/K_R^2 \ll 1$, we expand $V_L(K^2, R)$ around K_0^2 and retain only first-order terms:

$$V_L(K^2, R) \simeq V_L(K_0^2, R) + (K_R^2 + iK_I^2 - K_0^2) \left.\frac{\partial V_L(K^2, R)}{\partial K^2}\right|_{K^2 = K_0^2}. \tag{20}$$

This equation gives for the real and imaginary potentials:

$$W(R) = \left[1 + \left(\frac{2\mu_K(R)}{\hbar^2} \frac{\partial W_0(R)}{\partial K_0^2}\right)^2\right]^{-1} \frac{\mu_K(R)}{\mu} W_0(R),$$

$$U(R) - U_0(R) = \frac{2\mu_K(R)}{\hbar^2} W(R) \frac{\partial W_0(R)}{\partial K_0^2}, \tag{21}$$

where we have defined an effective mass for the α-particle such that:

$$\frac{\mu_K(R)}{\mu} = \left[1 + \frac{2\mu}{\hbar^2} \frac{\partial U_0(R)}{\partial K_0^2}\right]^{-1}. \tag{22}$$

Neglecting $\partial W_0/\partial K_0^2$ which always appears combined with the ratio μ_K/μ leads to a result similar to that of Negele *et al.* and Fantoni *et al.* for the nucleon potential in nuclear matter but with an effective mass which in finite nuclei depends on the distance:

$$U(R) = U_0(R),$$

$$W(R) = \frac{\mu_K(R)}{\mu} W_0(R). \tag{23}$$

In most of the works U_0 is calculated for different energies so that its energy derivative $\partial U_0(E, R)/\partial E$ is known while in general cases U_0 is not a simple function of K_0^2 (and k_0^2). Furthermore, the non-local potential $V^{(0)} + \Delta V$ depends on energy via its dependence upon K^2 (and k^2) only so that we can transform easily $\partial U_0/\partial K_0^2$ in terms of $\partial U_0/\partial E$. We get

$$\frac{2\mu}{\hbar^2} \frac{\partial U_0}{\partial K_0^2} = \frac{\partial U_0}{\partial E} \left(1 - \frac{\partial U_0}{\partial E}\right)^{-1} \tag{24}$$

with the result

$$\frac{\mu_K(R)}{\mu} = 1 - \frac{\partial U_0(E, R)}{\partial E} = \frac{\mu^*(R)}{\mu},$$

$$W(R) = \frac{\mu^*(R)}{\mu} W_0(R), \tag{25}$$

where μ^* is the generalization to the α-particle case of the usual total effective nucleon mass for a finite nucleus.

The potential U_0 has been calculated in ref.[4]). For a Brink and Boeker nucleon-nucleon interaction and α-Ca^{40} scattering a simple evaluation of the effective mass μ^*/μ from the energy dependence of the volume integral of U_0 leads to 0.6, 0.64, 0.8 and 0.96 at $R = 0, 2, 4$ and 6 fm respectively. The potential W is therefore much weaker (about half) than W_0 in the interior but very close to it at the surface.

The derivation of W from W_0 requires the knowledge of the derivative $\partial U_0/\partial E$ and therefore the knowledge of U_0 in a domain ΔE around E while in the computer program U_0 and W_0 are calculated at a given energy E. It has been shown[4]) that when the effective nucleon-nucleon interaction is a gaussian (or a sum of gaussians), $V^e(R, s)$ behaves almost like a gaussian (or a sum of gaussians) in terms of the s-variable. In this specific case $\partial U_0/\partial K_0^2$ is simply related to $V_L^e(R)$ the local term equivalent to $V^e(R, s)$. If β is the range of the gaussian form factor, eq. (2.5) can be written as:

$$W(R) \simeq \frac{W_0(R)}{1 - \frac{\mu}{2\hbar^2}\beta^2 V_L^e(R)}, \tag{26}$$

where $\beta^2 V_L^e(R)$ is replaced by a sum of such terms for a sum of gaussians.

If we express $\partial W_0/\partial K_0^2$ in terms of $\partial W_0(E, R)/\partial E$ we can also make an evaluation of $U - U_0$ from eqs. (21). The term $((\mu^*/\mu)(\partial W_0/\partial E))^2$ is always very small and can be neglected in the eq. (21) of W so that W is not modified and $U - U_0$ is given by

$$U(R) - U_0(R) = \frac{\mu^*}{\mu} W_0 \frac{\partial W_0}{\partial E}. \tag{27}$$

For high α-particle energies, $|W_0|$ slightly decreases with increasing energies so that $\partial W_0/\partial E$ is positive and U is more attractive than U_0 but the correction is negligible. On the contrary, for low energies $|W_0|$ increases quite fast – due in particular to the opening of new reaction channels – and U can be notably less attractive than U_0.

An alternative, but similar way to obtain an approximation to U and W is to use the oscillatory properties of Bessel functions. The successive derivatives of $j_0(x)$ are combinations of Bessel functions of different orders and are more and more oscillatory. Therefore, if we replace in eq. (13) the function $j_0(Ks)$ by its Taylor expansion around K_r, we need retain the first-order terms only, the higher terms being negligible because of the successive powers of K_i and because the integrals involving higher order derivatives of j_0 become smaller and smaller. Eqs. (16) are then replaced by the two equations:

$$U = V^d + 4\pi \int_0^\infty j_0(K_r s)[V^e(R, s) + \cos(k_r s)e^{-k_i s} g(R, s)]s^2 ds$$

$$-4\pi K_i \int_0^\infty \frac{dj_0(K_r s)}{dK_r} \sin(k_r s)e^{-k_i s} g(R, s)s^2 ds, \tag{28}$$

$$W = 4\pi \int_0^\infty j_0(K_r s)\sin(k_r s)e^{-k_i s}g(R,s)s^2 ds$$

$$+4\pi K_i \int_0^\infty \frac{dj_0(K_r s)}{dK_r}[V^e(R,s)+\cos(k_r s)e^{-k_i s}g(R,s)]s^2 ds. \quad (29)$$

The two first terms of U and the first term of W are, apart the exponential factor $e^{-k_i s}$, the same as in eqs. (16) for U_0 and W_0. The factor $e^{-k_i s}$ will damp down the oscillations of the non-local ΔV term but will not change the potential drastically. Added to these terms, we get in U a contributions of $\mathrm{Im}\Delta V$ while in W we have a contribution of $V^e + \mathrm{Re}\Delta V$. When realistic nucleon-nucleon effective interactions are used, the exchange term V^e is very large so that we expect a larger modification for W than for U compared to W_0 and U_0 respectively.

Eqs. (28)–(29) have a much simpler form than eq. (13). Since $dj_0(K_r s)/dK_r = -s j_1(K_r s)$ they involve integrals of the non-local potential multiplied by the Bessel function j_0 or j_1 of real arguments. They can be applied to the general case of a non-local potential $V(R,s)$ of the form

$$V(R,s) = V_0(R)\delta(s) + V_1(R,s) + iW_n(R,s)$$

leading to the local potential $U + iW$:

$$U = V_0 + 4\pi \int_0^\infty [j_0(K_r s)V_1(R,s) + K_i s j_1(K_r s)W_n(R,s)]s^2 ds,$$

$$W = 4\pi \int_0^\infty [j_0(K_r s)W_n(R,s) - K_i s j_1(K_r s)V_1(R,s)]s^2 ds, \quad (30)$$

where K_r and K_i are given by eq. (17a) in terms of U and W.

Making the same assumptions as previously made on the local potential of eqs. (28)–(29) leads back to the approximate local potential of eq. (26) and to $U \simeq U_0$.

4. Results

We have calculated ΔV of eq. (10) which determines the imaginary potential and a correction to the real folding model potential for energies above 50 MeV and several nuclei (Ca, Ni, Zr, Sn and Pb). The local nucleon-alpha interaction is given by eq. (9). In the potential ΔV, the target nucleus enters only in the average energy $\bar{E}_n$ of eq. (8) and in the local and non-local ground-state densities. For closed-shell nuclei we expect that the largest contribution to ΔV will come from collective states and assume $\bar{E}_n \simeq 1\hbar\omega = 40A^{-\frac{1}{3}}$ MeV. The sensitivity of ΔV upon this parameter is tested by

comparing the imaginary α-^{40}Ca potential calculated with $\bar{E}_n = 0$, 1 and $2\hbar\omega$. Indeed the recent paper by Bonaccorso and Brink [2]) shows that for uncorrelated particle-hole intermediate states, the $2\hbar\omega$ states give the largest contribution to the α-^{40}Ca potential for large energies. This result, obtained in the semi-classical limit of Feshbach's formula, suggests that $\bar{E}_n$ should depend on E. However in our calculation we kept $\bar{E}_n = 1\hbar\omega$. For open-shell nuclei, the low-lying level density is much larger and we take a small value for $\bar{E}_n$ as discussed later. The nuclear densities are calculated with harmonic oscillator states with an oscillator parameter fitted on the experimental rms radius [14]). For closed-shell nuclei, both the local and the non-local densities are easily derived in this model. For open-shell nuclei, the contribution of the valence nucleons is taken as the contribution of the corresponding closed sub-shell multiplied by a weighting factor ω/Ω where ω is the number of valence nucleons and Ω the degeneracy number of the sub-shell. Even in this simple calculation the non-local density would depend on the angle between $\boldsymbol{R}$ and $\boldsymbol{s}$ and, for simplifying the calculation of ΔV, we use for those nuclei the approximate density of eqs. (11). This approximation will be tested on the α-^{40}Ca potential.

The derivation of the local potential equivalent to ΔV according to eqs. (13)–(14) requires knowledge of the potential $V^{(0)}$ of eq. (1) in its non-local form. $V^{(0)}$ is the folding model potential for a non-local α-nucleon interaction and has been calculated in ref. [4]). Its analytical expression is directly introduced into our computing program for the B1 nucleon-nucleon interaction and the same non-local and local densities as used for the calculation of ΔV. Therefore both terms of eq. (1) are calculated with the same input except that in $V^{(0)}$ the non-local α-nucleon interaction is used while in ΔV it is replaced by its local equivalent. Eq. (13) which determines U and W is then solved by iteration for a given energy and a given nucleus. We take as our starting potential the real potential U_0 previously determined in ref. [4]) and W_0 determined by eq. (16b).

We first present the results obtained for α-^{40}Ca scattering and discuss in detail the different tests concerning the choice of $\bar{E}_n$, the approximation of eq. (11) for the non-local density and the comparison between U_0 and U, W_0 and W. Then we briefly report on the α-^{44}Ca imaginary potential compared to the α-^{40}Ca one. At the end of the paper we show the variation of the imaginary potential volume integral in terms of A, the mass number of the target nucleus.

4.1. THE α-^{40}Ca POTENTIAL

We show in fig. 1 the potential U_0 calculated at 100 MeV from the first-order term $V^{(0)}$ and the correction to U_0 due to the real part of ΔV. This correction is always attractive, peaked in the surface region but small. It never exceeds – even at the surface – 10 % of U_0 for all energies and nuclei considered in this work. From now on we drop this term and discuss only the imaginary potential due to the imaginary part of ΔV.

In figs. 2a, b is shown the potential W calculated at 50 MeV and 100 MeV respectively with harmonic oscillator densities for $\bar{E}_n = 0$, 1 and 2 $\hbar\omega$. At short distances the

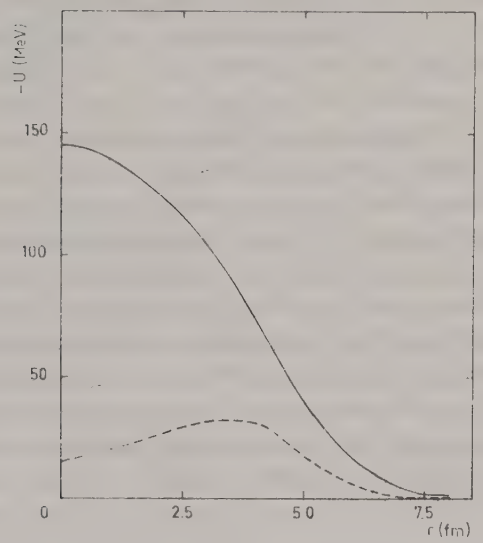

Fig. 1. Antisymmetrized double folding real α-^{40}Ca potential of eq. (12) (solid line) and the corrective term due to ΔV (dashed line) multiplied by five.

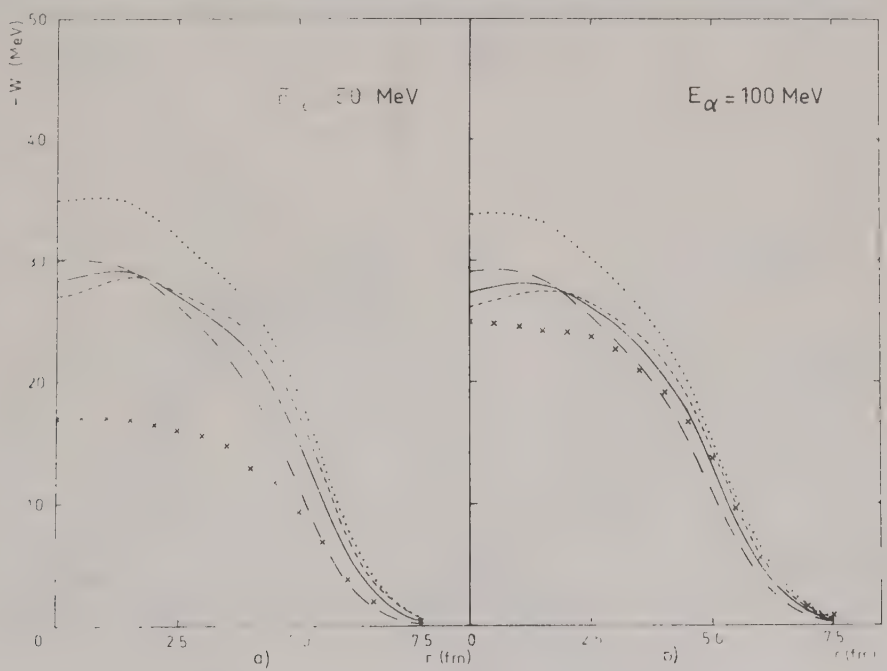

Fig. 2. Imaginary α-^{40}Ca potential at (a) $E = 50$ and (b) $E = 100$ MeV incident lab energies, calculated with $\bar{E}_n = |0\hbar\omega|$(dashed line), $1\hbar\omega$(solid line), $2\hbar\omega$(dot-dashed line) and $\bar{E}_n = 1\hbar\omega$ but with the approximated non-local density of eq. (11) (dotted line). The crosses correspond to the phenomenological potential A of ref. [15]).

differences between the three potentials are insignificant but are more important at large distances where the real potential is weaker and therefore k^2 more sensitive to a change of $\bar{E}_n$. At 50 MeV and in the tail of the potential the sensitivity to $\bar{E}_n$ is large and the potential much lower for $\bar{E}_n = 2\hbar\omega$ than for $\bar{E}_n = 0$ or $1\ \hbar\omega$. However, this average value of $2\hbar\omega$ is not very realistic at that energy and should be disregarded. At 100 and 150 MeV, $\bar{E}_n = 2\hbar\omega$ yields less absorption than $\bar{E}_n = 0$ and $1\hbar\omega$ but the three potentials are closer to each other when the incident energy increases. From now on, we discuss the potential calculated with $\bar{E}_n = 1\hbar\omega$ but should remember that, according to ref. [2]), we probably overestimate the absorption at large distances. In figs. 3a, b, the potential W calculated at 50 MeV and 100 MeV eq. (13) is compared with W' the potential of eq. (25), and with W_0 derived in the approximation of a real local momentum. In sect. 3, the effective mass which determines the ratio W'/W_0 was evaluated from the overall energy dependence of U_0 deduced from the energy dependence of its volume integral [4]), while here we have calculated dU_0/dE for each value of R. The values of μ^*/μ are slightly different from those given in sect. 3. The potential W' is very close to W obtained by solving exactly eq. (13). Therefore the approximation of eq. (25) or eq. (26), which is

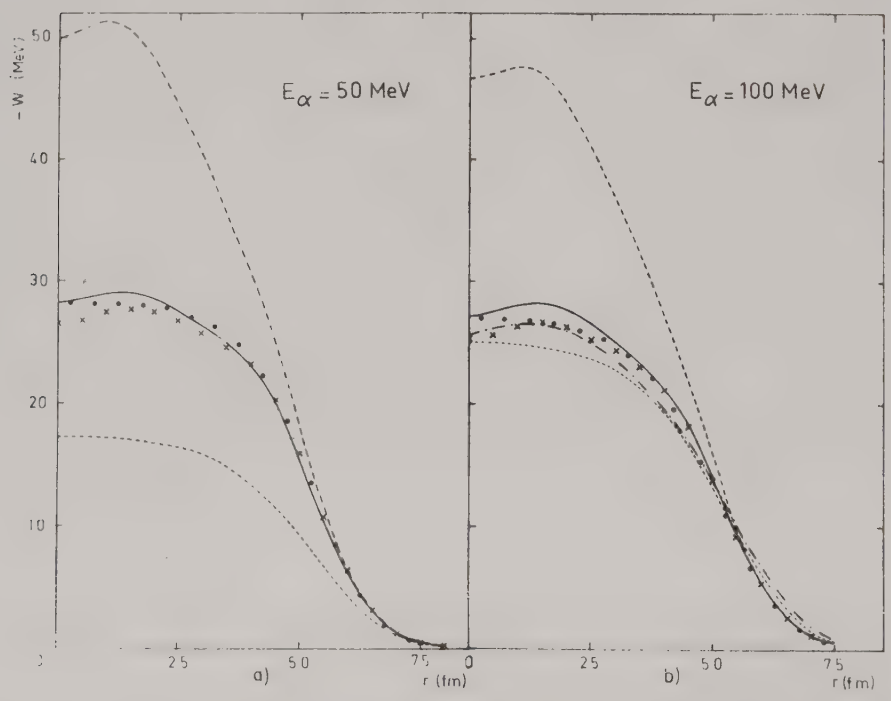

Fig. 3. Imaginary part of the α–^{40}Ca potential at (a) $E = 50$ and (b) $E = 100$ MeV: potential W of eq. (13) (solid line), potential W_0, eq. (16b) (dashed line, long dashes), potential W' of eq. (23) or (26) (crosses), (SW) [2] potential fitting W (points), potential A of ref. [15]) (dashed line, short dashes) and potential B of ref. [15]) (dot-dashed line).

identical to the approximation derived by Fantoni *et al.* [6]) and Negele *et al.* [7]) in nuclear matter, is excellent. The potential W_0 is much stronger than W in the interior but beyond 5 fm both are identical. This is a very important result which shows that all theoretical imaginary potentials calculated so far for α-nucleus or nucleon-nucleus scattering are largely overestimated mainly in the volume region. Finally, our potentials are compared at 50 and 100 MeV with the two phenomenological potentials of Delbar *et al.* [15]): the potential A has only volume absorption with a Saxon-Woods squared form factor, and potential B which has added to this volume term a surface term written as a derivative of $(SW)^2$. Obviously, 50 MeV is too low an energy for our approximations to be valid. At that energy, by using a closure relation over intermediate nuclear states, we certainly pick up many channels which should not yet contribute because of the energy threshold. At 100 MeV and 150 MeV, as shown in figs. 3b and 4, the overall agreement between our potentials and the empirical ones is very satisfactory, even though our potentials are systematically not absorptive enough at large distances. This lack of absorption in the surface region is at least partly due to our model which neglects the α-particle break-up channels. It has been shown [16]) that for energies much larger than the α-particle break-up threshold, the α-particle break-up probability increases for increasing α-particle energy with some saturation effect above ~ 150 MeV. Furthermore, the break-up probability has an essentially peripheral character which means that the break-up contribution to the optical potential would

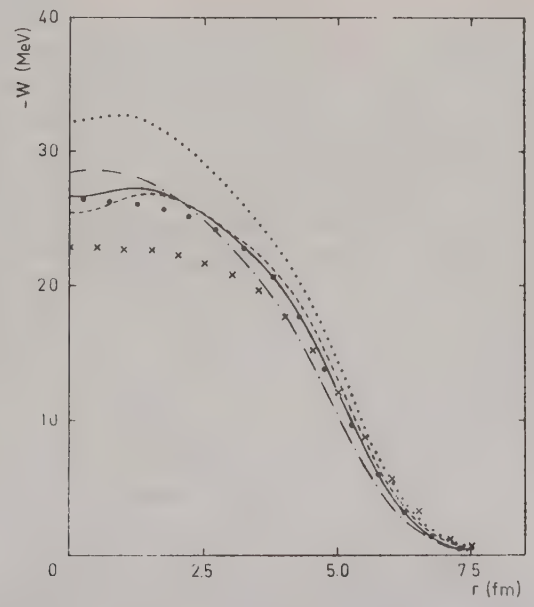

Fig. 4. Same as fig. 2 but for $E = 150$ MeV. The points corresponds to the $(SW)^2$ parametrization of the potential W (solid line).

essentially be concentrated in the surface region. Following this idea, it has been verified for α-particle energies greater than 100 MeV that with a weak adjustable surface term added to our theoretical potential one is able to reproduce the experimental α-particle elastic scattering [17]. In phenomenological analyses [18-20] it has also been found that adding a surface term to the usual imaginary volume potential improves significantly the fits of experimental data. Empirical analyses of data have shown the superiority of a Saxon-Woods squared imaginary potential over a Saxon-Woods one. This is confirmed by our calculation. Indeed, for 150 MeV α-particle energy we show in fig. 4 that a Saxon-Woods form factor fits our potential quite well. The geometrical parameters of the $(SW)^2$ imaginary potential are $R_W = 5.65$ fm (or $r_0 = 1.65$ fm) and $a_W = 0.95$ fm, very comparable to phenomenological parameters adjusted when both volume and surface absorption are considered. The same fit at 100 MeV leads to $R_W = 5.75$ fm and $a_W = 0.9$ fm and exhibits some weak energy dependence. Phenomenological fits do not generally show any definite energy dependence and, if they do, they seem to exhibit the opposite behaviour of increasing R and decreasing a in ^{40}Ca [ref. [18]]. In fig. 5 is given our imaginary potential volume integral as a function of energy. As discussed above, our closure approximation is not reliable below ~ 100 MeV and we cannot reproduce

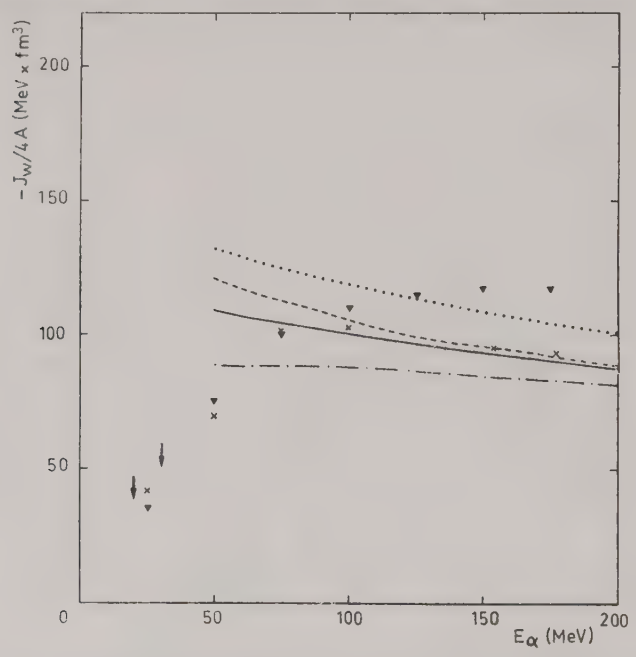

Fig. 5. Energy dependence of the volume integral per nucleon pair of the α-^{40}Ca potential calculated with $E_n = 0\hbar\omega$ (dashed line), $1\hbar\omega$ (solid line), $2\hbar\omega$ (dot-dashed line) and the exact non-local density, and with $E_n = 1\hbar\omega$ and the approximation of eq. (11) for the density (dotted line). The crosses and triangles refer to phenomenological results given respectively by potentials A and B of ref. [15]), and the arrows to the microscopic calculation of ref. [21]).

the fast increase of the absorption below 80 MeV. Our imaginary potential has a very weak energy dependence. Above 100 MeV it agrees with the energy dependence of the potential A of ref. [15]) but does not reproduce that of potential B, which however has been shown to be less successful in reproducing experimental data above 100 MeV. In the figure are also reported the volume integrals of the imaginary potentials of ref. [21]). These potentials were calculated at 20 and 30 MeV by taking explicitly into account the open inelastic channels which are described by RPA wave functions. The increasing of absorption with energy results from the progressive opening of new channels and is very similar to that of phenomenological potentials. The calculated volume integrals are slightly too high but they correspond to the potential W_0 and then are only an upper limit of the exact ones. As the absorption is mainly concentrated for those energies at the surface the volume integral of the potential W should not be very different, the expected reduction being at most 20 %. A similar potential was also obtained in ref. [22]) for 30 MeV α-particles.

For open-shell nuclei we use the approximate non-local density of eq. (11) and we finally make a test of this approximation on the α-^{40}Ca potential. This is given in figs. 2 and 4 where one sees that it systematically overestimates the potential. In the surface region, the most important for scattering properties, this overestimation of the potential is of the order of 10 %. The corresponding volume integrals are shown in fig. 5 where one sees a similar overestimation.

4.2. α–^{44}Ca POTENTIAL

The analysis of α-elastic scattering data in terms of optical model potentials shows much weaker absorption for ^{40}Ca than for ^{42}Ca and ^{44}Ca at low energies while above 50 MeV the three imaginary potentials become closer to each other. The differences between α-^{40}Ca and α-$^{42-44}$Ca are expected to come at least partly from the difference in level density of the low excitation energy spectrum for closed- or open-shell nuclei so that the strongly excited inelastic channels should appear at a much lower energy for $^{42-44}$Ca than for ^{40}Ca. This threshold effect does not enter explicitly in our model but it should manifest itself indirectly in the sense that our model should be valid for lower energies in the case of $^{42-44}$Ca compared to ^{40}Ca. On the other hand, the small difference at higher energies between the α-^{40}Ca and α-^{44}Ca [ref. [15])] imaginary potentials is contained in the expression (10) of our imaginary potential. This is illustrated in figs. 6 and 7 where the imaginary potentials for ^{40}Ca and ^{44}Ca at 50 and 100 MeV respectively are compared. Both are calculated with the approximate non-local density of eq. (11). For ^{44}Ca the most strongly excited states are expected to be at very low energy, a few MeV, and, because we are considering incident energies larger than 50 MeV, our potential is not sensitive to a modification of $\bar{E}_n$ by few MeV. Therefore we have used $\bar{E}_n = 5$ MeV in all the calculation. The difference between the two potentials comes from both the average energy of the most excited inelastic channels and the densities and is qualitatively in agreement with phenomenological analyses at 100 MeV

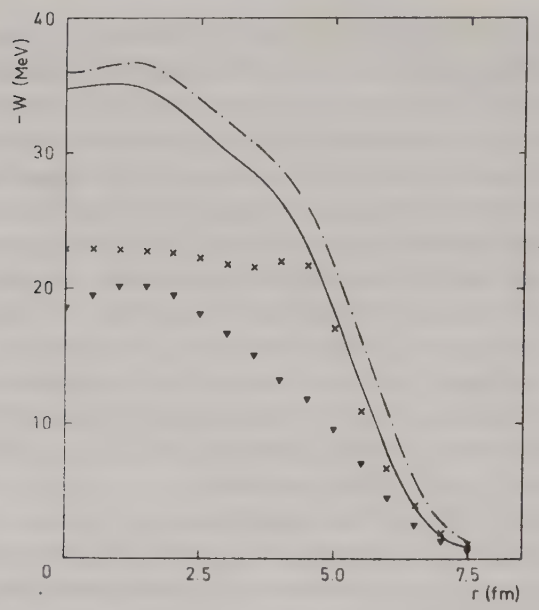

Fig. 6. Comparison at $E = 50$ MeV of the theoretical α-^{40}Ca (solid line) and α-^{44}Ca (dot-dashed line) potentials with the potential B of ref. [15]) for α-^{40}Ca (triangles) and for α-^{44}Ca (crosses).

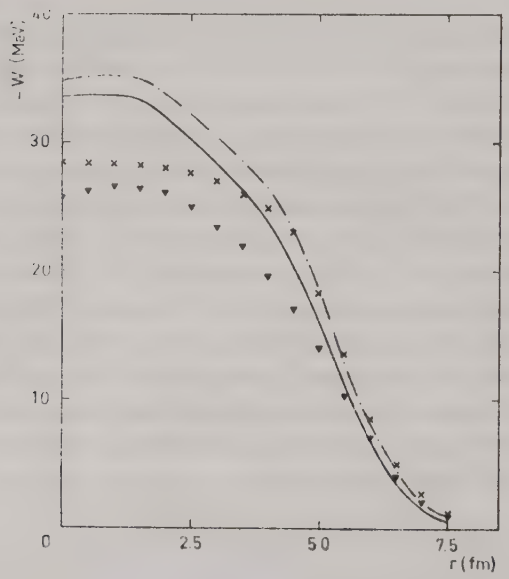

Fig. 7. Same as fig. 6 but for $E = 100$ MeV.

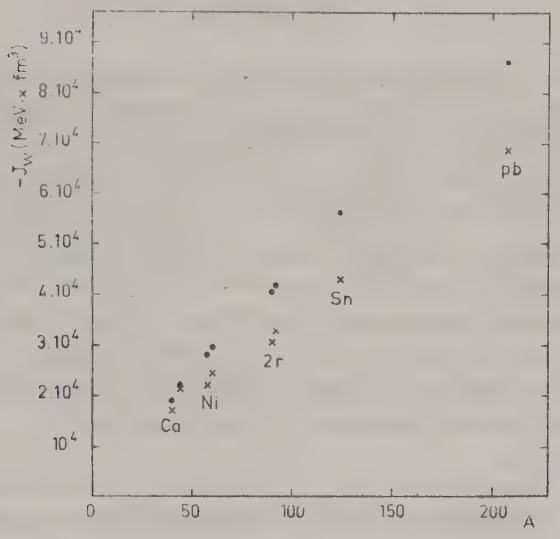

Fig. 8. Mass number dependence of the volume integral at $E = 100$ MeV: calculated (points) and phenomenological [15,18,19,23]) (crosses) values for ^{40,44}Ca, ^{58,60}Ni, ^{90,92}Zr, ^{124}Sn and ^{208}Pb.

but too small at 50 MeV where, as expected, the α-^{44}Ca potential is in better agreement with empirical potentials. As for ^{40}Ca we find a lack of absorption at high energy in the surface region, this effect being attenuated by our approximation of the non-local density.

4.3. MASS NUMBER DEPENDENCE OF THE IMAGINARY POTENTIALS

The imaginary potential is calculated for ^{58,60}Ni, ^{90,92}Zr, ^{124}Sn and ^{208}Pb following the same derivation and approximations as previously for ^{40,44}Ca. For all these nuclei we get the same general results as for calcium nuclei and it would not be of great interest to plot all these calculated potentials. However, it is interesting to study the global properties of the potentials and their variation with the target nucleus. In fig. 8, the volume integral J_W is plotted as a function of A, the mass number of the target nucleus, for $E = 100$ MeV. The A-dependence is almost linear with small jumps when one crosses closed-shell nuclei, in agreement with fitted potentials [15, 18, 19, 23]). In our model these jumps come as shown for Ca nuclei from the average energy $\bar{E}_n$ which has discontinuities for those nuclei. The general trend of J_W is very similar to that observed in phenomenological analyses but the calculated volume integrals are larger than the fitted ones. This overestimation of J_W can be interpreted as a consequence of our approximation on the non-local density. Indeed, it was shown previously (see fig. 5) that for ^{40}Ca this approximation leads to an overestimation of J_W of about 10 %. As this approximation neglects the angular dependence of the density, it is certainly less reliable for heavier nuclei. This is reflected in the figure where one sees that the difference between calculated and fitted values increases with A.

5. Conclusions

We have derived a simplified expression for the α-nucleus optical potential using the Feshbach formula. We have shown that the correction to the real folding model potential is small and have studied in detail the imaginary potential. Our imaginary potential is expressed in terms of the target ground-state densities, local and non-local, and an energy parameter $\bar{E}_n$ which is defined as the average energy of strongly excited target states. The derivation of a local imaginary potential equivalent to this non-local potential is discussed in detail. Comparison with fitted potentials shows an overall agreement for energies larger than 80–100 MeV with, however, an underestimation of absorption at the surface which is expected to be due to our neglect of α-particle break-up channels. The general trend of fitted potentials for the energy dependence as well as for the target mass number dependence are well reproduced.

It is pleasure to thank Dr. F. Duggan for his interest in this work at its early stage. One of us (M.L.) is very grateful to Dr. F. Michel for helpful discussions.

References

1a) N. Vinh Mau, Phys. Lett. **71B** (1977) 5
1b) N. Vinh Mau, Proc. Second Louvain-Cracow Seminar on the alpha-nucleus interaction, Louvain-la-Neuve, 1978, ed. G. Gregoire and K. Grotowski, p. 243
2) A. Bonaccorso and D. M. Brink, Nucl. Phys. **A384** (1982) 161
3) A. Faessler, T. Izumoto, S. Krewald and R. Sartor, Nucl. Phys. **A359** (1981) 509; S. B. Khadkikar, L. Rikus and A. Faessler, Nucl. Phys. **A369** (1981) 495
4) F. Duggan, M. Lassaut, F. Michel and N. Vinh Mau, Nucl. Phys. **A355** (1981) 141
5) A. Bouyssy, N. Vinh Mau and D. M. Brink, Phys. Lett. **102B** (1981) 109
6) S. Fantoni, B. L. Friman and V. R. Pandharipande, Phys. Lett. **104B** (1981) 89
7) J. W. Negele and K. Yazaki, Phys. Rev. Lett. **47** (1981) 71
8) M. Lassaut and N. Vinh Mau, Phys. Lett. **70B** (1977) 14; Nucl. Phys. **A349** (1980) 372; M. Lassaut, Thèse de troisième cycle, Orsay, 1978
9) X. Campi and A. Bouyssy, Phys. Lett. **73B** (1978) 263
10) See K. Grotowski, Proc. Fourth EPS Nuclear Physics Divisional Conference, ed. P. Blasi, Florence, 1977, for a list of references on this subject
11) F. G. Perey and D. S. Saxon, Phys. Lett. **10** (1964) 107
12) W. E. Frahn, Nucl. Phys. **66** (1965) 357
13) R. E. Peierls and N. Vinh Mau, Nucl. Phys. **A343** (1980) 1
14) G. D. Alkhazov, S. L. Belostotsky and A. A. Vorobyov, Phys. Reports **42C** (1978) 89
15) T. Delbar, G. Gregroire, G. Paic, R. Ceuleneer, F. Michel, R. Vanderpoorten, A. Budzanowski, H. Dabrowski, L. Freindl, K. Grotowski, S. Micek, R. Planeta, A. Strzalkowski and K. A. Eberhard, Phys. Rev. **C18** (1978) 1237
16) G. Baur, R. Shyam, F. Rösel and D. Trautmann, preprint
17) M. Lassaut and J. Van de Wiele, Nucl. Phys. **A386** (1982) 29
18) K. Grotowski, Proc. Second Louvain-Cracow Seminar on the alpha-nucleus interaction, Louvain-la-Neuve, 1978, ed. G. Gregroire and K. Grotowski, p. 1
19) Z. Majka and T. Grokowski, Acta. Phys. Polonica **B9** (1978) 75
20) A. M. Kobos, B. A. Brown, P. E. Hodgson, G. R. Satchler and A. Budzanowski, preprint 1982
21) M. Lassaut, Phys. Lett. **105B** (1981) 252
22) H. Dermawan, F. Osterfeld and V. A. Madsen, Phys. Rev. **C25** (1982) 140
23) A. Budzanowksi, H. Dabrowski, L. Freindl, K. Grotowski, S. Micek, R. Planeta, A. Strzalkowski, M. Bosman, P. Leleux, P. Macq, J. P. Meulders and C. Pirart, Phys. Rev. **C17** (1978) 951

CHAPITRE III

ETUDE AVEC NOS POTENTIELS MICROSCOPIQUES DE LA DIFFUSION ELASTIQUE (α,α) ET DE LA REACTION DE TRANSFERT (^{3}He,α)

L'article que nous présentons maintenant, publié dans Nuclear Physics, a été motivé par le fait qu'aucun des potentiels α-noyau déduits de la diffusion élastique (α,α) n'est capable au-delà de 100 MeV de reproduire de manière satisfaisante les sections efficaces de la réaction de transfert (^{3}He,α)dans le cadre de la DWBA[CH77, DJ80, VDW78] . Sachant que la réaction (^{3}He,α) est surtout sensible au potentiel dans la voie α, il nous a semblé intéressant d'essayer de décrire ces deux processus avec nos potentiels microscopiques calculés dans la première partie de notre thèse. Cette étude constitue un test supplémentaire de notre potentiel,qui complète notre analyse précédente de la diffusion élastique de particule alpha de 104 MeV à partir de notre potentiel réel.

Cet article est consacré à l'étude des deux processus (α,α) et (^{3}He,α) pour les trois noyaux ^{58}Ni, ^{90}Zr et^{208}Pb et pour des énergies comprises entre 100 et 283 MeV. Nous utilisons les trois potentiels α-noyau réels calculés précédemment avec la force B_1 de Brink et Boeker, et les interactions dépendant de la densité G-O de Banerjee-Campi-Sprung et JLM de Jeukenne-Lejeune-Mahaux,alors que le potentiel imaginaire est celui calculé dans l'article précédent.

Nous avons, dans une première analyse, renormalisé la partie réelle et la partie imaginaire de notre potentiel par deux constantes multiplicatives λ_R et λ_I,ajustées sur les données expérimentales de la diffusion élastique (α,α) disponibles pour les noyaux étudiés entre 100 et 218 MeV,puis utilisé le potentiel obtenu pour calculer les sections efficaces de la réaction (^{3}He,α) à l'approximation DWBA. Nous verrons qu'un tel potentiel conduit

à un accord global satisfaisant avec l'expérience en ce qui concerne la pente de distributions angulaires et conduit à des facteurs spectroscopiques compatibles avec ceux déterminés à basse énergie à partir des réactions (p,d) ou (d,t). Toutefois, une telle méthode de renormalisation conduit à une absorption beaucoup trop forte à l'intérieur et à des intégrales de volume du potentiel imaginaire peu réalistes. Les calculs des sections efficaces étant peu sensibles à l'absorption à l'intérieur du noyau, le facteur de renormalisation λ_I n'a probablement de sens qu'au-delà d'une certaine distance. Notre modèle négligeant toute voie de break-up de la particule alpha, dont on sait qu'elle apporterait une contribution à la surface [BA78, SH79, WA78, WU78], nous avons, dans une deuxième analyse, ajouté notre absorption calculée un terme de surface ajustable écrit comme la dérivée d'un potentiel de Saxon-Woods. Nous verrons que ce terme de surface très faible suffit, lorsqu'il est ajouté à notre potentiel , pour bien reproduire à la fois la diffusion élastique et la réaction de transfert. Enfin, de même que dans notre première étude de la diffusion élastique (α,α) à 104 MeV, nous constatons que les interactions nucléon-nucléon dépendant de la densité conduisent, pour chacune de ces analyses, au meilleur accord global avec les résultats expérimentaux pour ces deux processus.

Cette étude a été effectuée pour les seuls potentiels U_0 et W_0, correspondant à l'approximation du moment local par sa partie réelle. D'après le chapitre II, la résolution des équations couplées (II.17-18) conduit à un potentiel α-noyau dont la partie réelle U est proche du potentiel U_0, mais dont la partie imaginaire W est nettement plus faible que le potentiel W_0 pour la partie interne. Toutefois, les potentiels W et W_0 étant proches l'un de l'autre à la surface du noyau, les conclusions de notre analyse devraient rester qualitativement inchangées pour le potentiel α-noyau déterminé dans le chapitre précédent.

REFERENCES

[BA78] G. Baur, F. Rösel, R. Shyam and D Trautman, KFA Jülich, Annual Report (1978) p.131 et references internes

[CH77] N.S. Chant, H. Chen, D.A. Goldberg, A. Nadasen and P.G. Roos, University of Maryland, Progress Reports (1977), p.72.

[DJ80] A. Djaloeis, C. Alderliesten, J. Bojowald, C. Mayer-Böricke, W. Oelert and P. Turek, Nucl. Phys. A342(1980) 252.

[VDW78] J. Van de Wiele, E. Gerlic, H. Langevin-Joliot and G. Duhamel, Nucl. Phys. A297(1978) 61 et references internes

[WA78] N.S. Wall, A.A. Cowley and R.C. Johnson, Phys. Rev. C17(1978) 1315.

[WU78] J.R. Wu, C.C. Chang and H.D. Homgren, Phys. Rev. Lett. 40(1978) 1013.

Nuclear Physics **A386** (1982) 29–44
© North-Holland Publishing Company

DESCRIPTION OF α-ELASTIC SCATTERING AND (^{3}He, α) REACTION AT INTERMEDIATE ENERGY WITH A MICROSCOPIC α-NUCLEUS POTENTIAL

M. LASSAUT

Division de Physique Théorique, Institut de Physique Nucléaire, F-91406 Orsay Cedex, France*

and

J. VAN DE WIELE

Division de Recherche Expérimentale, Institut de Physique Nucléaire, F-91406 Orsay Cedex, France

Received 30 March 1982

Abstract: An attempt is made to describe both the α-elastic scattering and the (^{3}He,α) reaction on ^{58}Ni, ^{90}Zr and ^{208}Pb for energies ranging from 100 to 283 MeV where the phenomenological α-nucleus potentials adjusted on elastic scattering data are unable to reproduce correctly the transfer reaction cross sections. In a first step the real and the imaginary part of the microscopic α-nucleus potential are renormalized by multiplicative constants by fitting the α-elastic scattering data then used to calculate the (^{3}He, α) cross sections within the DWBA approximation. We show that such a potential leads to a satisfactory agreement with experiment in what concerns the shape of the angular distribution of transfer reaction and gives C^2S compatible with those determined at low energy from (p, d) and (d, t) reactions. In a second step we show that adding to the microscopic absorptive potential a quite weak surface term is equivalent to the former renormalization of the imaginary potential in the sense that it is sufficient to describe both the α-elastic scattering and the transfer reaction but is, physically, more satisfying.

1. Introduction

At high energy (i.e. for incident energies E_α above 140 MeV) the description of transfer reaction (^{3}He, α) in the DWBA approximation has raised many problems. Contrary to the situation at low energy the α-nucleus potentials adjusted to elastic scattering data above 140 MeV fail to reproduce the transfer reaction cross sections. This has been shown in particular by Chant *et al.* [1]) and Djaloeis *et al.* [2]) at $E_{^3\mathrm{He}} = 132$ MeV and Van de Wiele *et al.* [3]) at $E_{^3\mathrm{He}} = 205$ MeV. The real part of phenomenological potentials used in α-elastic scattering has a Woods–Saxon form factor or in a recent analysis of Van de Wiele [4]) has a Woods–Saxon-squared form factor and is characterized by the fact that it is shallow (of the order of 100 MeV at the origin). To describe the (^{3}He, α) reaction at 205 MeV Van de Wiele *et al.* [3]) have resorted to an empirical α-nucleus potential relevant for transfer reaction more specifically which is constructed as the sum of a ^{3}He-nucleus and a nucleon–nucleus potential. This potential has a deep real part (160 MeV at the origin) and

* Laboratoire associé au CNRS.

leads to a satisfactory reproduction of angular distributions of transfer reaction. Nevertheless it reproduces the α-elastic scattering at forward angles only and one is left with an unsatisfactory situation where simultaneous phenomenological analysis of both elastic scattering and transfer reaction seems to be impossible. The motivation of the present work is to see if elastic scattering and transfer reaction can be fitted simultaneously. We start with a theoretical α-nucleus potential which has been shown to reproduce correctly elastic scattering at 104 MeV [ref. [5])] even though it is not identical to phenomenological potentials.

We have used the microscopic α-nucleus potential derived in the model of Vinh Mau [6]) which, in contrast to earlier works, determines both the real and the imaginary potential. As shown in a previous analysis for the real α-^{40}Ca potential at 104 MeV [5]) the α-nucleus potential has to be renormalized. We have then introduced a renormalization constant λ_R for the real part of the optical potential as is done in ref. [5]) and another one λ_I for the imaginary potential which is assumed first to be also corrected by a multiplicative factor. The renormalized potentials are then tested against the transfer reaction experimental data. Nevertheless the renormalization of the imaginary potential by a multiplicative constant is certainly not the most appropriate way to get the best optical potential. Indeed λ_I is designed to simulate processes which are not taken into account in the microscopic calculation as the break-up of the α-particle. This particular process has been shown to increase with incident energy and to take place essentially at the surface of the nucleus [7]). This has suggested to us to add an adjustable surface term to the theoretical absorptive potential. This approach has been tested against the previous one in what concerns the α-elastic scattering and the transfer reaction.

In sect. 2 we recall the construction of the microscopic α-nucleus potential following refs.[5,6,8]). In sect. 3 we examine the ability of the microscopic α-nucleus potential to reproduce the elastic cross sections and determine a couple of values (λ_R, λ_I) leading to a global satisfactory reproduction of the α-nucleus scattering for energies ranging from 104 to 218 MeV. These parameters are used to calculate the transfer reaction cross sections which are compared in sect. 4 to the experimental data. In sect. 5 we show that the correction of the imaginary potential by a surface term, simulating the break-up processes, is sufficient to reproduce correctly both the α-elastic scattering and the transfer reaction. Our conclusions are presented in sect. 6.

2. The microscopic α-nucleus optical potential

The microscopic α-nucleus interaction used in this work has been calculated within the model of ref. [6]]. Assuming that the α-particle is an elementary particle the α-nucleus potential is calculated as the nucleon–nucleus one where the NN interaction in the latter is replaced by the α-nucleon potential. Nevertheless by considering the projectile as a particle (therefore distinguishable from the nucleons

in the target) no exchange term arises between target and projectile. Consequently the α-nucleus optical potential is given by the Feshbach formula [9]):

$$V_{\alpha N} = V_{\alpha N}^{(0)} + \Delta V_{\alpha N}$$
$$= \left\langle \psi_0 \left| \sum_{i=1}^{A} V_{\alpha N}(i) \right| \psi_0 \right\rangle + \sum_{M \neq 0} \lim_{\varepsilon \to 0^+} \int\!\!\!\!\!\!- \sum_a$$
$$\times \frac{\langle \psi_0 | \sum_{i=1}^{A} V_{\alpha N}(i) | \psi_M \varphi_a \rangle \langle \varphi_a \psi_M | \sum_{j=1}^{A} V_{\alpha N}(j) | \psi_0 \rangle}{E + i\varepsilon - \varepsilon_a - E_M}, \qquad (1)$$

where ψ_0 and A are respectively the ground-state wave function and the mass number of the target, ψ_M and E_M the wave function and energy of its excited states M, φ_a and ε_a the wave function and energy of the α-particle in its intermediate state a and E denotes the c.m. energy of the projectile.

Eq. (1) shows clearly, because the α-nucleon potential is real at least for energies E below 100 MeV [ref. [10])], that the first term $V_{\alpha N}^{(0)}$ is real and that the imaginary part of the α-nucleus interaction is generated by the second term $\Delta V_{\alpha N}$ alone. On the other hand the real part of $\Delta V_{\alpha N}$ gives a correction to the first term $V_{\alpha N}^{(0)}$. Although this correction is expected to be weak [6,8]), it has been taken into account in the present calculation.

The real potential $V_{\alpha N}^{(0)}$ evaluated starting from different α-nucleon interactions derived by Lassaut and Vinh Mau [10]) is studied in detail in ref. [5]). The calculation of the second term has been performed refining the previous approximations of Vinh Mau [6]). We have then worked under the following assumptions:

– the α-particle propagator in eq. (1) is calculated in the eikonal approximation accordingly to ref. [11]),

– ψ_0 is a Slater determinant,

– to simplify the calculation, we suppose that the α-nucleon interaction is gaussian,

– the energy E is high enough so that all strongly excited states contribute to the sum over M and that their energy E_M can be replaced by an average value $\bar{E}_M$ namely $E - E_M \simeq E - \bar{E}_M$. This will be the case in this work as we consider α-particle lab energies above 100 MeV.

It is then possible to use a closure relation on intermediate states of the target nucleus. The derivation of $\Delta V_{\alpha N}$ following refs. [6,8]), where the case $\bar{E}_M = 0$ MeV was treated, is straightforward and therefore not reproduced here. The final expression of $\Delta V_{\alpha N}$, given in ref. [8]) involves the target ground-state density, the parameters of the gaussian α-nucleon interaction and the average energy $\bar{E}_M$. The target densities used in this paper are those derived by Alkhazov *et al.* [12]) which have been modified as explained in ref. [5]). The gaussian α-nucleon interaction is the parametrization of the α-N potential derived in ref. [10]) from the B_1 force of Brink and Boeker [13]) and $\bar{E}_M$ has been evaluated as being $\bar{E}_M = 1\hbar\omega$ MeV for a closed shell nucleus. To have a consistent calculation of the optical potential we

have used the potential $V^{(0)}_{\alpha N}$ derived with the same B_1 force. This potential is from now on labelled M_I.

However a preliminary test of the real part of α-^{40}Ca potential [5]) against the experimental data at 104 MeV has shown that using density dependent NN interactions [like the G-0 force of Banerjee–Campi–Sprung [14]) or that of Jeukenne, Lejeune and Mahaux (JLM) [15])] instead of the density-independent B_1 force leads to a better reproduction of the α-elastic scattering. The fact that, in contrast to the B_1 force, the G-0 interaction yields an α-nucleon potential unable to be represented by a gaussian, prevents from using it in the calculation of the second term. Nevertheless to test our optical potential in the study of the $(^3He, \alpha)$ reaction, we have considered two additional potentials that we have labelled M_{II} and M_{III}; their real parts are respectively the potentials G-0^{RT} and the potential JLMI constructed as explained in ref. [5]) from the G-0 and the JLM forces respectively while their imaginary part is that of potential M_I.

3. Elastic scattering cross section at 140, 166 and 218 MeV for ^{58}Ni, ^{90}Zr and ^{208}Pb

A previous analysis of the real part of the potential tested with an adjustable imaginary potential of WS^2 shape against the α-^{40}Ca elastic scattering data at 104 MeV [ref. [5])], has pointed out the necessity of renormalizing the real potential to describe the elastic cross sections. This has prompted us to consider the potential:

$$V = \lambda_R V_R + i\lambda_I V_I , \tag{2}$$

where V_R and V_I are the microscopic real and imaginary potential while λ_R and λ_I are parameters designed to be adjusted on the α-elastic scattering data.

3.1. DETERMINATION OF λ_R AND λ_I AT FIXED ENERGY FOR A GIVEN NUCLEUS

As the transfer reaction will be studied for ^{58}Ni, ^{90}Zr and ^{208}Pb above 100 MeV, we have considered the α-elastic experimental cross sections of Goldberg *et al.* at the incident lab energy $E_\alpha = 140$ MeV for ^{58}Ni and ^{208}Pb [16]) and those of Bimbot *et al.* at $E_\alpha = 166$ MeV for these three nuclei [17]). We have also taken into account in our analysis the recent measurement of the α-^{208}Pb cross section at 218 MeV acquired by Marty *et al.* [18]).

The couple of parameters λ_R and λ_I is varied in a modified version of the automatic search code JIB3 [ref. [19])] to yield a minimum of χ-square per degree of freedom χ^2/F. The resulting values of λ_R and λ_I are presented in table 1 together with the volume integral per nucleon pair J and the rms radius of the real and imaginary part of potential of eq. (2). The elastic cross sections calculated with the renormalized potential have been compared to the experimental data and are presented in fig. 1. For all potentials M_I, M_{II} and M_{III} the agreement is relatively

TABLE 1

Renormalization constants, volume integrals per nucleon pair and rms radii of renormalized α-nucleus potentials and those of phenomenological potentials for different energies and nuclei

Nucleus	Energy (MeV)	Potential	Real part			Imaginary part			χ^2/F	Ref.
			λ_R	J_R	$\langle r^2\rangle_R^{1/2}$	λ_I	J_I	$\langle r^2\rangle_I^{1/2}$		
^{58}Ni	104	M_I	0.72	298	4.74	1.62	225	4.63		
		M_{II}	0.68	310	4.76	1.69	235	4.63		
		M_{III}	1.00	397	4.42	1.53	213	4.63		
		phenom		315	4.69		93	5.27		[27]
^{58}Ni	140	M_I	0.74	282	4.75	1.38	180	4.59	88	
		M_{II}	0.64	283	4.77	1.29	168	4.59	68	
		M_{III}	0.88	323	4.41	1.16	151	4.59	58	
		phenom		298	4.76		95	5.23		[16]
^{58}Ni	166	M_I	0.71	255	4.76	1.28	161	4.56	66	
		M_{II}	0.61	265	4.78	1.27	159	4.56	42	
		M_{III}	0.95	329	4.41	1.31	164	4.56	28	
		phenom		283	4.72		101	5.12		[17]
^{90}Zr	166	M_I	0.69	244	5.29	1.11	133	5.17	4.5	
		M_{II}	0.59	253	5.30	1.13	135	5.17	3.6	
		M_{III}	0.86	298	4.94	1.04	124	5.17	1.7	
		phenom		284	5.21		89	5.78		[17]
^{208}Pb	140	M_I	0.86	304	6.36	2.08	239	6.28	24	
		M_{II}	0.76	316	6.37	2.20	253	6.28	34	
		M_{III}	1.17	417	6.04	2.07	238	6.28	21	
		phenom		283	6.58		81	7.36		[16]
^{208}Pb	166	M_I	0.69	231	6.38	1.46	164	6.28	23	
		M_{II}	0.59	241	6.39	1.52	171	6.28	35	
		M_{II}	0.97	326	6.04	1.57	176	6.28	32	
		phenom		276	6.40		74	7.28		[17]
^{208}Pb	218	M_I	0.75	224	6.40	1.30	138	6.22	74	
		M_{II}	0.61	239	6.41	1.35	143	6.22	83	
		M_{III}	1.02	305	6.03	1.90	201	6.22	30	
		phenom		264	6.60		68	7.38		[18]

The "experimental" cross sections at 104 MeV are those calculated from the phenomenological potential of Rebel *et al.* [27]).

satisfactory for ^{58}Ni and ^{90}Zr at 140 and 166 MeV up to $\theta_{c.m.} = 30$–$35°$ but at larger angles the theoretical cross sections are larger than the experimental ones. A satisfactory agreement is observed for the ^{208}Pb at $E_\alpha = 140$, 166 and 218 MeV. Fig. 1 shows clearly that the elastic cross sections are the best reproduced, in particular the minima, with potential M_{III} and that the overall agreement is better for M_{II} than for M_I. This is confirmed by results of table 1 which display the best values of χ^2/F for potential M_{III} and better χ^2/F for M_{II} than for M_I.

Examination of table 1 shows that λ_R is always lower than unity, except for potential M_{III}, the strongest deviation corresponding to potential M_{II} and the

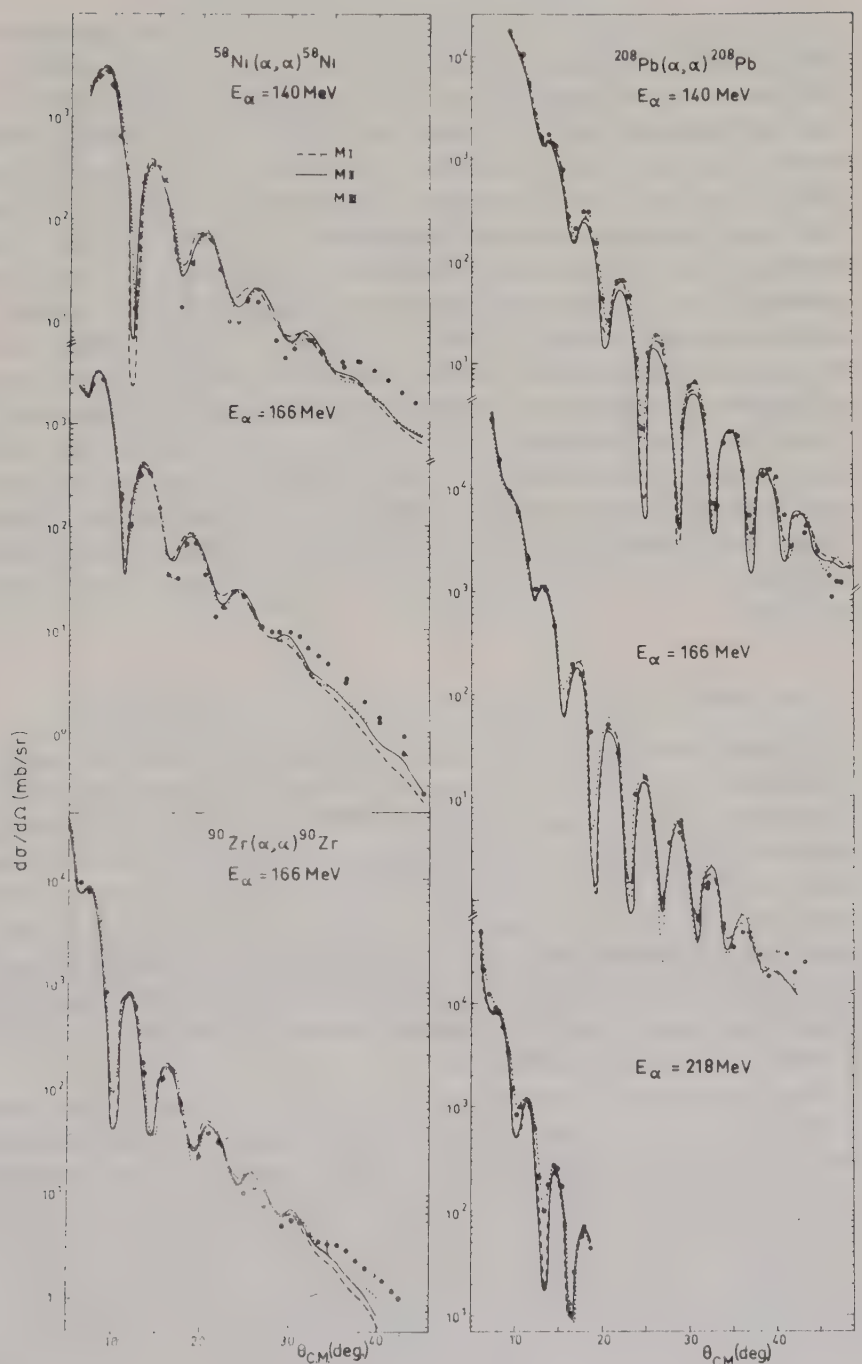

Fig. 1. α-elastic cross sections calculated for potentials M_I, M_{II} and M_{III} renormalized according to eq. (2) with parameters of table 1.

weakest to potential M_{III}. It leads to values of J close to the phenomenology for the real part of potentials M_I and M_{II} which have an rms radius in excellent agreement with the phenomenological results, while J is larger by a factor 1.2–1.3 than the phenomenological values for potential M_{III} which displays systematically too weak a radius. The renormalization constant λ_I of the imaginary potential is always larger than one (of the order of 1.5) and leads to volume integral much larger than those predicted by the phenomenology while the rms radii are noticeably smaller. In figs. 2a–d we have displayed the real and imaginary part of the α-^{58}Ni potential at 140 and 166 MeV renormalized according to table 1 together with the phenomenological potential of refs.[16,17]). One sees that our potentials are close to the phenomenology at the surface but differ in the interior mainly for the real part of potential M_{III} (deeper by a factor of 2) and the imaginary potential five times deeper than the phenomenology. The same trend is observed for other nuclei and energies. It seems that the fitting procedure determines the renormalization constants from the surface region only disregarding the interior. This means that correcting the potential and mainly the imaginary one by a multiplicative constant at all distances is certainly not a reliable way to get the best optical potential.

3.2. DETERMINATION OF λ_R AND λ_I IN ALL THE ENERGY DOMAIN

We have attempted to get an unique couple of parameters λ_R and λ_I leading through eq. (2) to a satisfactory overall agreement for all energies and if possible all nuclei. The previous analysis displays values of λ_R and λ_I much scattered with the energy and the nucleus, mainly for the renormalization constant of the imaginary potential. This situation is inherent to the method of determination of the parameters by a minimization procedure: indeed we have checked that a rather large change of both parameters λ_R and λ_I can produce only small modifications of the χ^2/F. This makes it doubtful to extrapolate the unique couple of parameters from the punctual results of table 1. Therefore we have repeated the analysis developed in subsect. 3.1 in a quite different way.

In a previous work [5]), we have noticed that the behaviour with the energy of the volume integral of the real α-^{40}Ca potential is close to phenomenology. This has suggested to us an adjustment of the volume integral of the microscopic real potential on that of the phenomenological potential. For incident energies E_α below 200 MeV we get parameters λ_R very stable with the energy and the target nucleus and we have then extracted an unique value, given in table 2. Nevertheless the parameters λ_R vary by about 10% for the α-^{208}Pb M_I and M_{III} potentials between 166 and 218 MeV which could be explained by the fact that the experimental data at 218 MeV extend on a very weak angular range, $\theta_{c.m} < 20°$, generating some uncertainties on the phenomenological potential. This has led us to disregard the results at 218 MeV and keep the value of λ_R listed in table 2.

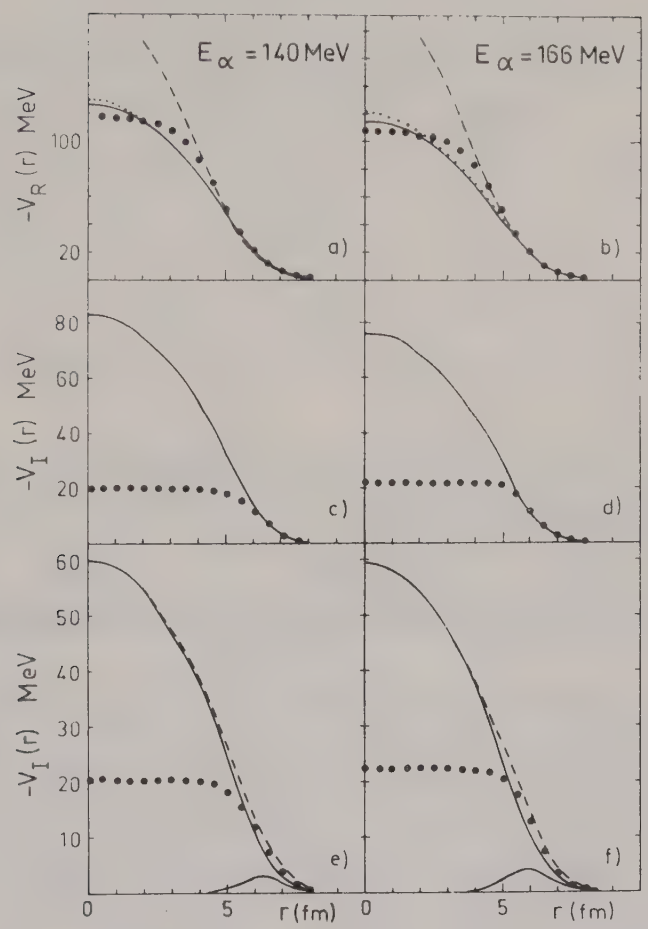

Fig. 2. (a), (b): Real part of the α-^{58}Ni potential renormalized following eq. (2) with parameters of table 1: potentials M_I, solid line; M_{II}, dotted line and M_{III} dashed line. (c), (d): Imaginary part of the α-^{58}Ni potential M_I renormalized via eq. (2) with parameters of table 1: solid line. (e), (f): Microscopic α-^{58}Ni potential, solid line; this potential plus the surface term, dashed line. In all figures the dots refer to phenomenological potentials of ref. [16]) for $E_\alpha = 140$ MeV and ref. [17]) for $E_\alpha = 166$ MeV.

A similar attempt would fail for the imaginary potential as the volume integral of the microscopic potential does not vary in the same way as the phenomenological one. Consequently starting from the value of λ_R of table 2, we have made a search restricted to parameter λ_I only. For ^{58}Ni the renormalization constants of the imaginary potential are nearly constant with the energy. We have reproduced their average value in table 2. It leads to value of χ^2/F close to those of table 1 for ^{58}Ni and ^{90}Zr but very large χ^2/F as compared to the results of table 1 for the ^{208}Pb. In this latter case, the search for λ_I displays values scattered with the energy but because of uncertainties due to the existence of discrete ambiguities at 140 MeV

TABLE 2

Parameters λ_R and λ_I used for calculation of the $(^3He, \alpha)$ reaction cross sections

Potential	Nucleus	λ_R	λ_I
M_I	^{58}Ni, ^{90}Zr	0.79	1.52
	^{208}Pb		1.82
M_{II}	^{58}Ni, ^{90}Zr	0.67	1.40
	^{208}Pb		1.83
M_{III}	^{58}Ni, ^{90}Zr	0.81	1.05
	^{208}Pb		1.47

and to the fact that the angular range of experimental points is not extended enough at 218 MeV, we use at all energies the value determined by the search code at 166 MeV which is listed in table 2.

4. Study of transfer reaction at high energy with the renormalized microscopic potential

We have calculated the cross sections corresponding to the following final states $\frac{7}{2}^-$ at 2.56 MeV of ^{57}Ni, $\frac{9}{2}^+$ ground state of ^{89}Zr and $\frac{13}{2}^+$ at 1.63 MeV of ^{207}Pb and compared our results to the experimental cross sections acquired at $E_{^3He} = 132$ MeV for ^{58}Ni and ^{90}Zr [refs. [2,20])], at 205 MeV for ^{58}Ni, ^{90}Zr and ^{208}Pb [ref. [3])] and 283 MeV for ^{90}Zr and ^{208}Pb [refs. [21,22])]. At high energy the so-called DWBA zero-range approximation is no longer adequate ref. [23]). We have then performed exact finite-range calculations with the microscopic range function of ref. [4]), by using a modified version of code MARY [24]). In the incident channel we consider the phenomenological ^3He-nucleus potentials induced from elastic scattering data by Chant *et al.* [1]) at $E_{^3He} = 132$ MeV lab energy for ^{58}Ni and ^{90}Zr and by Willis *et al.* [25]) at $E_{^3He} = 205$ MeV for ^{58}Ni, ^{90}Zr and ^{208}Pb. At 283 MeV the ^3He-nucleus elastic scattering has not yet been measured. We have then extrapolated the ^3He-^{208}Pb potential of Willis *et al.* at 205 MeV by lowering the strength of its real part from 78 MeV up to 70 MeV taking into account the available phenomenological results about the energy dependence of the ^3He-nucleus optical potential. The optical potentials for the α-particle are the potentials M_I, M_{II} and M_{III} renormalized with coefficients of table 2.

Some of the resulting angular distributions are presented in fig. 3 [curves (a)]. For all nuclei and energies considered the shape of the angular distribution is correctly reproduced. According to a previous analysis of Van de Wiele [4]) the sensitivity of the shape of angular distribution to the α-nucleus potential is the weakest as the nucleus is heavy. Indeed the ^{208}Pb leads to results very close to

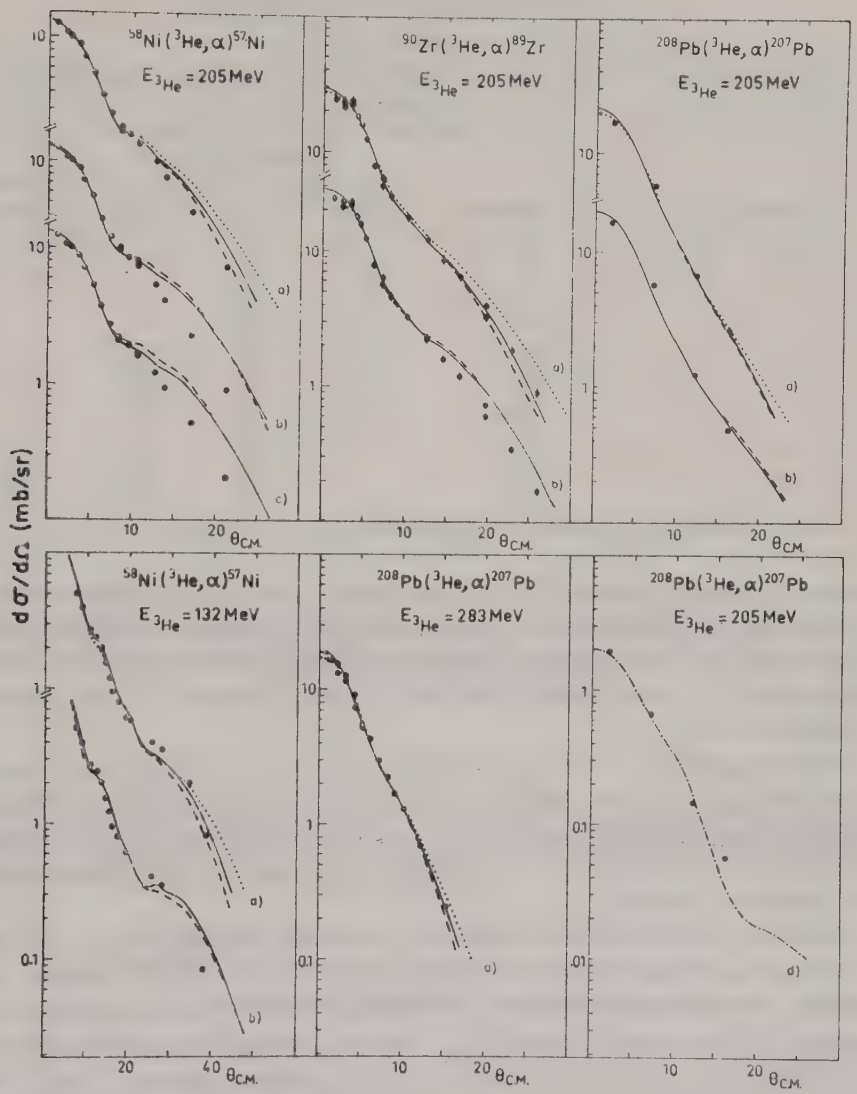

Fig. 3. Angular distributions of the $(^3He, \alpha)$ reaction calculated with potential M_I, dashed line; M_{II}, solid line and M_{III}, dotted line; the curves (a) refer to calculations where the imaginary potential is renormalized by λ_I, the curves (b) correspond to calculations where a surface term is added to the microscopic absorptive potential and the curves (c) refer to the same calculations as curves (b) but with another surface term (see text). The curve (d) corresponds to a calculation involving the α-^{208}Pb phenomenological potential of ref. [18]). The dots represent the experimental data.

each other for potentials M_I, M_{II} and M_{III} while for ^{58}Ni and ^{90}Zr we observe a better agreement with the experimental points for potentials M_I and M_{II}.

The spectroscopic factors extracted (C^2S) are listed in table 3 and compared to those determined at low energy from (p, d) and (d, t) transfer reaction [3]). Our

TABLE 3

Comparison of spectroscopic factors deduced from DWBA calculations with potentials of eq. (2) with reference data (see text)

Nucleus	*nlj*	Potential	Energy (MeV) 132	205	283	Reference data
^{57}Ni	$1f_{7/2}$	M_I	2.15	2.1		
		M_{II}	2.0	2.3		3
		M_{III}	1.1	1.5		
^{89}Zr	$1g_{9/2}$	M_I	7.5	5.75	5.9	
		M_{II}	7.4	6.2	7.85	8
		M_{III}	4.75	3.9	3.8	
^{207}Pb	$1i_{13/2}$	M_I		6.9	8.4	
		M_{II}		7	10.9	10
		M_{III}		4.7	6	

spectroscoscopic factors are always lower but the agreement is relatively satisfactory, except may be for potential M_{III} where the C^2S is always smaller by a factor of 2 than the previous ones. The agreement for the α-^{208}Pb M_{III} potential is improved if one uses $\lambda_I = 1.92$, a value arising from the adjustment on the experimental data of Marty *et al.* [18]).

Following Sakai [21]), we have examined the behaviour with the energy of the integrated pick-up cross section. The calculated and experimental total pick-up cross sections corresponding to the $1i_{13/2}$ state at 1.63 MeV of ^{207}Pb are presented for different energies in fig. 4. The variation with energy is reasonably reproduced at least above 100 MeV.

We have shown that our microscopic potentials renormalized on the available α-elastic scattering data are able to reproduce the shape of the transfer reaction angular distributions and lead to C^2S compatible with results obtained at low energy. Consequently they allow a coherent description of both the α-elastic scattering and the $(^3\text{He}, \alpha)$ reaction at high energy contrary to the α-nucleus phenomenological potentials which failed to reproduce the transfer reaction angular distributions [as an example we display in fig. 3 [curve (d)] the angular distribution of the $^{208}\text{Pb}(^3\text{He}, \alpha)^{207}\text{Pb}$ reaction at 205 MeV given by the potential of ref. [18])].

The calculated cross sections depend on the microscopic finite range function and the ^{3}He-nucleus potential. We have studied the influence of this latter potential on the shape of the angular distributions and the absolute value of the cross sections for ^{208}Pb at 283 MeV by shallowing the strength of the real part of the ^{3}He-^{208}Pb potential from 70 to 55 MeV. These two values can be regarded as the upper and lower limits we get by extrapolating the ^{3}He-^{208}Pb potential at 205 MeV. The angular distribution calculated with the shallowest potential decreases more rapidly and leads to a disagreement with the experimental points while the C^2S are hardly

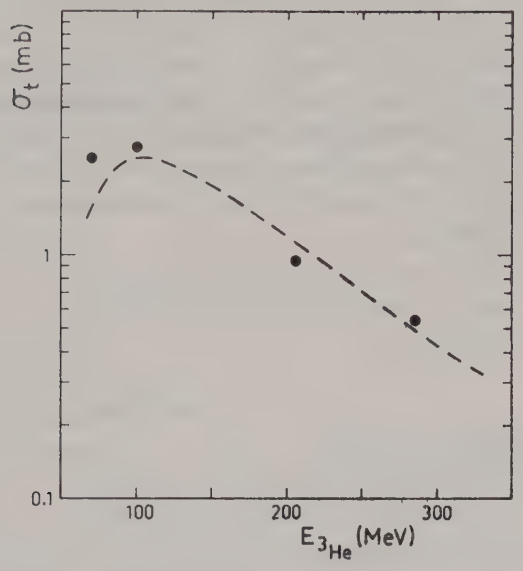

Fig. 4. Variation with incident energy $E_{^3He}$ of the integrated pick-up cross section for ^{208}Pb. Dashed line, our calculation; dots, experimental results at $E_{^3He} = 70$ MeV [ref. [28])], 100 MeV [ref. [29])], 205 MeV [ref. [3])] and 283 MeV [ref. [22])].

changed. This suggests to us that our results could be improved by using instead of a ^{3}He-nucleus potential adjusted on ^{3}He-elastic scattering a microscopic ^{3}He-nucleus potential as is done for the α-channel.

5. Simulation of α-particle break-up effects and its influence on α-elastic scattering and transfer reaction

The volume integral of the imaginary part of the renormalized potential is too large by a factor of two as compared to phenomenology. This very large value has two sources. First, the microscopic potential is overestimated in the interior mainly due to the neglect of the imaginary part of the local momentum involved in the Green propagator and in the Perey–Saxon approximation [26]). Second, the way we renormalize the potential by a multiplicative factor is not adapted to our potential. Indeed the fitting procedure tends to correct the imaginary potential at the surface only where it is not absorptive enough, increasing the strength of the potential at all distances.

The lack of absorption of our imaginary potential at the surface would be corrected by taking into account the α-particle break-up in the microscopic calculation. Indeed the α-particle break-up cross sections increase with the energy [7]) and correspond to a reaction essentially peripheral. We have attempted to simulate

these effects by adding to our microscopic imaginary potential a term contributing to the potential at the surface only.

This surface term is determined only qualitatively by using our previous fitting results. The difference $W_{ph} - W_{th}$ (for r large enough) between the phenomenological potential or equivalently the renormalized potential and the unrenormalized potential is peaked at the surface region and behaves like an exponential function asymptotically. This has suggested to us a parametrization of the surface term by a derivative of a WS:

$$W = W_S \frac{e^x}{(1+e^x)^2}, \tag{3}$$

where

$$x = (r - r_S A^{1/3})/a_S . \tag{4}$$

The α-nucleus potential is now

$$V = \lambda_R V_R + i(V_I + W) . \tag{5}$$

The real potential is the same as in our previous analysis with $\lambda_R = 0.79$ for M_I and 0.67 for M_{II}. (We have disregarded the potential M_{III} as its real part displays too weak a radius and it does not reproduce the transfer reaction so well as M_I and M_{II}). The potential V_I is the microscopic potential and W is given by eq. (3). Its diffusivity and position are directly determined from the function $W_{ph} - W_{th}$ where W_{ph} is chosen as the phenomenological potential of Goldberg *et al.* [16]) at $E_\alpha = 140$ MeV for ^{58}Ni and those of Bimbot *et al.* [17]) at 166 MeV for ^{58}Ni, ^{90}Zr and ^{208}Pb. Its strength is fitted on the α-elastic scattering data starting from the potential of eq. (5). We have listed in table 4 the values of parameters W_S, r_S and a_S for the potential M_I together with the χ^2/F, the volume integral per nucleon pair and the rms radius of the modified imaginary potential. The χ^2/F are comparable to those obtained by using the parameter λ_I of table 2 ($\chi^2/F = 91$ and 81 for ^{58}Ni at 140 and 166 MeV; 6.07 and 86 for ^{90}Zr and ^{208}Pb at 166 MeV) except for ^{208}Pb where the χ^2/F has become 1.6 times larger. A comparison between

TABLE 4

Parameters of the surface term, eq. (3), volume integral per nucleon pair and rms radius of imaginary part of potential of eq. (5) and χ^2/F given by potential of eq. (5)

Nucleus	W_S	r_S	a_S	$r_S A^{1/3}$	$J/4A$	$\langle r^2 \rangle^{1/2}$	χ^2/F
^{58}Ni	2.63×4 [a])	1.58 [a])	0.62 [a])	6.12 [a])	144 [a])	4.82 [a])	104 [a])
	4.19×4	1.50	0.52	5.81	142	4.77	92
^{90}Zr	2.57×4	1.50	0.60	6.72	129	5.34	6.07
^{208}Pb	3.09×4	1.54	0.78	9.12	125	6.69	86

The label [a]) refers to results obtained at $E_\alpha = 140$ MeV, otherwise $E_\alpha = 166$ MeV.

tables 1 and 4 indicates that the volume integral and the rms radius of the new imaginary potential have improved as compared to the phenomenological values. Figs. 2e,f display the microscopic α-^{58}Ni imaginary potential and this potential plus W at 140 and 166 MeV both compared to phenomenology. At the surface the modified potential is close to the empirical one and to our first renormalized potential.

The imaginary potential of eq. (5) is now used for the calculation of the cross sections of the (^{3}He, α) reaction on ^{58}Ni at $E_{^3He} = 132$ MeV and on ^{58}Ni, ^{90}Zr and ^{208}Pb at 205 MeV. At 132 MeV we use the parameters of table 4. At 205 MeV we have taken the difference between the microscopic potential and the potential α_{III} of ref. [3]) without any further fit.

The angular distributions drawn in fig. 3 [curves (b)] can be directly compared to those given by the potential of eq. (2). It can be seen that the shape of the angular distribution is correctly reproduced even though the agreement is slightly less satisfactory than by using the imaginary potential renormalized by λ_I. However this is, in some measure, not very surprising since unlike the constant λ_I the parameters of W have not been determined (excepted the strength of W at 140 MeV) in order to get the best fits with α-elastic scattering cross sections. The spectroscopic factors given in table 5, are either unchanged or slightly improved. As previously, the best results occur for potential M_{II}.

TABLE 5

Spectroscopic factors deduced from DWBA calculations with the potential of eq. (5)

Nucleus	Potential	Energy (MeV)	
		132	205
^{57}Ni	M_I	2.4	2.1
	M_{II}	2.25	2.3
^{89}Zr	M_I		6.1
	M_{II}		6.4
^{207}Pb	M_I		6.9
	M_{II}		7.0

We have tested the influence of the position and the depth of the surface term by repeating the calculation of ^{58}Ni(^{3}He, α)^{57}Ni reaction cross section with the term W determined for α-^{58}Ni elastic scattering at 166 MeV, located at 5.8 fm instead of 5.4 fm and 4.19 MeV deep instead of 2.59 MeV. The results are practically unchanged in what concerns the angular distributions [see fig. 3, curves (c)] but the C^2S are improved of 10% ($C^2S = 2.35$ for M_I and 2.55 for M_{II}).

References

1. N.S. Chant, H. Chen, D.A. Goldberg, A. Nadasen and P.G. Roos, University of Maryland, Progress Reports (1977), p. 72
2) A. Djaloeis, C. Alderliesten, J. Bojowald, C. Mayer-Böricke, W. Oelert and P. Turek, Nucl. Phys. **A342** (1980) 252
3) J. Van de Wiele, E. Gerlic, H. Langevin-Joliot and G. Duhamel, Nucl. Phys. **A297** (1978) 61, and references therein
4) J. Van de Wiele, thèse de doctorat d'Etat, Orsay (1980)
5) F. Duggan, M. Lassaut, F. Michel and N. Vinh Mau, Nucl. Phys. **A355** (1981) 141
6) N. Vinh Mau, Phys. Lett. **71B** (1977) 5; Proc. Second Louvain–Cracow Seminar on the alpha-nucleus interaction, Louvain-la-Neuve, 1978, ed. G. Grégoire and K. Grotowski, unpublished, p. 243
7) G. Baur, F. Rösel, R. Shyam and D. Trautmann, KFA Jülich, Annual Report (1978) p. 131, 132, and references therein;
   R. Shyam, G. Baur, F. Rösel and D. Trautmann, Phys. Rev. **C19** (1979) 1246, and references therein;
   N.S. Wall, A.A. Cowley and R.C. Johnson, Phys. Rev. **C17** (1978) 1315;
   J.R. Wu, C.C. Chang and H.D. Holmgren, Phys. Rev. Lett. **40** (1978) 1013
8) M. Lassaut and N. Vinh Mau, to be published
9) H. Feshbach, Ann. of Phys. **5** (1958) 357
10) M. Lassaut and N. Vinh Mau, Phys. Lett. **70B** (1977) 14; Nucl. Phys. **A349** (1980) 372
11) A. Bouyssy, N. Vinh Mau and D.M. Brink, Phys. Lett. **102B** (1981) 109
12) G.D. Alkhazov, S.L. Belostotsky and A.A. Vorobyov, Phys. Reports **42C** (1978) 89
13) D.M. Brink and E. Boeker, Nucl. Phys. **A91** (1967) 1
14) D.W.L. Sprung and P.K. Banerjee, Nucl. Phys. **A168** (1971) 273;
   X. Campi and D.W.L. Sprung, Nucl. Phys. **A194** (1972) 401
15) J.P. Jeukenne, A. Lejeune and C. Mahaux, Phys. Rev. **C16** (1977) 80
16) D.A. Goldberg, S.M. Smith, H.G. Pugh, P.G. Roos and N.S. Wall, Phys. Rev. **C7** (1973) 1938
17) L. Bimbot, B. Tatischeff, I. Brissaud, Y. Le Bornec, N. Frascaria and A. Willis, Nucl. Phys. **A210** (1973) 397;
   L. Bimbot, thèse de doctorat d'Etat, Orsay (1973)
18) C. Djalali, thèse de 3è Cycle, Orsay (1981)
19) F. Perey, private communication
20) J.P. Didelez, A. Djaloeis, A. Galonsky and W. Oelert, K.F.A. Jülich, Annual Report (1976) p. 16
21) M. Sakai, private communication
22) H. Langevin-Joliot, E. Gerlic, J. Guillot, M. Sakai, J. Van de Wiele, A. Devaux, P. Force and G. Landaud, to be published
23) N.S. Chant and J.N. Craig, Phys. Rev. **C14** (1976) 1763;
   N.S. Chant, Nucl. Phys. **A211** (1973) 269
24) N.S. Chant, Computer code MARY, University of Maryland, private communication
25) N. Willis, I. Brissaud, Y. Le Bornec, B. Tatischeff and G. Duhamel, Nucl. Phys. **A204** (1973) 454
26) J.W. Negele and K. Yazaki, Phys. Rev. Lett. **47** (1981) 71; S. Fantoni, B.L. Friman and V.R. Pandharipande, Phys. Lett. **104B** (1981) 89
27) H. Rebel, R. Löhken, G.W. Schweimer, G. Schatz and G. Hauser, Z. Phys. **256** (1972) 258
28) S. Galès, G.M. Crawley, D. Weber and B. Zwieglinski, Phys. Rev. **C18** (1978) 2475
29) J. Guillot, J. Van de Wiele, H. Langevin-Joliot, E. Gerlic, J.P. Didelez, G. Duhamel, G. Perrin, M. Buenerd and J. Chauvin, Phys. Rev. **C21** (1980) 879

CONCLUSION

Notre étude du potentiel optique α-noyau a mis en évidence un certain nombre d'effets importants qui doivent être pris en compte et permettent de mieux reproduire ses propriétés déduites des analyses phénoménologiques de la diffusion élastique (α,α). Notre travail,reposant sur la théorie de Feshbach,suppose que la particule alpha conserve sa structure au cours du processus de collision, hypothèse qui implique que nous négligeons dès le départ les voies inélastiques correspondant au break-up de la particule alpha. Néanmoins,ces voies sont importantes pour des énergies supérieures à 100 MeV et nous en avons tenu compte dans la discussion de nos résultats.

Dans notre modèle, l'interaction de départ est l'interaction α-nucléon qui, lorsqu'elle est calculée à partir d'une interaction nucléon-nucléon qui possède les bonnes propriétés de saturation, a une forte composante non locale, seule responsable en fait du caractère attractif de l'interaction α-nucléon, qui de plus a un rayon de non localité proche de sa portée. Alors que cette interaction α-nucléon était, dans toutes les études précédentes de la partie réelle du potentiel α-noyau, remplacée par une interaction locale, nous avons montré qu'il était indispensable de l'utiliser sous sa forme originale, sa composante non locale introduisant trois effets importants sur le calcul du potentiel optique α-noyau, effets complètement détruits par l'utilisation d'une interaction α-nucléon locale équivalente. Le potentiel réel, ainsi calculé comme produit de convolution de l'interaction α-nucléon non locale par la densité du noyau cible,est un potentiel non local

dont le rayon de non localité est faible comparé à sa portée. La dérivation du potentiel local qui lui est équivalent est donc moins ambiguë. Elle conduit à un potentiel réel beaucoup moins profond à courtes distances dont la forme est modifiée : gaussienne pour une interaction α-nucléon locale, elle est maintenant proche d'une forme de puits de Woods-Saxon élevé à une puissance supérieure à 2. De plus, son intégrale de volume par paires de nucléons n'est plus une constante comme précédemment, mais une fonction décroissante du nombre A de nucléons du noyau cible, avec une rupture de pente nette pour le ^{58}Ni, conformément aux informations apportées par les analyses phénoménologiques de diffusion. Enfin, et c'est là un résultat très important, la non localité du potentiel réel a une grande influence sur la détermination du potentiel imaginaire local. En effet, le potentiel imaginaire local, résultant de la dérivation du potentiel local équivalent au potentiel α-noyau non local, parties réelle et imaginaire, est fortement réduit par rapport au potentiel imaginaire dérivé en supposant le potentiel réel purement local. Le facteur de réduction, approximativement égal à $\frac{m^*_\alpha(r)}{m_\alpha}$, où m^*_α est la masse effective de la particule alpha, est voisin de 0.6 à l'intérieur, puis croît et devient proche de 1 à la surface. Il modifie donc à la fois la forme et la profondeur du potentiel imaginaire.

Outre son caractère non local, l'interaction α-nucléon, calculée pour des interactions nucléon-nucléon effectives déduites d'études effectuées dans la matière nucléaire, dépend de la densité aux points 1 et 2, caractérisant la position des deux nucléons en interaction. Alors que pour le système α-nucléon, décrit dans l'approximation de Hartree-Fock, cette densité est simplement reliée à la densité à un corps de la particule alpha, pour le système α-noyau, où l'un des deux nucléons en interaction est dans la particule

alpha et l'autre dans le noyau, la relation entre la densité $\rho(1,2)$ et les densités non perturbées de l'alpha et du noyau n'est plus aussi clairement définie. Nous avons utilisé une relation qui, à l'encontre de celle couramment utilisée qui est la somme des densités de l'alpha et du noyau, ne conduit jamais à des valeurs de ρ excédant la densité nucléaire normale, mais qui par contre sous-estime vraisemblablement l'effet de la densité aux grandes distances. Nous avons aussi montré,dans ces deux cas,que tenir compte de la densité du noyau cible dans l'interaction effective modifie la profondeur du potentiel à courtes distances et permet de mieux reproduire sa dépendance en A.

Ces résultats correspondent au potentiel réel du modèle de convolution,qui représente le premier terme du potentiel de Feshbach. Nous avons également calculé la correction à ce potentiel apportée par le second terme du potentiel de Feshbach, correction qui n'excède jamais 5%, augmente la profondeur du potentiel et ne peut donc expliquer les facteurs de renormalisation que nous devons introduire pour reproduire les sections efficaces de la diffusion élastique. Ces facteurs de renormalisation, toujours inférieurs à l'unité et plus petits pour les interactions dépendant de la densité,proviennent plutôt de notre traitement incomplet de l'antisymétrisation et, dans le cas des interactions dépendant de la densité, du traitement de cette dépendance en densité. En particulier, nous avons montré que l'inclusion des termes de réarrangement du potentiel Hartree-Fock diminue sensiblement la profondeur du potentiel α-noyau. Malheureusement, les calculs deviennent alors très compliqués et nous n'avons pu les mener à bien que sous certaines hypothèses. Cependant, une renormalisation globale de la profondeur de nos potentiels, indépendante de l'énergie, suffit pour reproduire les sections efficaces ce qui montre que la forme de nos potentiels

ainsi que leur dépendance en énergie, sont très satisfaisantes, l'accord étant meilleur pour les interactions nucléon-nucléon dépendant de la densité.

Alors que pour le potentiel réel, qui a fait l'objet de nombreuses études dans le cadre du modèle de convolution, nous nous sommes attachés, à l'intérieur du modèle de convolution, à traiter le mieux possible tous les effets qui nous semblaient importants, pour le potentiel imaginaire, qui n'a suscité que peu d'études théoriques et dont la détermination à partir des données expérimentales reste encore ambiguë, nous nous sommes limités à une recherche de ses propriétés globales et avons utilisé des approximations qui nous ont permis de simplifier son calcul. En particulier, l'interaction α-nucléon est remplacée par l'interaction locale dérivée de l'interaction de Brink et Boeker. Nous avons aussi obtenu une expression du potentiel imaginaire qui est facilement utilisable pour tous les noyaux, puisqu'elle ne fait intervenir que les densités locales et non locales de l'état fondamental du noyau cible et un paramètre qui représente l'énergie moyenne des états nucléaires les plus fortement excités dans une réaction α-noyau. Cependant, ces approximations ne sont valables que pour des énergies relativement grandes par rapport à cette énergie moyenne, et pour des énergies plus faibles nous devons tenir compte explicitement de toutes les voies inélastiques ouvertes. Pour des énergies supérieures à 80-100 MeV, notre potentiel imaginaire est de forme Woods-Saxon carré, corroborant les analyses phénoménologiques récentes qui semblent montrer une préférence pour de telles formes. L'intégrale de volume de nos potentiels varie peu avec l'énergie mais montre une légère décroissance. Ce comportement est compatible avec les résultats des analyses phénoménologiques, qui ont cependant une grande dispersion, pour des énergies

supérieures à approximativement 80 MeV pour le ^{40}Ca, 50 MeV pour le ^{44}Ca par exemple. Comme nous pouvions nous y attendre, la limite de validité de nos approximations dépend du noyau,en liaison avec l'énergie moyenne des états les plus excités qui est plus élevée pour les noyaux à couches fermées que pour les noyaux ayant plusieurs nucléons de valence. Cette différence des énergies moyennes dans l'un et l'autre type de noyaux se reflète également dans la variation de l'intégrale de volume avec A, le nombre de masse du noyau cible. En effet,nous avons obtenu une variation linéaire avec des écarts pour les noyaux à couches fermées. Dans le domaine d'énergies compatibles avec nos approximations, ces écarts sont faibles et décroissent avec l'énergie. Ce problème de différences entre potentiels absorptifs des noyaux à couches fermées et des noyaux voisins est particulièrement intéressant à basse énergie où les écarts sont importants. Malheureusement, il n'est pas facile à traiter même si intuitivement la théorie de Feshbach nous en suggère l'origine. En effet, l'absorption, due à l'excitation des voies inélastiques ouvertes énergétiquement, doit être, à basse énergie, plus forte dans un noyau dont la densité de niveaux de faible énergie d'excitation est plus élevée et dont les sections efficaces de diffusion inélastique sont plus grandes, comme c'est le cas quand on compare les noyaux à couches ouvertes aux noyaux à couches fermées. Pour calculer ces potentiels, il faut inclure explicitement la contribution de chaque état excité dont l'énergie est inférieure à l'énergie incidente. Nous avons fait ce calcul dans le seul cas du ^{40}Ca, en utilisant les fonctions d'onde RPA. Ces calculs conduisent à une faible absorption à 20 MeV,avec une augmentation très rapide quand l'énergie croît.
Les résultats,obtenus à basse énergie pour le ^{40}Ca d'une part,et ceux obtenus précédemment pour le ^{40}Ca et le ^{44}Ca d'autre part,semblent globalement compatibles avec la dépendance en énergie et en A suggérée par les

analyses des résultats expérimentaux.

Avec nos potentiels calculés, nous avons étudié simultanément la diffusion élastique (α,α) et la réaction de transfert $(^3He,\alpha)$ pour des énergies supérieures à 100 MeV, là où les analyses phénoménologiques semblaient échouer. Nos potentiels microscopiques nous ont permis de reproduire simultanément les sections efficaces de la diffusion élastique et de la réaction de transfert. Toutefois, notre modèle néglige les voies de break-up de la particule alpha et l'on doit s'attendre à une absorption sous-estimée à la surface. Nous avons vérifié qu'ajouter un terme de surface très faible à notre absorption calculée conduit au même type d'accord ou désaccord qu'en introduisant une constante de renormalisation globale pour le potentiel imaginaire.

Notre travail, qui nous a permis de mieux comprendre un certain nombre de propriétés des potentiels déduits des analyses de diffusion, souffre encore d'un certain nombre de défauts. Entre autres, alors que nous avons montré qu'il était indispensable de travailler avec l'interaction α-nucléon non locale, les effets de cette non localité sur le potentiel imaginaire ont été négligés aussi bien que les effets dus à la dépendance en densité de l'interaction effective. Ces effets pourraient modifier nos résultats. Un effet certainement plus important provient du fait que nous avons négligé la contribution des voies de break-up de la particule alpha, que nous avons ajoutée phénoménologiquement mais qui devrait être calculée. Cependant, nous avons pu obtenir des résultats au moins qualitativement intéressants qui ont incité d'autres auteurs à tenter une généralisation de notre modèle simple pour décrire l'absorption dans une diffusion d'ions lourds. Cette

généralisation est délicate, en particulier parce que toutes les simplifications justifiées quand on a une particule alpha doivent être reconsidérées.

Résumé

Une étude microscopique du potentiel α-noyau est effectuée dans le cadre de la théorie de Feshbach pour des énergies comprises entre 20 et 200 MeV. Le potentiel réel du modèle de convolution est calculé directement à partir de l'interaction α-nucléon non locale déduite à l'approximation Hartree-Fock de diverses interactions nucléon-nucléon. Pour les interactions dépendant de la densité, nous avons proposé un choix différent de densité locale et inclus les termes de réarrangement, qui se sont révélés importants à courtes distances. Notre étude montre l'importance des effets de non-localité de l'interaction α-nucléon et de dépendance en densité du noyau de l'interaction nucléon-nucléon effective pour la détermination du potentiel réel. A basse énergie, nous avons calculé le potentiel absorptif α-^{40}Ca en tenant compte de tous les états qui peuvent être excités et en utilisant les fonctions d'onde RPA du ^{40}Ca. Aux énergies intermédiaires, nous avons dérivé une expression simple du potentiel imaginaire et de la correction au modèle de convolution pour tous les noyaux, en utilisant la relation de fermeture sur la base complète des états du noyau. Nous montrons que la correction au modèle de convolution est très faible. La détermination du potentiel imaginaire local équivalent au potentiel de Feshbach est fortement influencée par la non-localité du potentiel réel. Nos potentiels α-noyau reproduisent correctement les propriétés globales des potentiels déduits des analyses de diffusion et nous ont permis une description cohérente de la diffusion élastique (α,α) et de la réaction de transfert (^{3}He, α) au-delà de 100 MeV.

Mots-clés

Interaction α-noyau - Potentiel optique -
Diffusion élastique - Réaction de transfert.